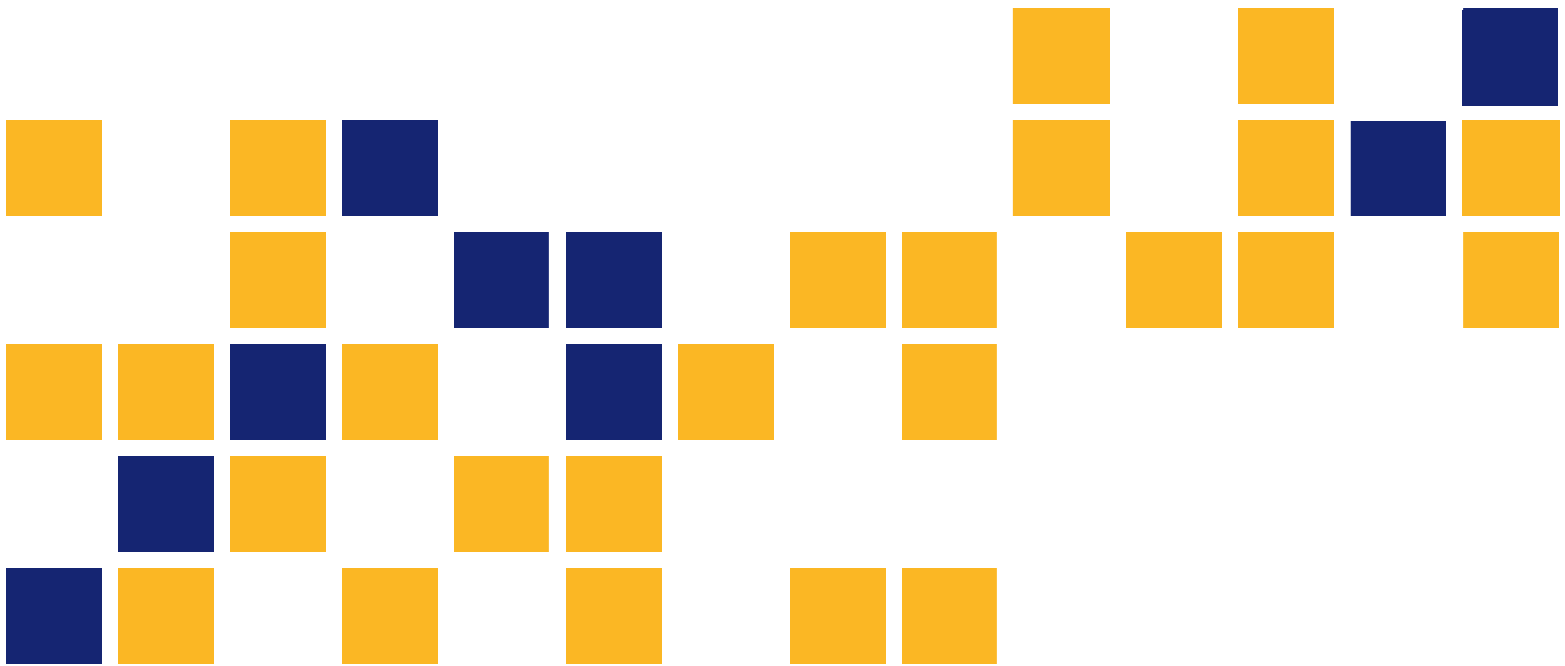# Kansas Department of Transportation Column Expert: Ultimate Shear Capacity of Circular Columns Using the Simplified Modified Compression Field Theory

AlaaEldin Abouelleil, M.S.
Hayder Rasheed, Ph.D., P.E., FASCE

Kansas State University Transportation Center

Kansas
Department of Transportation

1	Report No. K-TRAN: KSU-14-4	2	Government Accession No.	3	Recipient Catalog No.
4	**Title and Subtitle** Kansas Department of Transportation Column Expert: Ultimate Shear Capacity of Circular Columns Using the Simplified Modified Compression Field Theory			5	**Report Date** September 2015
				6	**Performing Organization Code**
7	**Author(s)** AlaaEldin Abouelleil, M.S., and Hayder Rasheed, Ph.D., P.E., FASCE			7	**Performing Organization Report No.**
9	**Performing Organization Name and Address** Kansas State University Transportation Center Department of Civil Engineering 2126 Fiedler Hall Manhattan, Kansas 66506			10	**Work Unit No. (TRAIS)**
				11	**Contract or Grant No.** C1972
12	**Sponsoring Agency Name and Address** Kansas Department of Transportation Bureau of Research 2300 SW Van Buren Topeka, Kansas 66611-1195			13	**Type of Report and Period Covered** Final Report July 2013–June 2015
				14	**Sponsoring Agency Code** RE-0625-01
15	**Supplementary Notes** For more information write to address in block 9.				

The importance of the analysis of circular columns to accurately predict their ultimate confined capacity under shear-flexure-axial force interaction domain is recognized in light of the extreme load event imposed by the current American Association of State Highway and Transportation Officials (AASHTO) Load and Resistance Factor Design (LRFD) Bridge Construction Specifications (AASHTO, 2014). In this study, various procedures for computing shear strength are reviewed. Then, the current procedure adopted by AASHTO LRFD specifications, based on the Simplified Modified Compression Field Theory, is evaluated for non-prestressed circular concrete bridge piers. This evaluation is benchmarked against experimental data available in the literature, and against Response 2000 freeware program that depicts interaction diagrams based on AASHTO (1999) LRFD requirements. Differences in results are discussed and future improvements are proposed. A new approach is presented to improve the accuracy of AASHTO LRFD calculations. The main parameters that control the cross section shear strength are discussed based on the experimental results and comparisons.

17	**Key Words** Shear Capacity, Circular Columns, Concrete Shear Resistance	18	**Distribution Statement** No restrictions. This document is available to the public through the National Technical Information Service www.ntis.gov.
19	**Security Classification (of this report)** Unclassified	20	**Security Classification (of this page)** Unclassified	21	**No. of pages** 129	22	**Price**

Form DOT F 1700.7 (8-72)

This page intentionally left blank.

Kansas Department of Transportation Column Expert: Ultimate Shear Capacity of Circular Columns Using the Simplified Modified Compression Field Theory

Final Report

Prepared by

AlaaEldin Abouelleil, M.S.
Hayder Rasheed, Ph.D., P.E., FASCE

Kansas State University Transportation Center

A Report on Research Sponsored by

KANSAS DEPARTMENT OF TRANSPORTATION
TOPEKA, KANSAS

and

KANSAS STATE UNIVERSITY TRANSPORTATION CENTER
MANHATTAN, KANSAS

September 2015

PREFACE

The Kansas Department of Transportation's (KDOT) Kansas Transportation Research and New-Developments (K-TRAN) Research Program funded this research project. It is an ongoing, cooperative and comprehensive research program addressing transportation needs of the state of Kansas utilizing academic and research resources from KDOT, Kansas State University and the University of Kansas. Transportation professionals in KDOT and the universities jointly develop the projects included in the research program.

NOTICE

The authors and the state of Kansas do not endorse products or manufacturers. Trade and manufacturers names appear herein solely because they are considered essential to the object of this report.

This information is available in alternative accessible formats. To obtain an alternative format, contact the Office of Public Affairs, Kansas Department of Transportation, 700 SW Harrison, 2nd Floor – West Wing, Topeka, Kansas 66603-3745 or phone (785) 296-3585 (Voice) (TDD).

DISCLAIMER

The contents of this report reflect the views of the authors who are responsible for the facts and accuracy of the data presented herein. The contents do not necessarily reflect the views or the policies of the state of Kansas. This report does not constitute a standard, specification or regulation.

Abstract

The importance of the analysis of circular columns to accurately predict their ultimate confined capacity under shear-flexure-axial force interaction domain is recognized in light of the extreme load event imposed by the current American Association of State Highway and Transportation Officials (AASHTO) Load and Resistance Factor Design (LRFD) Bridge Construction Specifications (AASHTO, 2014). In this study, various procedures for computing shear strength are reviewed. Then, the current procedure adopted by AASHTO LRFD specifications, based on the Simplified Modified Compression Field Theory, is evaluated for non-prestressed circular concrete bridge piers. This evaluation is benchmarked against experimental data available in the literature, and against Response 2000 freeware program that depicts interaction diagrams based on AASHTO (1999) LRFD requirements. Differences in results are discussed and future improvements are proposed. A new approach is presented to improve the accuracy of AASHTO LRFD calculations. The main parameters that control the cross section shear strength are discussed based on the experimental results and comparisons.

Acknowledgements

Table of Contents

List of Tables

List of Figures

Chapter 1: Introduction

1.1 Overview

Even though the behavior of concrete elements subjected to shear force has been studied for many years, researchers do not have a full agreement on concrete shear resistance. This is mainly because of the many different mechanisms that affect the shear transfer process of concrete, such as aggregate interlock, interface shear transfer across cracks, shear transfer in compression zone, dowel action, and residual tensile stresses normal to cracks. However, researchers agree that aggregate interlock and shear transfer in compression zone are the key components to understanding concrete behavior under full field shear, flexural, and axial stresses.

1.2 Objectives

The importance of the analysis of circular reinforced concrete columns to accurately predict their confined load carrying capacity under full interaction domain (moment-shear force-axial force) is recognized in light of the extreme load event imposed by the current American Association of State Highway and Transportation Officials (AASHTO) Load and Resistance Factor Design (LRFD) Bridge Construction Specifications (AASHTO, 2014), based on the Simplified Modified Compression Field Theory (SMCFT). Since these provisions are relatively new to the specification, a detailed evaluation of their predictions is warranted. Objective judgment may be reached if the generated interaction diagrams are compared to experimental results available in the literature. It is also valuable to compare the results against other programs, especially those making similar assumptions and based on the same theory.

1.3 Scope

This report is composed of eight chapters covering the development of calculations, analysis procedures, benchmarking, and practical applications.

Chapter 1 introduces the work, highlighting the objectives and scope of the report. Chapter 2 details the literature review as it relates to the shear models and the experimental studies addressing the behavior of circular reinforced concrete columns under different load

combinations. Chapter 3 describes the present formulation used in the analysis procedure to predict the full domain of column sections. Chapter 4 discusses the implementation procedure to utilize the formulated equations and limits to generate interaction diagrams that represent the extreme load event of the sections. Chapter 5 provides the final results and comparisons of this study with brief discussions and comments. Chapter 6 briefs the reader on the software development that was coded using the proposed procedure, and describes the program interface design and features. Chapter 7 provides full database comparisons against the experimental studies. Chapter 8 discusses the conclusions and provides recommendations for future relevant work.

Chapter 2: Literature Review

2.1 Overview

This section provides a general review of shear strength provisions implemented by various design codes and proposed models, followed by a number of experimental studies to investigate shear strength mechanism experimentally. Most design codes are based on concrete strength and transverse reinforcement strength to determine the shear capacity of reinforced concrete sections. These two components are simply added together to provide the full shear capacity of the section in the presence of flexure and axial force.

2.2 Theoretical Treatments

2.2.1 Approach of Priestley, Verma, and Xiao (1994)

Priestley, Verma, and Xiao (1994) proposed a model for the shear strength of reinforced concrete members under cyclic lateral load as the summation of strength capacities of concrete (V_c), steel (V_s), and an arch mechanism associated with axial load (V_p).

$$V = V_c + V_s + V_p \qquad \qquad \textbf{Equation 2.1}$$

Where $V_c = k\sqrt{f_c'A_e}$, $A_e = 0.8\,A_g$ **Equation 2.2**

Where (k) within plastic end regions depends on the member's ductility.

$$V_s = \frac{\pi A_h f_{yh} D' \cot(\theta)}{2s} \qquad \qquad \textbf{Equation 2.3}$$

In which (D') is the spiral/hoop diameter and (Ah) is area of a single hoop/spiral.

The angle of the critical inclined flexure-shear cracks to the column axis is taken as $\theta = 30°$, unless limited to larger angles. The shear strength enhancement resulting from axial compression is considered as a variable, and is given by:

$$V_p = P * tan\alpha = \frac{D-c}{2a}P$$
Equation 2.4

> Where (D) is the diameter of circular column, (c) is the depth of the compression zone, and (a) is the shear span.
>
> For a cantilever column, (α) is the angle formed between the column axis and the strut from the point of load application to the center of the flexural compression zone at the column plastic hinge critical section.

2.2.2 Standards New Zealand (1995)

Standards New Zealand (1995) adapted the following equations based on a 45° truss model for the nominal shear strength of concrete columns. In determination of (V_c) inside the plastic hinge zone, the longitudinal steel amount and the axial load effect are considered. However, the axial load effect is applied only if the axial load ratio exceeds 0.1. If the axial load ratio is less than or equal to 0.1, the concrete contribution to shear strength is ignored. The shear strength carried by concrete is thus calculated as follows:

$$V_c = \left(0.01 + 1.45\frac{A_s}{bs}\right)\sqrt{f_c'}\sqrt{\frac{P}{f_c'A_g} - 0.1}\,b\,d \quad \text{(ksi)}$$
Equation 2.5

> In which (A_s) is the area of transverse reinforcement within spacing (s), and (b) is the width of the column. For circular columns, (b) is taken as the column diameter (D).
>
> The shear strength carried by transverse reinforcement is based on analysis of effective shear resistance provided by transverse hoops assuming a 45° truss mechanism (Ang, Priestley, & Paulay, 1989).

$$V_s = \frac{\pi A_{sp} f_{yh} D_{sp}}{2s}$$
Equation 2.6

> Where (A_{sp}) is the cross-sectional area of transverse steel, (D_{sp}) is the core diameter of circular section defined by the center-to-center diameter of transverse steel, (f_{yh}) is yield stress of transverse steel, and (s) is vertical distance between transverse steel.

2.2.3 Applied Technology Council Report ATC-32 Shear Design Equations

The design approach of Applied Technology Council Report Number ATC-32 (Nutt, 1996) also uses the combination of concrete shear resistance (V_c) and steel shear resistance (V_s).

$$V_n = V_c + V_s \qquad\qquad \textbf{Equation 2.7}$$

$$V_s = \frac{\pi A_h f_{yh} D' \cot(\theta)}{2s} \qquad\qquad \textbf{Equation 2.8}$$

$$V_c = 0.024\left(K_1 + \frac{P}{K_2 A_g}\right)\sqrt{f_c'}\,(0.8\,A_g) \;\; \text{(ksi)} \qquad\qquad \textbf{Equation 2.9}$$

> Where (K_1) = 1.0, except in plastic hinge regions of ductile columns, where (K_1) = 0.5, and (K_2) = 13.8 for compressive axial load (P) and (K_2) = 3.45 for tensile axial load where (P) has the negative sign. (θ) is the angle of the inclined flexure-shear cracks to the column axis.

2.2.4 California Department of Transportation Memo 20-4 (2010)

The California Department of Transportation (Caltrans) shear strength equations are primarily intended as an assessment tool for determining the shear strength of existing bridge columns, and were developed based on the Kowalsky and Priestley (2000) approach. This approach recognizes the effect of displacement ductility on column shear strength, and shear strength is based on the following equations for (V_c) and (V_s):

$$V_s = \frac{\pi A_{sp} f_{yh} D_{sp}}{2s} \qquad\qquad \textbf{Equation 2.10}$$

$$V_c = v_c A_e = F_1 F_2 \sqrt{f_c'}\,\left(0.8 A_g\right) \le 0.048\sqrt{f_c'}\,A_g \;\; \text{(ksi)} \qquad\qquad \textbf{Equation 2.11}$$

> The shear stress of concrete (v_c) is a function of the product of F_1 and F_2, which are the terms related to the shear strength dependent on displacement ductility level (μ) and axial load ratio (P/A_g). Displacement ductility level is estimated by the ratio of measured maximum displacement (Δ_D) to measured yield displacement (Δ_y) under cyclic loading.

2.2.5 Joint ASCE-ACI Task Committee 426 (1973) Shear Strength Approach

Committee 426, a joint ASCE-ACI committee on shear strength of concrete members, has produced a design equation based on the additive model (Joint ASCE-ACI Task Committee 426, 1973).

$$V_n = V_c + V_s$$ **Equation 2.12**

The committee does not consider the influence of ductility to estimate total shear strength of circular columns (Priestley et al., 1994).

The shear strength carried by concrete (V_c) is calculated by:

$$V_c = v_b \left(1 + \frac{3P}{f_c' A_g}\right) A_e$$ **Equation 2.13**

Where (A_e) is the effective shear area of circular column with diameter (D), calculated as:

$$A_e = 0.8 A_g$$ **Equation 2.14**

(v_b) is the nominal concrete shear stress from the following equation:

$$v_b = (0.0096 + 1.45 \rho_t)\sqrt{f_c'} \leq 0.03\sqrt{f_c'} \text{ (ksi)}$$ **Equation 2.15**

In which (ρ_t) is the longitudinal tension steel ratio and it is calculated in terms of the gross area of the column.

In order to calculate the transverse steel shear strength contribution (V_s), the committee assumed a diagonal compression strut model at 45° to the member longitudinal axis.

$$V_s = \frac{\pi}{2}\frac{A_h f_{yh} D'}{s}$$ **Equation 2.16**

In which (D') is the spiral/hoop diameter and (A_h) is area of a single hoop/spiral.

2.2.6 ACI Committee 318 (2011)

The American Concrete Institute (ACI) code ACI 318-11 considers a portion of the design shear force to be carried by the concrete shear resistance (V_c), with the remainder carried by transverse steel (V_s), as done by earlier codes and models. The ACI code presents the following equation for calculating (V_c) for members subjected to combined shear, moment, and axial compression (ACI Committee 318, 2011):

$$V = V_c + V_s \qquad\qquad\qquad \textbf{Equation 2.17}$$

$$V_s = \frac{A_v f_{y_t}(\sin\alpha + \cos\alpha)d_s}{s} \qquad\qquad\qquad \textbf{Equation 2.18}$$

$$V_c = 0.002\left(1 + \frac{P}{2000A_g}\right)\lambda\sqrt{f_c'}\,bd \quad \text{(ksi)} \qquad\qquad \textbf{Equation 2.19}$$

Where (P) is axial load subjected to the section, (A_g) is gross cross-sectional area, (f'_c) is concrete compressive strength, (b) is the width of section, and (d) is the effective depth of section. (A_v) is the area of transverse reinforcement within the spacing (s), (f_{yt}) is the yield stress of transverse steel, (α) is the angle between inclined stirrups and longitudinal axis of the member, and (λ) is a modification factor to account for lightweight concrete.

2.2.7 Modified Compression Field Theory

In the 1980s, after testing different reinforced concrete members elements subjected to pure shear, pure axial load, and a combination of shear and axial load, a theory called the Modified Compression Field Theory (MCFT) was developed based on the Compression Field Theory (Vecchio & Collins, 1986). The MCFT was able to accurately predict the shear behavior of concrete members subjected to shear and axial forces. The main key of this theory is that significant tensile stresses could exist in the concrete between the cracks, even at very high values of average tensile strains. In addition, the value for angle θ of diagonal compressive stresses was considered as variable compared to the fixed value of 45 assumed by the ACI code.

To simplify the process of predicting the shear strength of a section using the MCFT, the shear stress is assumed to remain constant over the depth of the cross section, and the shear

strength of the section can be determined by considering the axial stress and the shear stress at one location in the web. This was the basis of the sectional design model for shear implemented by the AASHTO (2014) LRFD Bridge Design Specifications, based on the work of Bentz, Vecchio, and Collins (2006).

Even though the AASHTO LRFD procedure to predict the shear strength of a section was relatively straightforward in earlier versions of the specification, the prediction of the contribution of concrete to shear strength of a section, which is a function of β and varying angle θ, was required to be determined using the tables provided by AASHTO LRFD. In the most recent version of the specifications, β and θ were defined using equations instead of the tables approach. The factor β indicates the ability of diagonally-cracked concrete to transmit tension and shear. The modified compression field theory was further more simplified when simple and direct equations were developed by Bentz et al. (2006) for β and θ to replace the iterative procedure using the tables that was implemented by earlier versions of AASHTO specifications. These simplified equations were then used to predict the shear strength of different reinforced concrete sections and the results were compared to those obtained from MCFT, as shown in Figure 2.1.

Consequently the shear strength predicted by the Simplified Modified Compression Field Theory (SMCFT) and the MCFT were compared with experimental results of various beams. It was found that the results of the SMCFT and the MCFT were similar and both matched properly the experimental results. In addition, the results were also compared with the ACI code, where it was inconsistent in particular for panels with no transverse reinforcements (Bentz et al., 2006), see Figure 2.1.
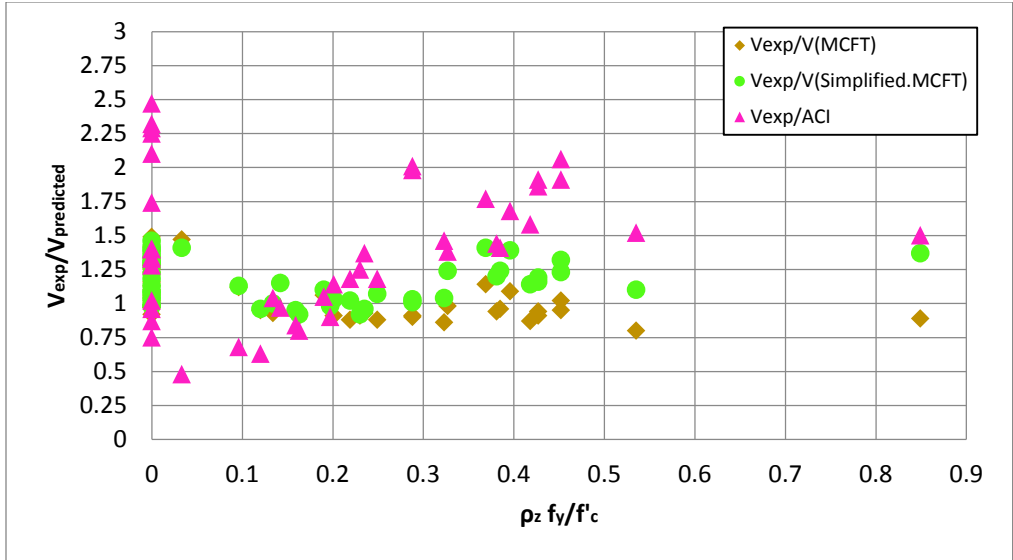
Figure 2.1: Ratio of Experimental to Predicted Shear Strength of Different Models
Note: Graph is reproduced from data collected by Bentz et al. (2006)

Before discussing the Modified Compression Field Theory, it is important to define the basic membrane element used to develop the approach. The reinforced concrete element is defined to have a uniform thickness and a relatively small size. It consists of an orthogonal grid of reinforcement with the longitudinal steel in (X) direction and the transverse steel in (Y) direction, see Figure 2.2.
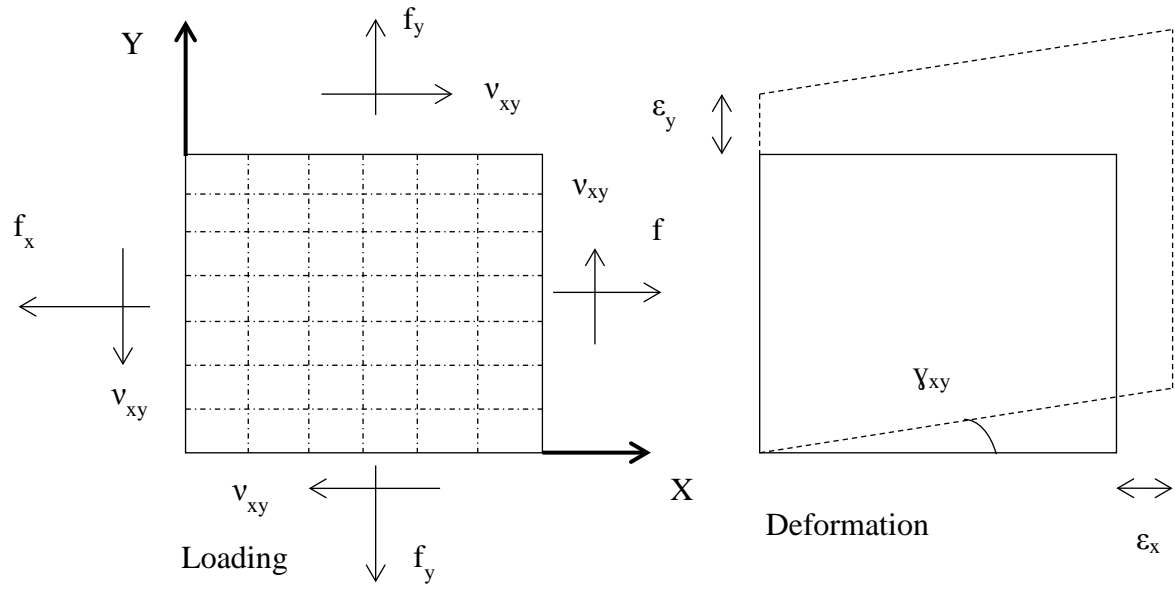
Figure 2.2: Loading and Deformation for MCFT Membrane Element

9

Uniform axial stresses (f_x), (f_y) and a uniform shear stress (v_{xy}) are acting on the element, causing two normal strains (ε_x) and (ε_y) in addition to a shear strain (γ_{xy}), see Figure 2.2. The main target is to develop a relationship between the stresses and the strains in the member. In order to achieve this relationship, some reasonable assumptions were made:

1. Each strain state is corresponding to one stress state.
2. Stresses and strains could be calculated in terms of average values when taken over areas large enough to include several cracks.
3. A perfect bond exists between the steel and the concrete.
4. A uniform longitudinal and transverse steel distribution over the element.

2.2.7.1 Compatibility Conditions

Assuming a perfect bond between the concrete and the reinforcement requires that any change in concrete strain will cause an equal change in steel strain in the same direction.

$$\varepsilon_c = \varepsilon_s = \varepsilon$$ **Equation 2.20**

By knowing the three strains ε_x, ε_y, and γ_{xy}, the strain in any other direction can be calculated from the geometry of Mohr's circle of strain, see Figure 2.3.
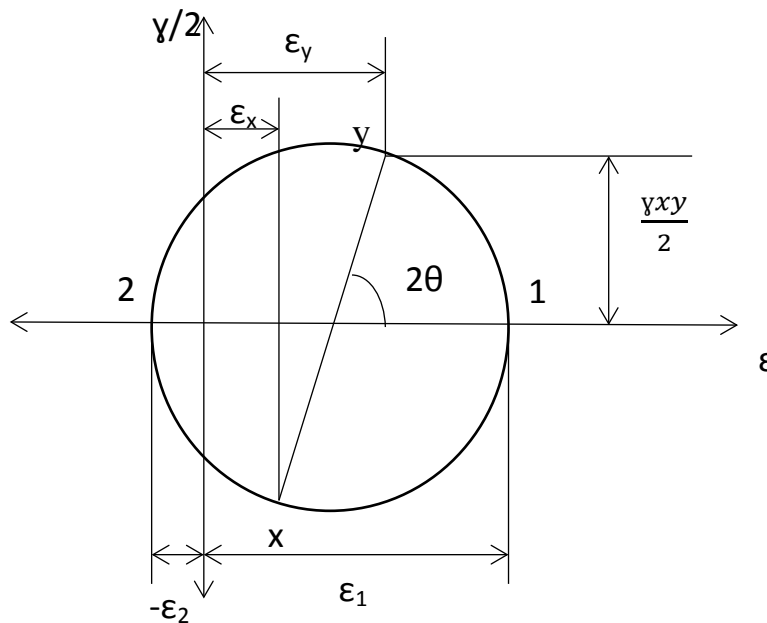
Figure 2.3: Mohr's Circle of Strains

In Figure 2.3, (ε_1) represents the principal tensile strain, while (ε_2) represents the principal compressive strain. The angle of the principal direction with respect to the horizontal direction is represented by (θ).

2.2.7.2 Equilibrium Conditions

In order to achieve equilibrium, the summation of the applied forces and the resisting forces generated in the element should equal zero in each direction. In (x) direction (see Figure 2.2), the state of equilibrium is:

$$\int f_x \, dA = \int f_{cx} dA_c + \int f_{sx} dA_s \qquad \qquad \textbf{Equation 2.21}$$

Where (f_{cx}) and (A_c) are the stress in concrete and area of concrete, and (f_{sx}) and (A_s) are the stress in steel and area of steel.

Ignoring the reduction in concrete area due to the steel presence:

$$f_x = f_{cx} + \rho_s f_{sx} \qquad \qquad \textbf{Equation 2.22}$$

Similarly,

$$f_y = f_{cy} + \rho_s f_{sy} \qquad \qquad \textbf{Equation 2.23}$$

$$v_{xy} = v_{cx} + \rho_s v_{sx} \qquad \qquad \textbf{Equation 2.24}$$

$$v_{xy} = v_{cy} + \rho_s v_{sy} \qquad \qquad \textbf{Equation 2.25}$$

2.2.7.3 Stress-Strain Relationship

The stress-strain relationships for the concrete and the reinforcement are assumed to be completely independent of each other. The axial stress in steel would be only a result of the axial strain in the steel. Also, shear stresses in the steel on a plane perpendicular to the steel longitudinal axis are assumed to be zero. Regarding the steel axial stress-axial strain relationship, the usual bilinear relationship is assumed, see Figure 2.4.

$$f_s = E_s \varepsilon_s \le f_y \qquad\qquad \textbf{Equation 2.26}$$

$$v_s = 0 \qquad\qquad \textbf{Equation 2.27}$$

Where (E_s) is the modulus of elasticity of steel, and (f_y) is the yielding stress in steel.
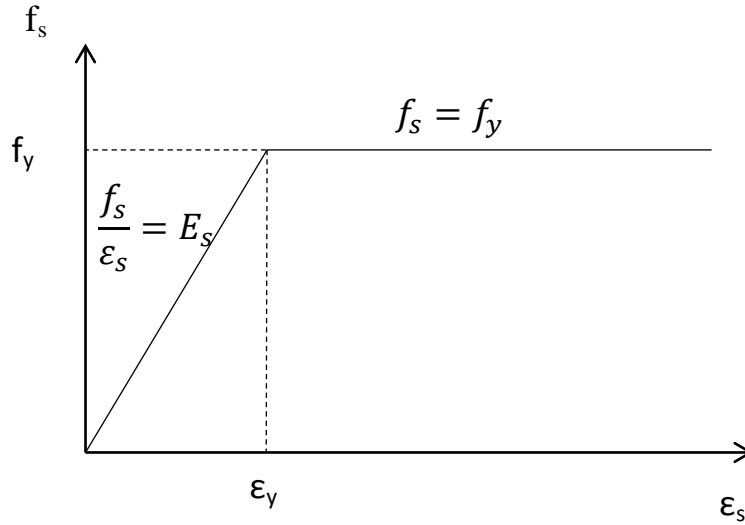
Figure 2.4: Steel Bilinear Relationship

In regard to the concrete stress-strain relationships, 30 reinforced concrete elements were tested under different loading conditions, including pure shear, uniaxial compression, biaxial compression, and combined shear and axial load. Longitudinal and transverse steel ratios and concrete strength were also variables in these tests. More details are discussed in this literature review under the experimental works section.

It was assumed that the principal strain direction in concrete (θ) and the principal stress direction in concrete (θ_c) have the same angle, $\theta_c = \theta$. However, it was observed that the direction of the principal strain in the concrete deviated from the direction of the principal stress in concrete, $\theta_c = \theta \pm 10$ (Vecchio & Collins, 1986).

Although the principal compressive stress in the concrete (f_{c2}) was found to be a function in both the principal compressive strain (ε_2) and the accompanied principal tensile strain (ε_1), for

12

this reason the cracked concrete under tensile strains normal to the compression is weaker than concrete standard cylinder test, and the suggested relationship is:

$$f_{c2} = f_{c2\max}(\frac{2\varepsilon_2}{\varepsilon'_c} - (\frac{\varepsilon_2}{\varepsilon'_c})^2)$$
Equation 2.28

Where (ε'_c) is the strain corresponding to the $(f_{c2\max})$. It is a good observation to mention that the suggested equation is similar in behavior to Hognestad's concrete parabola, only differing in the maximum values; see Figure 2.5.
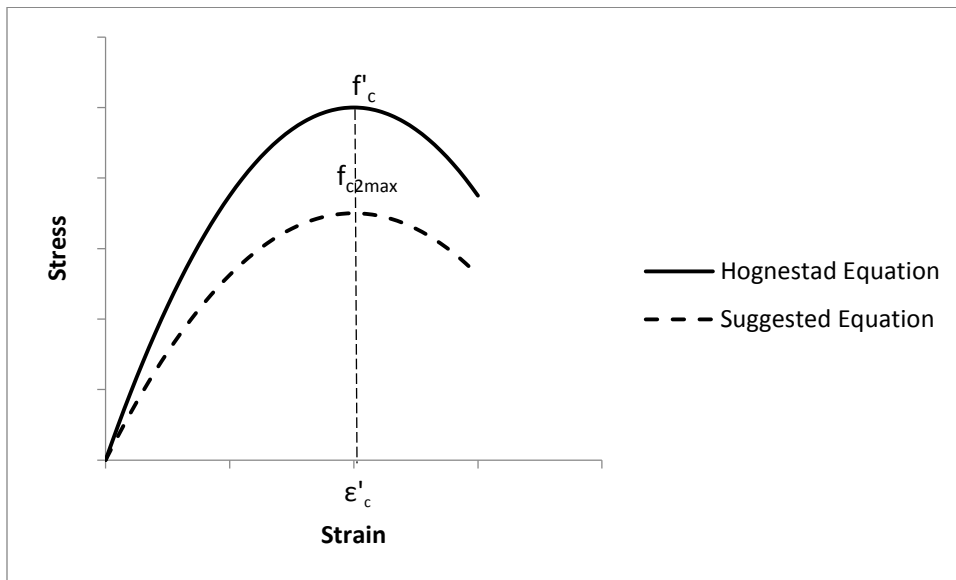
Figure 2.5: Relationship between Hognestad's Equation and MCFT Suggested Equation for the Principal Compressive Stress

In tension, it was suggested to use the linear stress-strain relationship to define the relationship between the principal tensile stress and the principal tensile strain in concrete prior to cracking.

$$f_{c1} = E_c\varepsilon_1$$
Equation 2.29

Where (E_c) is the modulus of elasticity of concrete.

13

After cracking, the suggested equation is:

$$f_{c1} = \frac{f_{cr}}{1 + \sqrt{200\varepsilon_1}}$$

Equation 2.30

Where (f_{cr}) is the concrete rupture stress.

2.2.7.4 Average Stresses and Average Strains Concept

The MCFT considers average stresses and average strain across the crack. It does not provide an approach corresponding to local stress/strain variations. The concrete tensile stresses would be minimum value at cracks, and it would reach a value higher than the average in the distance between the two successive cracks. The steel tensile stresses would be higher than the average at cracks, and it would have a lower value between the cracks due to the contribution of concrete tensile resistance.

2.2.7.5 Transmitting Shear/Tension Across Cracks

The applied stresses, (f_x), (f_y), and (v_{xy}), and the internal stresses should establish a state of equilibrium in the element. Furthermore, the internal stress at a crack plane (plane a-a) should equal the stresses at a parallel plane in the distance between two successive cracks (plane b-b), see Figure 2.6. The internal stresses at the crack are steel stresses (f_{scr}), shear stresses (v_c), and minor compressive stresses (f_c). The internal stresses at the uncracked plane parallel to the crack plane are average stresses (f_{c1}) and steel stresses (f_s). In terms of average strain, the average shear stress is zero at plane (b-b). By assuming a unit cross area along the crack, the stresses equilibrium in (x) and (y) directions is calculated.

At (x) direction:

$$\rho_s f_s \sin(\theta) + f_{c1} \sin(\theta) = \rho_s f_{scr} \sin(\theta) - f_c \sin(\theta) - v_c \cos(\theta)$$

Equation 2.31

At (y) direction:

$$\rho_s f_s \cos(\theta) + f_{c1} \cos(\theta) = \rho_s f_{scr} \cos(\theta) - f_c \cos(\theta) + v_c \sin(\theta)$$

Equation 2.32

From Equations 2.31 and 2.32, equilibrium can't be achieved without the shear stresses, especially when the reinforcement at cracking (f_{scr}) is approaching the yielding, as the concrete contribution will then be negligible.

The shear stresses are caused due to the aggregate interlock, see Figure 2.7. Due to the high strength of the aggregate, the concrete crack occurs along the interface of the aggregate. The shear stress across the crack (v_c) is a function in maximum aggregate size (a), crack width (w), and the compressive stress on the crack (f_c; Walraven, 1981).
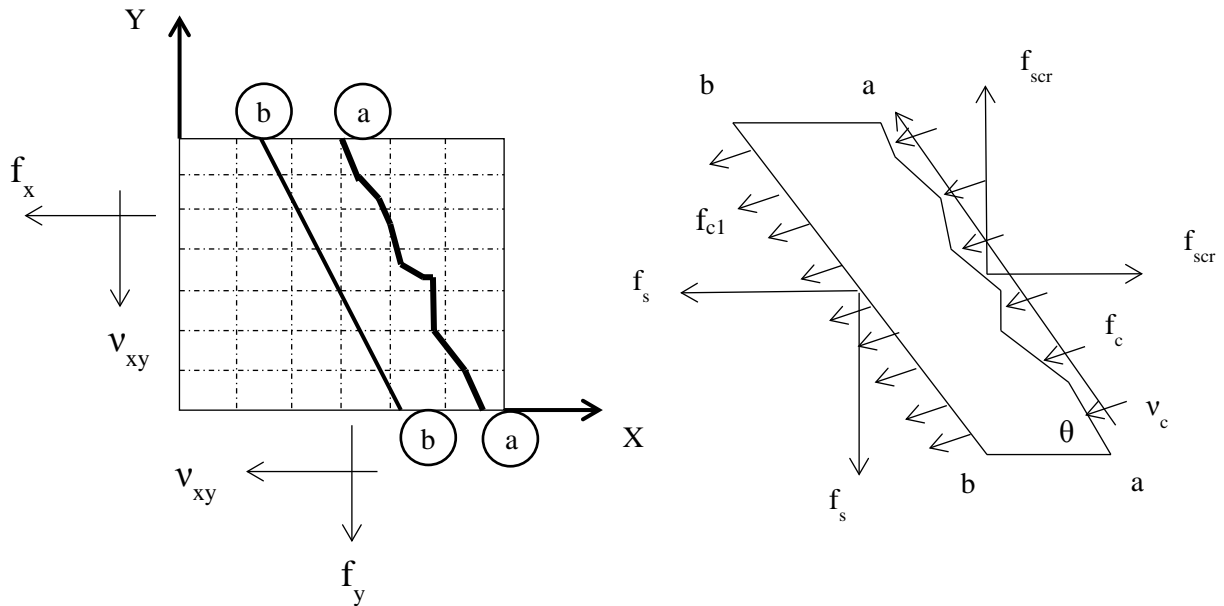
Figure 2.6: State of Equilibrium for Plane (a-a) and Plane (b-b)

Walraven (1981) suggested the following equation based on experimental results.

$$v_c = 0.18v_{cmax} + 1.64f_c - \frac{0.82f_c^2}{v_{cmax}}$$ **Equation 2.33**

Where

$$v_{cmax} = \frac{12\sqrt{-f_c'}}{0.31 + 24\frac{w}{a + 0.63}}$$ **Equation 2.34**

Where (a) is the maximum aggregate size in inches, (w) is the crack width in inches, and the concrete maximum compressive strength (f'_c) is in psi. In Equation 2.34, ($f'c$) should be substituted with a negative value as a representation of compression.

15
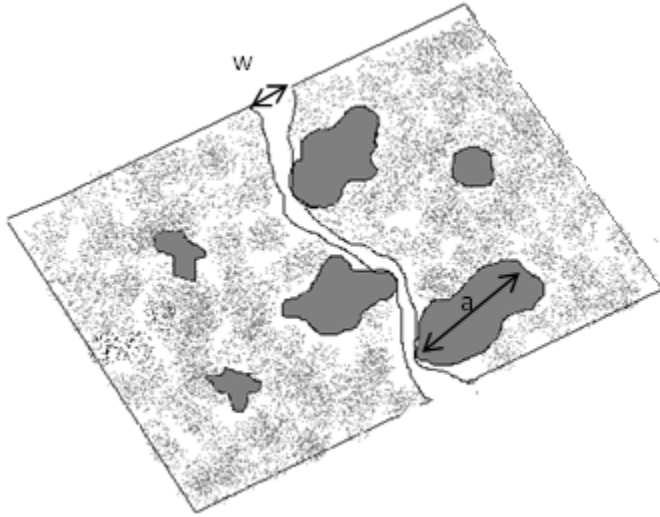
Figure 2.7: Aggregate Interlock

2.3 Experimental Studies

This section provides a general review of experimental studies on the behavior of circular reinforced concrete columns under combined loading cases. The applied forces on the columns varied between shear-moment and shear-moment and axial force. Although the main target is to investigate the shear behavior of columns, some of the experimental studies discussed in this section were held using a square reinforced-concrete prism, as in the case of the MCFT tests. This prism was chosen in order to test pure shear without developing a significant moment which might cause a shear-moment failure instead of pure shear failure.

Ang, Priestley, and Paulay (1985) tested 25 cantilever circular columns under cyclic lateral loading and different constant axial forces (P). The circular cantilever columns were subjected to constant axial force and a slow lateral cyclic loading with gradually increasing displacement limits to simulate earthquake effects. The ratios of the length of the column to its diameter were 1.5, 1.75, 2.0, and 2.5. This ratio tends also to relate the applied lateral force to the resulting moment according to the following relationship:

16

$$\frac{M}{VD} = \frac{L}{D}$$

Where (M) is the moment at the base of the cantilever, (V) is the applied shear force, (D) is column diameter, and (L) is the effective length of the column.

In case of a cantilever column, the effective length is the full length of the column.

The level of axial compression force $(P/(f'_cA_g))$ were 0, 0.1, and 0.2. The volumetric hoop reinforcement content varied between 0.0038 and 0.00102. Table 2.1 shows column details and capacities.

Ohtaki, Benzoni, and Priestley (1996) tested four circular reinforced-concrete columns under cyclic lateral loading and different axial loads. The four columns were exposed to a double bending mechanism test. The specimens (CS1, CS2, CS3, and CS4) had the same length to diameter ratio (L/D) of 2, and also had the same reinforcement and geometrical details. The first two columns (CS1 and CS2) were subjected to axial load ratio (P/f'_cA_g) of 0.35 as compression and -0.087 as tension. The last two specimens (CS3 and CS4) were subjected to a varied axial load calculated based on the applied lateral force. Table 2.2 describes the columns' details and results. Unit CS4 showed major widening of existing cracks at ductility factor μ=1.5, while the maximum lateral forces for the other three specimens occurred at ductility factor μ=2. The tests of the first three columns continued till μ=6 without steel fracture.

Nelson (2000) tested four circular reinforced-concrete columns to evaluate the effects of earthquakes on "in place" bridge piers. The length to diameter ratio for the four identical columns was 3, and the geometry and reinforcement details of these columns were similar to Washington State Department of Transportation columns built prior to the mid-1970s. The four columns were subjected to different lateral loading. Table 2.3 illustrates the four columns' details and results.

Vecchio and Collins (1986) proposed the Modified Compression Field Theory, which deals with the reinforced cracked concrete as a new composite material as described in the theoretical approaches presented in this literature review. In order to justify their approach, 30 reinforced concrete elements were subjected to different load combinations. Two-thirds of the

elements were subjected to pure shear, and one-third of the elements were subjected to a combination of shear and axial compression/tension force. Longitudinal steel, transverse steel, and concrete strength were also variables in this experimental program. Table 2.4 shows the loading conditions and also shows the longitudinal and transverse steel ratio and concrete strength for each element. The test specimens were a thin square prism ($35 \times 35 \times 2.75$ inches). They were reinforced with two layers of welded wire mesh, with the wires parallel to the square edge. A clear cover of 0.25 inches was provided from the longitudinal steel to the element surface. The loads were applied using hydraulic jacks on five steel shear keys pre-casted into each of the four edges, see Figure 2.8. The direct output of these experiments was to determine the average strains and average stresses in the reinforcement. By knowing the external applied forces, the cracked concrete contribution could be calculated. In Table 2.4, compression is represented by a negative sign and tension is represented by a positive sign. Longitudinal steel ratio and transverse steel ratio are (ρl) and (ρs), respectively.
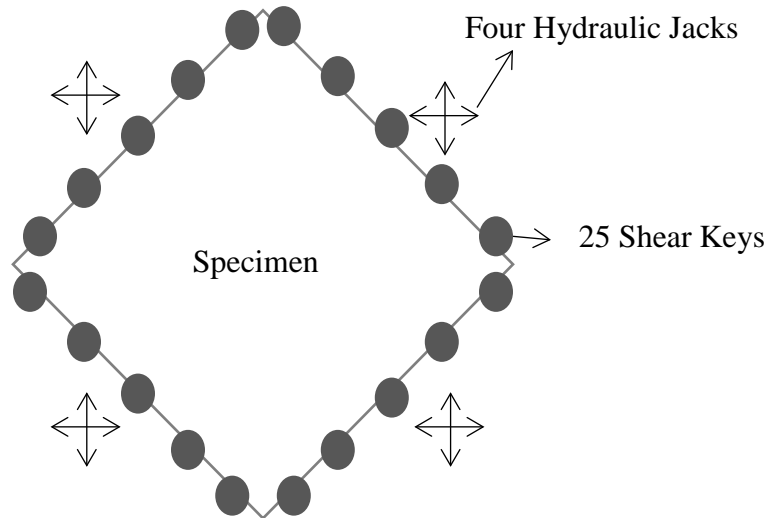
Figure 2.8: Modified Compression Field Theory Specimen Loading Installation

Table 2.1: Ang et al. (1985) Columns Details and Results

Unit	D (in.)	Clear cover (in.)	L/D	Number of bars	Longitudinal bar diameter (in.)	fy (ksi)	Transverse bar diameter (in.)	fyt (ksi)	Spacing (in.)	f'c (ksi)	Axial force (kip)	Shear force (kip)	Moment (k.ft)
1	15.75	0.59	2	20	0.63	63.22	0.24	47.56	2.36	5.4375	0	72.25	189.6563
2	15.75	0.59	2	20	0.63	42.92	0.24	47.56	2.36	5.394	0	49.61	130.2263
3	15.75	0.59	2.5	20	0.63	63.22	0.24	47.56	2.36	5.22	0	62.09	203.7069
4	15.75	0.59	2	20	0.63	63.22	0.39	45.82	6.5	4.437	0	65.01	170.6513
5	15.75	0.59	2	20	0.63	63.22	0.24	47.56	1.57	4.5095	0	74.39	195.2738
6	15.75	0.59	1.5	20	0.63	63.22	0.24	47.56	2.36	4.3645	0	88.04	173.2921
7	15.75	0.59	2	20	0.63	64.96	0.24	53.94	3.15	4.2775	0	63.09	165.6113
8	15.75	0.59	2	20	0.63	64.96	0.24	53.94	1.18	4.1615	162.08	104.54	274.4175
9	15.75	0.59	2.5	20	0.63	64.96	0.24	53.94	1.18	4.335	168.82	88.3	289.27
10	15.75	0.59	2	20	0.63	64.96	0.47	48.14	4.72	4.524	176.24	101.39	266.1488
11	15.75	0.59	2	20	0.63	64.96	0.24	53.94	2.36	4.3355	168.82	91.52	240.24
12	15.75	0.59	1.5	20	0.63	64.96	0.24	53.94	1.17	4.147	80.7	118.44	233.1294
13	15.75	0.59	2	20	0.63	63.22	0.24	47.27	1.18	5.249	102.28	98.99	259.8488
14	15.75	0.43	2	9	0.94	61.48	0.24	47.27	2.36	4.8865	0	71.12	186.69
15	15.75	0.59	2	12	0.63	63.22	0.24	47.27	2.36	5.046	0	51.78	135.9225
16	15.75	0.59	2	20	0.63	63.22	0.24	47.27	2.36	4.843	94.42	83.68	219.66
17	15.75	0.59	2.5	20	0.63	63.22	0.24	47.27	2.36	4.9735	96.89	73.12	239.8945
18	15.75	0.59	2	20	0.63	63.22	0.24	47.27	2.36	5.075	98.91	113.49	297.9113
19	15.75	0.59	1.5	20	0.63	63.22	0.24	47.27	3.15	4.988	97.11	98.34	193.5659
20	15.75	0.59	1.75	20	0.63	69.89	0.24	47.27	3.15	5.3215	181.41	109.4	251.2553
21	15.75	0.59	2	20	0.63	63.22	0.24	47.27	3.15	4.814	0	60.8	159.6
22	15.75	0.59	2	20	0.63	63.22	0.39	44.95	8.66	4.4805	0	64.03	168.0788
23	15.75	0.59	2	20	0.63	63.22	0.47	48.14	6.3	4.6835	0	74.75	196.2188
24	15.75	0.59	2	20	0.63	63.22	0.39	44.95	4.33	4.7995	0	76.54	200.9175

Table 2.2: Ohtaki et al. (1996) Columns Details and Results

Unit	D (in.)	Clear cover (in.)	L/D	Number of bars	Longitudinal bar diameter (in.)	fy (ksi)	Transverse bar diameter (in.)	fyt (ksi)	Spacing (in.)	f'c (ksi)	Axial force (kip)	Shear force (kip)	Moment (k.ft)
CS1	18.1	0.6	2	20	0.63	67	0.25	53.5	3.75	4.25	380	110.8	334.2467
CS2	18.1	0.6	2	20	0.63	67	0.25	53.5	3.75	5.19	-115	72.39	218.3765
CS3	18.1	0.6	2	20	0.63	67	0.25	53.5	3.75	5.37	380	92	277.5333
CS4	18.1	0.6	2	30	0.75	67	0.25	53.5	3.75				

Table 2.3: Nelson (2000) Columns Details and Results

Unit	D (in.)	Clear cover (in.)	L/D	Number of bars	Longitudinal bar diameter (in.)	fy (ksi)	Transverse bar diameter (in.)	fyt (ksi)	Spacing (in.)	f'c (ksi)	Axial force (kip)	Shear force (kip)	Moment (k.ft)
Col1	20	0.75	3	10	0.63	66	0.18	66	4	8.15	326	69.32	346.6
Col2	20	0.75	3	10	0.63	66	0.18	66	4	8.27	279	65.95	329.75
Col3	20	0.75	3	10	0.63	66	0.18	66	4	8.265	256	61.89	309.45
Col4	20	0.75	3	10	0.75	66	0.18	66	4	7.65	256	59.64	398.2

Table 2.4: Modified Compression Field Theory Experimental Program

Panel	Loading ratio v-fx-fy	ρl	fy (ksi)	ρs	fyt (ksi)	f'c (ksi)	vu (ksi) (failure)
PV1	1:00:00	0.0179	70.035	0.0168	70.035	-5.0025	1.1629
PV2	1:00:00	0.0018	62.06	0.0018	62.06	-3.4075	0.1682
PV3	1:00:00	0.0048	95.99	0.0048	95.99	-3.857	0.44515
PV4	1:00:00	0.0106	35.09	0.0106	35.09	-3.857	0.41905
PV5	1:00:00	0.0074	90.045	0.0074	90.045	-4.1035	0.6148
PV6	1:00:00	0.0179	38.57	0.0179	38.57	-4.321	0.65975
PV7	1:00:00	0.0179	65.685	0.0179	65.685	-4.495	0.98745
PV8	1:00:00	0.0262	66.99	0.0262	66.99	-4.321	0.96715
PV9	1:00:00	0.0179	65.975	0.0179	65.975	-1.682	0.5423
PV10	1:00:00	0.0179	40.02	0.01	40.02	-2.1025	0.57565
PV11	1:00:00	0.0179	34.075	0.0131	34.075	-2.262	0.5162
PV12	1:00:00	0.0179	68.005	0.0045	68.005	-2.32	0.45385
PV13	1:00:00	0.0179	35.96	0	0	-2.639	0.29145
PV14	1:00:00	0.0179	65.975	0.0179	65.975	-2.958	0.7598
PV15	00:-1:00	0.0074	36.975	0.0074	36.975	-3.1465	-2.842
PV16	1:00:00	0.0074	36.975	0.0074	36.975	-3.1465	0.3103
PV17	00:-1:00	0.0074	36.975	0.0074	36.975	-2.697	-3.0885
PV18	1:00:00	0.0179	62.495	0.0032	59.74	-2.8275	0.4408
PV19	1:00:00	0.0179	66.41	0.0071	43.355	-2.755	0.57275
PV20	1:00:00	0.0179	66.7	0.0089	43.065	-2.842	0.6177
PV21	1:00:00	0.0179	66.41	0.013	43.79	-2.8275	0.72935
PV22	1:00:00	0.0179	66.41	0.0152	60.9	-2.842	0.88015
PV23	1:-0.39:-0.39	0.0179	75.11	0.0179	75.11	-2.9725	1.28615
PV24	1:-0.83:-0.83	0.0179	71.34	0.0179	71.34	-3.451	1.1513
PV25	1:-0.69:-0.69	0.0179	67.57	0.0179	67.57	-2.784	1.3224
PV26	1:00:00	0.0179	66.12	0.0101	67.135	-3.0885	0.78445
PV27	1:00:00	0.0179	64.09	0.0179	64.09	-2.9725	0.92075
PV28	1:0.32:0.32	0.0179	70.035	0.0179	70.035	-2.755	0.841
PV29	Changing	0.0179	63.945	0.0089	46.98	-3.1465	0.85115
PV30	1:00:00	0.0179	63.365	0.0101	68.44	-2.7695	0.74385

Chapter 3: Present Formulation

3.1 Overview

This section provides the proposed approaches to generate the interaction domain (moment-shear force-axial force) for non-prestressed reinforced concrete columns. The first approach is based on the SMCFT and AASHTO (2014) LRFD Bridge Construction Specifications.

3.2 AASHTO (2014) LRFD Approach

The present procedure is based on the SMCFT originally developed by Bentz, Vecchio, and Collins (2006), and adopted by AASHTO (2014) LRFD specifications. This theory was derived based on the MCFT developed earlier by Vecchio and Collins (1986). In this section, shear equations used in this study are presented and specialized for the present application of non-prestressed circular reinforced concrete columns.

3.2.1 Minimum Transverse Steel

The following empirical equation is adopted to signify the minimum transverse reinforcement allowed by AASHTO (2014):

$$A_v \geq .0316\sqrt{f_c'}\,\frac{b_v s}{f_y} \quad (A_v \geq .083\sqrt{f_c'}\,\frac{b_v s}{f_y})$$
    (AASHTO, 2014) **Equation 3.1**

Where:

A_v = area of transverse reinforcement within spacing (s) in in^2 (mm^2)

f'_c = concrete compressive capacity in ksi (MPa)

b_v = effective web width taken as the minimum web width, measured parallel to the neutral axis, between the tensile resultant and compressive force due to flexure, or for circular sections, it is taken as the diameter of the section in inches (mm); see Figure 3.1.

s = spacing of transverse reinforcement in inches (mm)

f_y = yield strength in transverse steel in ksi (MPa)

A minimum amount of transverse reinforcement is necessary to control the growth of shear diagonal cracking. Based on this equation, there are two cases of analysis as described below.

3.2.2 Shear Resistance

The section nominal shear capacity is determined as the summation of concrete shear contribution and transverse steel shear contribution. Concrete shear contribution is a function in the effective shear area (b_v*d_v), concrete strength, and (β), which indicates the ability of the diagonally-cracked concrete to transmit shear along its axis. Transverse steel shear contribution depends on the transverse steel yielding strength, area of transverse steel, the angle of cracking (θ), and the angle of inclination of transverse reinforcement to the longitudinal axis (α).

$$V_n = V_c + V_s \qquad \text{(AASHTO, 2014)} \textbf{ Equation 3.2}$$

In which

$$V_c = .0316\beta\sqrt{f_c'}\,b_v d_v \ \ (V_c = \beta\sqrt{f_c'}\,b_v d_v) \qquad \text{(AASHTO, 2014)} \textbf{ Equation 3.3}$$

$$V_s = \frac{\pi}{2}\frac{A_v f_y d_v (cot\theta + cot\alpha)sin\alpha}{s} \qquad \text{(AASHTO, 2014)} \textbf{ Equation 3.4}$$

Where

V_c = concrete shear strength that relies on the tensile stresses in concrete in ksi (MPa)

V_s = steel shear strength that relies on the tensile stresses in transverse steel in ksi (MPa)

d_v = effective shear depth taken as the distance, measured perpendicular to the neutral axis, between the tensile resultant and compressive force due to flexure. It needs not be taken to be less than the greater of $0.9d_e$ or $0.72h$ in inches (mm); see Figure 3.1.

β = factor indicating ability of diagonally-cracked concrete to transmit tension and shear

θ = angle of inclination of diagonal compressive stresses (˚)

α = angle of inclination of transverse reinforcement to longitudinal axis (˚); see Figure 3.2.
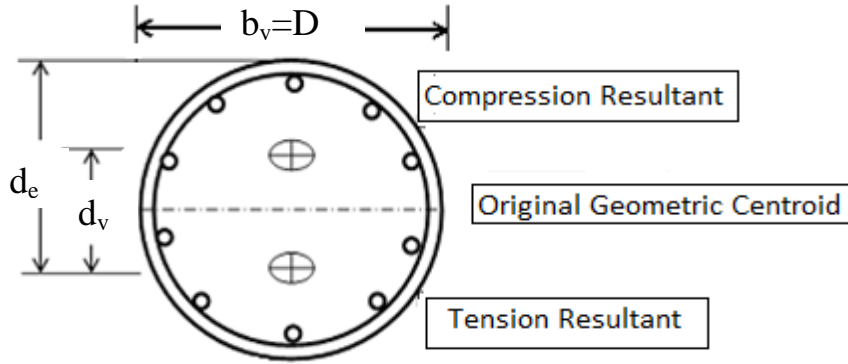
Figure 3.1: Illustration of b_v and d_v Parameters
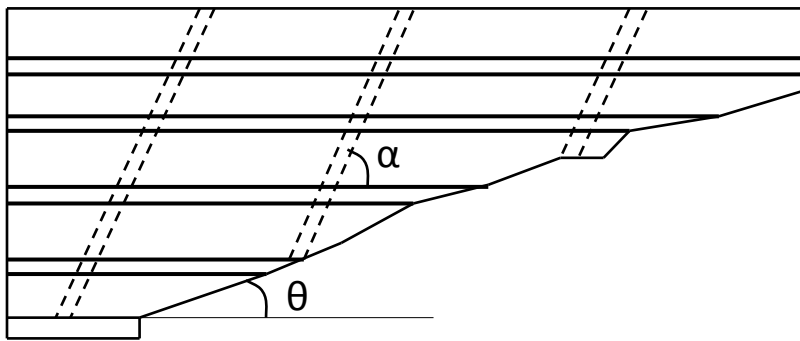
Figure 3.2: Illustration of Angle (θ) and Angle (α)

3.2.3 Determination of β and θ

In the case that the transverse steel is more than the minimum transverse steel required by AASHTO (2014) LRFD Bridge Construction Specifications (see Equation 3.1), β and θ are calculated based on the longitudinal axial strain at the centroid of tensile steel (εs). This is identified as Case 1 in this study:

$$\beta = \frac{4.8}{1+750\varepsilon_s} \quad (\beta = \frac{0.4}{1+750\varepsilon_s}) \qquad \text{(AASHTO, 2014)} \textbf{ Equation 3.5}$$

$$\theta = 29(degree) + 3500\varepsilon_s \ \leq 75° \qquad \text{(AASHTO, 2014)} \textbf{ Equation 3.6}$$

Note that Equation 3.5 is for the kip-in. units (SI units) system.

In the case that the transverse steel is less than the minimum transverse steel required by AASHTO (2014) LRFD specifications (see Equation 3.1), β and θ are calculated based on the longitudinal axial strain at the centroid of tensile steel (ε_s) and crack spacing parameter (s_{xe}). This is identified as Case 2 in this study:

$$\beta = \frac{4.8}{1+750\varepsilon_s}\frac{51}{39+s_{xe}} \quad (\beta = \frac{0.4}{1+750\varepsilon_s}\frac{1300}{1000+s_{xe}}) \qquad \text{(AASHTO, 2014)} \textbf{ Equation 3.7}$$

$$\theta = (29(degree) + 3500\varepsilon_s) \qquad \text{(AASHTO, 2014)} \textbf{ Equation 3.8}$$

$$s_{xe} = s_x\frac{1.38}{a_g+0.63} \quad (s_{xe} = s_x\frac{35}{a_g+16}) \geq 12\ in \qquad \text{(AASHTO, 2014)} \textbf{ Equation 3.9}$$

s_x = the lesser of d_v or the vertical distance between horizontal layers of longitudinal crack control reinforcement in inches (mm)

a_g = maximum aggregate size in inches (mm); has to equal zero when $f'_c \geq 10\ ksi\ (69\ MPa)$

Note that Equations 3.7 and 3.9 are for the kip-in. units (SI units) system.

If the section has transverse steel less than the minimum transverse steel defined by AASHTO (2014) LRFD Specifications (Case 2), the specification allows for checking the shear contribution due to aggregate size (1.38/(ag+0.63)) and longitudinal steel (S_x). However, if there is enough longitudinal steel and the aggregate size is efficient, (S_{xe}) must not be less than 12 inches so the factor $\left(\frac{51}{39+s_{xe}}\right) \leq 1$.

3.2.4 Calculation of Longitudinal Axial Strain (ε_s)

Longitudinal axial strain (ε_s) is calculated based on the superimposed effect of the forces in the tension side of the section, as follows (see Figure 3.3):

$$\varepsilon_s = \frac{\frac{|M|}{d_v}+0.5N+V}{A_sE_s} \qquad \text{(AASHTO, 2014)} \textbf{ Equation 3.10}$$

ε_s must not exceed 0.006 to maintain a reasonable crack widening.

If the value of (ε_s) computed from this case is negative, which means the section is under compression, the concrete rigidity is added to the denominator:

$$\varepsilon_s = \frac{\frac{|M|}{dv} + 0.5N + V}{(A_s E_s + A_c E_c)}$$ (AASHTO, 2014) **Equation 3.11**

Where

M = moment in k.in (N.mm)

V = shear force in kip (Newton)

N = axial force, taken as positive if tensile and negative if compressive in kip (Newton)

A_s = area of non-prestressed steel on the flexural tension side of the section in in^2 (mm^2). This is considered to be the area of flexural reinforcement under the original geometric centroid of the section.

A_c = area of concrete on the flexural tension side of the section in in^2 (mm^2). This is considered to be the area of concrete below the original geometric centroid of the section.

E_s = modulus of elasticity of steel in ksi (MPa).

E_c = modulus of elasticity of concrete in ksi (MPa).

This procedure assumes a constant distribution of shear stress over an area of depth d_v and width b_v. That means the direction of principal compressive stresses doesn't change over the depth, and also that shear stresses could be computed from any point of this area.

Sections containing at least the minimum transverse steel have the capacity to redistribute shear stresses uniformly over the section (Case 1). Sections containing less than the minimum transverse steel have less capacity to redistribute shear stresses uniformly over the section (Case 2). That is why the crack axial parameter (S_{xe}) and the maximum aggregate size (a_g) are included for further calculations.

$$\varepsilon_s = \frac{M_u/d_v}{E_s A_s}$$

Moment

$$\varepsilon_s = \frac{V_u}{E_s A_s}$$

Shear force

$$\varepsilon_s = \frac{0.5 N_u}{E_s A_s}$$
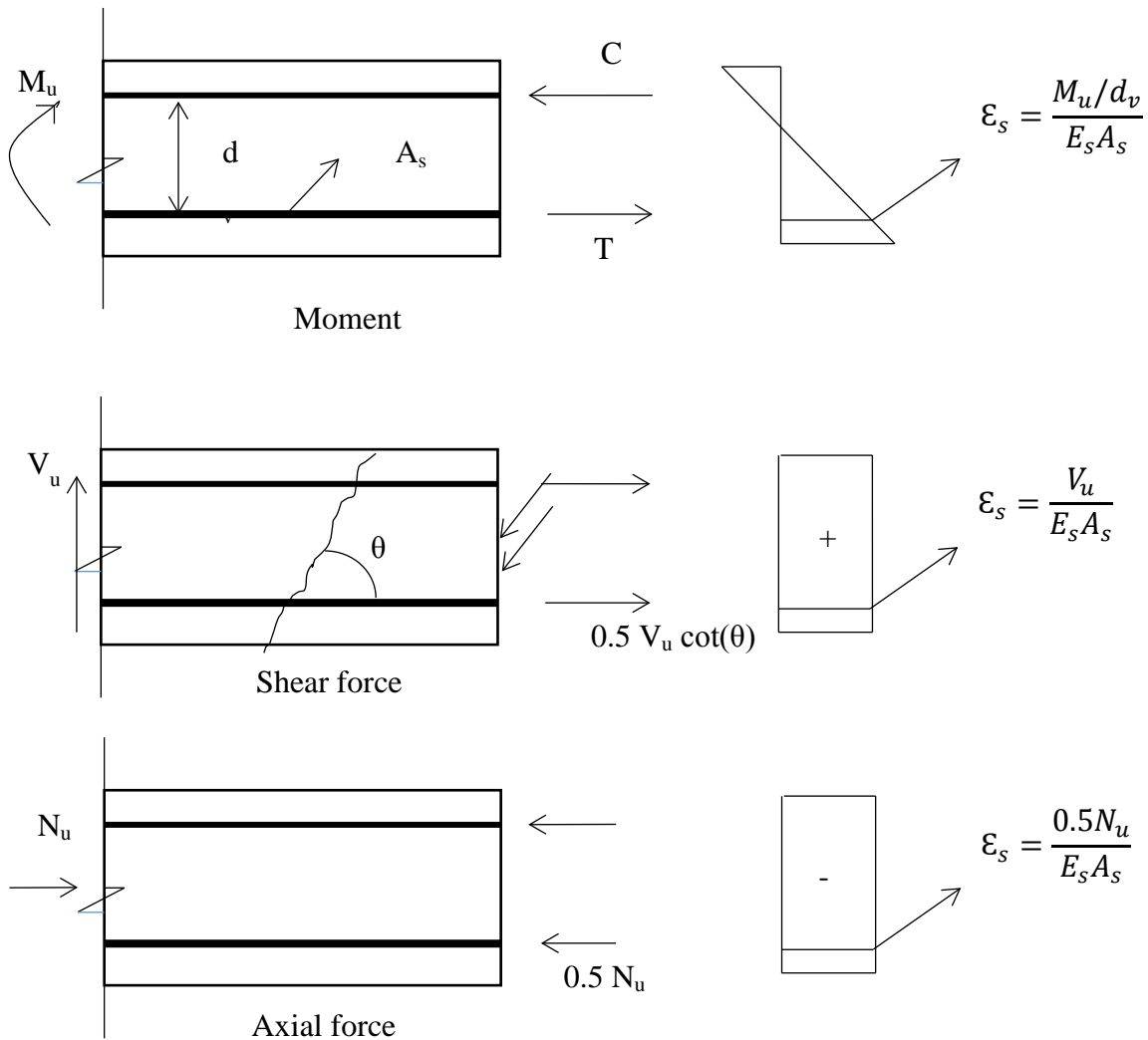
Axial force

Figure 3.3: Strain Superimposition Due to Moment, Shear, and Axial Force

3.2.5 Angle of Inclination of Transverse Reinforcement to Longitudinal Axis (α) Calculations

In order to calculate the angle of inclination (α) of transverse spiral reinforcement with respect to the longitudinal axis, the normalized tangent vector of Helix/Spiral equation is calculated. By computing the dot product of the unit tangent vector and the unit vector in the axial direction, the angle of inclination of the transverse spiral reinforcement is determined.

A circular helix of radius ($D_r/2$; core radius) and pitch/spacing (s) is described by the following parameterization, see Figure 3.4 for helix 3D plotting:

$$x(g) = \frac{D_r}{2}\cos(g)$$ **Equation 3.12**

$$y(g) = \frac{D_r}{2}\sin(g)$$ **Equation 3.13**

$$z(g) = \frac{s}{2\pi}g$$ **Equation 3.14**

Tangent vector $= <-\frac{D_r}{2}\sin(g), \frac{D_r}{2}\cos(g), \frac{s}{2\pi}>$

$||\text{Tangent vector}|| = \sqrt{\left(\frac{D_r}{2}\right)^2 + \left(\frac{s}{2\pi}\right)^2}$

Unit tangent vector $(t) = \frac{\text{Tangent vector}}{||\text{Tangent vector}||}$

Unit vector in the axial direction of the column $(k) = <0, 0, 1>$

The dot product of $<k>.<t> = \frac{s/2\pi}{\sqrt{\left(\frac{D_r}{2}\right)^2 + \left(\frac{s}{2\pi}\right)^2}} = 1 * 1 * \cos\alpha.$

In the case that the section contains transverse reinforcement of hoops, the angle of inclination of transverse steel to the axial direction (α) is 90°. For sections that contain spiral transverse reinforcement:

$$\alpha = \cos^{-1}\left(\frac{s/2\pi}{\sqrt{\left(\frac{D_r}{2}\right)^2 + \left(\frac{s}{2\pi}\right)^2}}\right)$$

3.2.6 Effective Number of Legs of Transverse Steel in Shear Resistance Calculation

Most design codes assume two legs of transverse steel are resisting the shear force, taking $A_v=2A_h$ for circular and rectangular sections. However, a new value for the effective number of legs in circular sections has been defined based on a 45° angle of diagonal cracking (Ang et al., 1989). The new assigned value equals to ($\pi/2$) as an average integrated value along a 45° crack, see Figure 3.5 for the geometrical details.
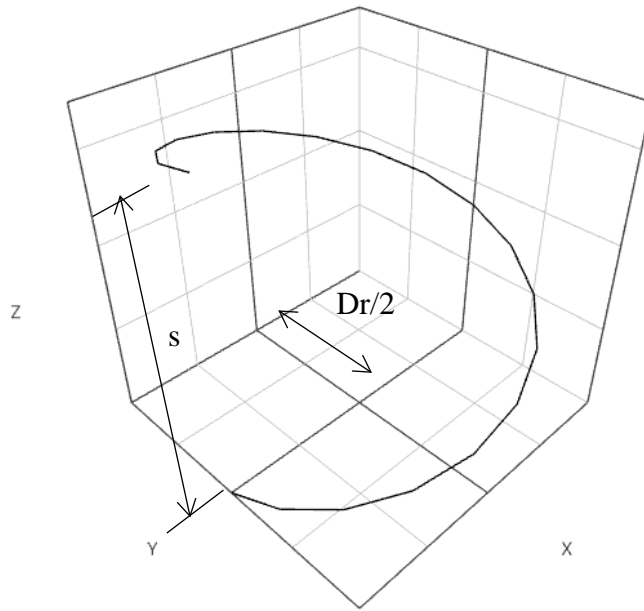
Figure 3.4: Helix/Spiral 3D Plot
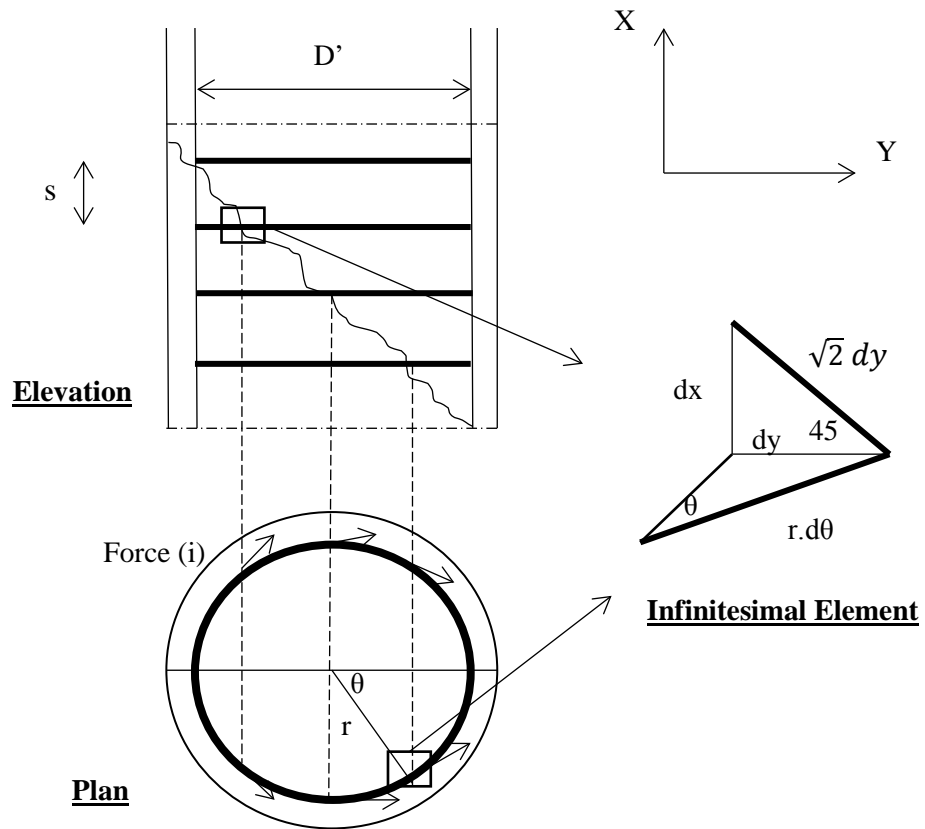
Figure 3.5: Shear Carried by Transverse Steel in Circular Column

The average total force in the transverse steel over the crack length is the summation of each hoop force divided by the length of the crack ($\sqrt{2}\,D'$)—in other words, it is the integration of the forces over the length of the crack.

$$V_s = \frac{\int_0^{D'} Forces(i).\sqrt{2}\,dy}{\sqrt{2}\,D'}$$ **Equation 3.15**

Where

Vs = transverse steel shear resistance.

Force (i) = the transverse steel force in the hoop at the crack location, see Figure 3.5.

In each single hoop, the force in (Y) direction is calculated as follows:

$$Force(i) = 2A_{sh}f_y\sin(\theta)$$ **Equation 3.16**

Where

A_{sh} = transverse steel single hoop area

Substitute in Equation 3.15,

$$V_s = \frac{\int_0^{D'} 2A_{sh}f_y\sin(\theta).\sqrt{2}\,dy}{\sqrt{2}\,D'}$$ **Equation 3.17**

But from geometry,

$$dy = rd\theta\sin(\theta)$$ **Equation 3.18**

$$D' = 2r$$ **Equation 3.19**

Then,

$$V_s = 2\int_0^{\pi/2} 2A_{sh}f_y\sin^2(\theta).d\theta$$ **Equation 3.20**

$$V_s = 2\int_0^{\pi/2} 2A_{sh}f_y\frac{1-\cos(2\theta)}{2}\,d\theta$$ **Equation 3.21**

$$V_s = 2A_{sh}f_y\left[\frac{\theta}{2} - \frac{\sin2\theta}{2}\right]_0^{\pi/2}$$ **Equation 3.22**

$$V_s = \frac{\pi}{2}A_{sh}f_y$$ **Equation 3.23**

Chapter 4: Implementation

4.1 Overview

      As a general guideline for our numerical solution approach, the mathematical procedure is based on finding the shear capacity of the section corresponding to a certain level of moment and axial force. By applying this procedure for the full range of moments under a constant axial force, we were able to develop a 2D moment-shear force interaction diagram under a specific axial force. The collection of all the 2D interaction diagrams yielded a 3D interaction diagram of a circular reinforced-concrete cross section.

4.2 Input Parameters

      In order to apply our numerical approach, a set of parameters needs to be pre-defined. These parameters could be classified into material properties, reinforcement, and geometry.

1. Material Properties: Yielding strength for longitudinal (f_y) and transverse bars (f_{yh}), concrete compressive strength (f'_c), and modulus of elasticity of steel (E_s) were defined as the material properties. Modulus of elasticity of concrete (E_c) was calculated based on the concrete compressive strength $E_c = 57\sqrt{f'c}$ ($E_c = 4700\sqrt{f'c}$), where f'_c is in psi (MPa) units and E_c is in ksi (MPa) units.

2. Reinforcement Properties: The reinforcement parameters are the number of longitudinal bars, cross section dimensions of longitudinal bars (diameter, area [A_s]), cross section dimensions of transverse bars (diameter, area [A_v]), the type of transverse reinforcement (hoop or spiral), and the transverse bar spacing (s).

3. Geometric Properties: Circular cross section diameter (d) and clear cover (cc) were the two direct geometrical parameters used in this analysis. Effective shear depth (d_v) and effective web width (b_v) are two indirect geometrical parameters needed to calculate steel and concrete shear capacities.

4.3 Effective Shear Area

In our case of reinforced-concrete circular sections, it was agreed to use the effective web width as the diameter of the circular section per the AASHTO (2014) requirements, although it is less conservative, as it increases the value of concrete shear capacity (V_c). It also seems to contradict the main definition of effective web width as the minimum web width of the section. However, according to the specifications, circular members typically have the longitudinal steel uniformly distributed around the perimeter of the section, and when the member cracks, the highest shear stresses occur near the mid-depth of the cross section. It is for this reason the effective web width was be taken by AASHTO to be the diameter. For the centroid location of the tensile force, the neutral axis of the cross section is assumed by AASHTO LRFD specifications to be always across the middle of the section at a depth equals d/2. This assumption was expected to decrease the moment capacity of the section, which is more conservative; see Figure 3.1.

4.3.1 Effective Shear Depth Calculation (d$_v$)

d_v = Max{0.72h,0.9d$_e$,d$_v$}

d_e = the distance from the upper compressive fiber to the resultant of tensile forces in inches (mm)

$$d_e = d/2 + d_r/\pi \qquad\qquad \text{(AASHTO, 2014) \textbf{Equation 4.1}}$$

d = diameter of section in inches (mm)

d_r = diameter of the circle passing through the centers of the longitudinal bars in inches (mm)

The second term in Equation 4.1 represents the geometric centroid of a semicircular ring.

d_v = distance between the compressive resultant point of action and the tensile resultant point of action in inches (mm). According to AASHTO (2014) specification (d$_v$) could be approximated as follows by assuming ALL the tensile steel to yield:

$$d_v = \frac{M}{A_s f_y} \qquad\qquad \text{(AASHTO, 2014) \textbf{Equation 4.2}}$$

4.4 Analysis Procedure

Under a constant axial compressive force (N), the moment-shear interaction diagram is determined by increasing the value of the moment from zero to the ultimate confined moment capacity corresponding to zero-shear, while solving for the total shear capacity under every moment step. The ultimate confined moment capacity at zero-shear and axial force (N) is readily available from the procedure developed earlier by Abd El-Fattah, Rasheed, and Esmaeily (2011). At a zero moment value, the shear capacity is estimated first based on a 45° angle of shear crack (cot θ=1) and a concrete strength based on ($\varepsilon_s = 0.00457$, β= 1.084). This shear capacity is then used along with the axial force (N) to determine (ε_s), based on Equation 3.10. The longitudinal strain at the centroid of tensile reinforcement (ε_s) is then used to compute θ and β based on Equations 3.6 and 3.10 or Equations 3.7, 3.8, and 3.9 for sections having less transverse steel than minimum transverse steel defined by AASHTO (2014) LRFD specifications, see Equation 3.1. The concrete and steel shear capacities are determined next using Equations 3.3 and 3.4, and totaled using Equation 3.2 to update the section shear strength (V). If that value is equal to the initially estimated shear capacity, then convergence is achieved. Otherwise, the updated shear capacity is used to reiterate until convergence of the newly updated shear capacity, see Figure 4.2. Once the new moment step is input, the shear capacity of the previous step, along with (N), is used to compute (ε_s), and iterations are resumed until the new shear capacity convergences. The interaction diagram is concluded when the moment step reaches the ultimate confined moment capacity corresponding to zero-shear, see Figure 4.1.
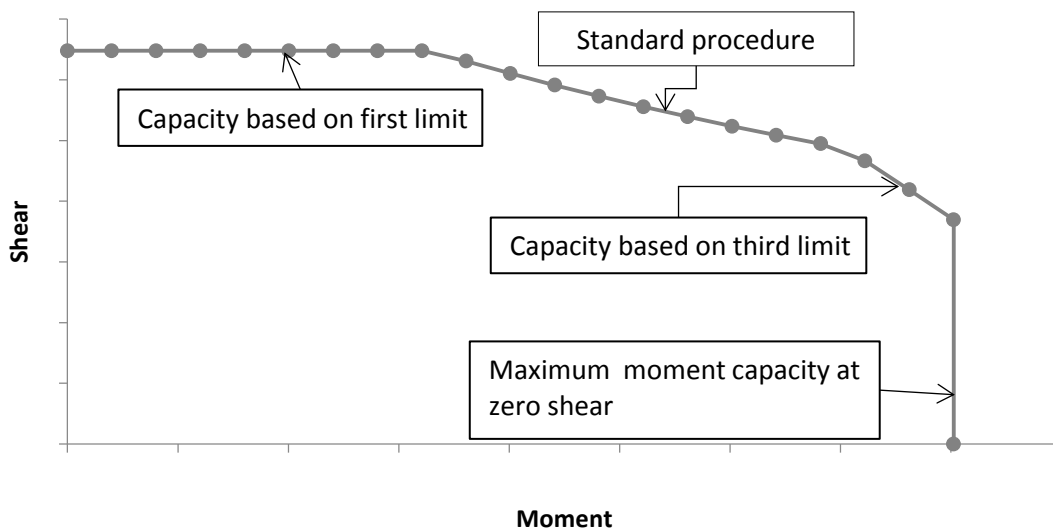

Figure 4.1: Moment-Shear Interaction Diagram Under a Constant Axial Compression Force
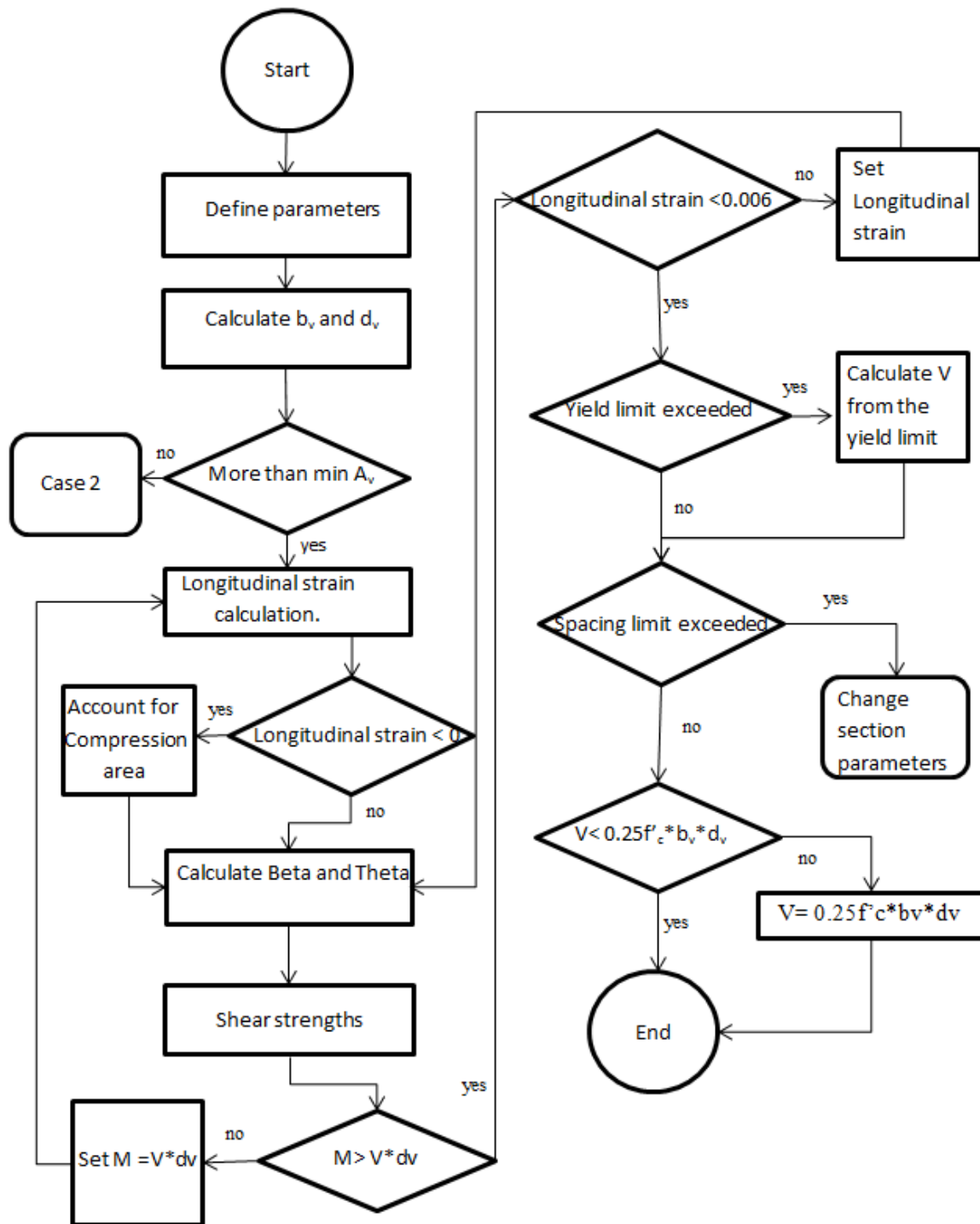
Figure 4.2: Flow Chart of Present Procedure (Case 1: Sections with More than Minimum Transverse Steel).

4.4.1 Limits of Constraints

The value of the shear capacity (V) should satisfy five other limits according to AASHTO (2014) LRFD Bridge Construction Specifications.

1. The first limit is $[M \geq V d_v]$. If this limit is not achieved at a moment step, the iteration should be repeated with an initial value of moment (M) equals to (V.d$_v$).

2. The second limit is $[\mathcal{E}_s \leq 0.006]$. If not, ($\mathcal{E}_s$) is set to 0.006, and the shear capacity (V) is directly calculated.

3. The third limit or the yield limit is $[A_s f_y \geq \frac{M}{d_v} + \frac{N}{2} + V \cot(\theta) - 0.5V_s \cot(\theta)]$. If not, the shear capacity value (V) should be reduced according to this limit.

4. The forth limit is the spacing limit; if $[v_u = \frac{V}{b_v d_v} < 0.125 f_c']$, then the max spacing equals $0.8 * dv \leq 24$ $in.$ (609.6 mm). And if $[v_u = \frac{V}{b_v d_v} \geq 0.125 f_c']$, then the max spacing equals $0.4 * dv \leq 12$ $in.$ (304.8 mm). If this limit is not achieved, the analysis is stopped, warning the user to decrease the spacing to satisfy this limit.

5. The fifth limit is $[V \leq 0.25 * f'c * dv * bv]$, otherwise the shear value is set to be $[V = 0.25 * f'c * dv * bv]$.

The first limit controls when the moment value approaches the point of zero moment (e.g. simple beam support). The specification assigned a moment value equal to V.d$_v$ over the length where moment is negligible. This limit causes a horizontal line at the top of shear-moment interaction diagram, see Figure 4.1. The second limit illustrates that the tensile strain of longitudinal steel on the tension side should not exceed an excessive value in order to keep cracks width within a reasonable value to effectively transmit tension along the member. The third limit formula could be derived from Figure 4.3 by taking the moment summation around point (o), and it aims to ensure that the force in the longitudinal steel is equal to or less than the maximum force that could be carried by the steel. The fourth limit is to minimize the diagonal shear crack width by having enough transverse steel within the spacing (s) to resist shear

stresses. The fifth limit was intended to ensure that the concrete strut will not crush before the transverse steel yields.
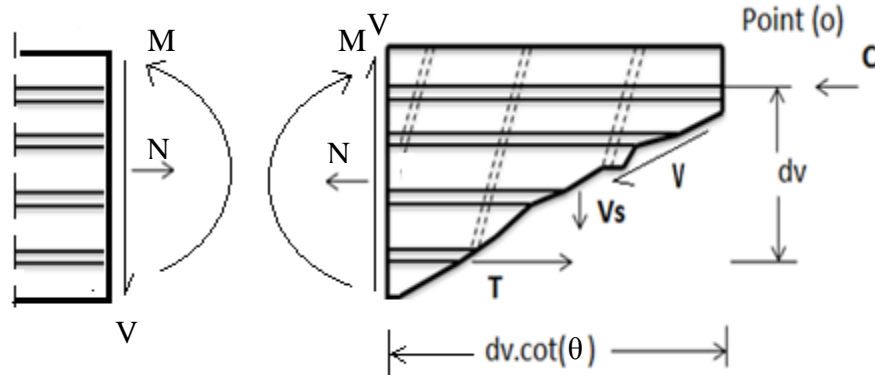
Figure 4.3: Derivation of the Yielding Stress Limit

There are two more conditions that cause the AASHTO (2014) LRFD specifications to consider the section invalid if one of them is met, and new section properties are then recommended.

The first condition is in the case of sections having less than the minimum transverse steel defined by AASHTO (2014) LRFD specifications, see Equation 3.1. If the section doesn't have enough longitudinal steel to control cracks along its diameter according to the following equation, the section is considered invalid:

$$A_{layer} = 0.003b_v s_x$$ **Equation 4.3**

Where (A_{layer}) is the area of longitudinal steel in each layer of reinforcement (in^2). More longitudinal bars or bigger bars are then recommended to control cracks.

The second condition is to make sure that there is a clear yielding zone in the steel stress-strain curve. Thus, the steel yielding strength should not exceed 100 ksi, see Figure 4.4. This value was verified for both prestressed and non-prestressed members for nonseismic applications (Shahrooz, Miller, Harries, & Russell, 2011).
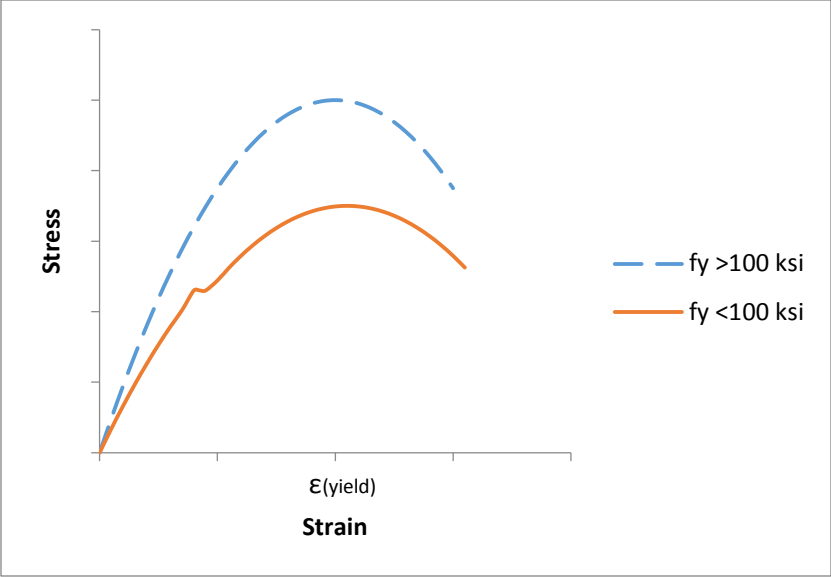
Figure 4.4: Yielding Zone for Different Yielding Strength

Chapter 5: Experimental Verification

5.1 Overview

The proposed formulations were verified against a large pool of experimental data performed by different researchers in different countries. In this section, a full database and the experimental parameters for the sections are presented in Tables 5.3 to 5.33. Full database comparisons against experimental studies and interaction diagrams are shown in Chapter 7. Randomly selected sections are discussed in detail with necessary comments in this chapter. A comparison against the experimental studies and another against Response 2000 were applied in this chapter to verify the accuracy of the proposed methods. Response 2000 is a structural tool that was developed based on AASHTO (1999) LRFD Bridge Construction Specifications and the MCFT, and it also predicts shear strength and moment-shear interaction diagrams at specific levels of axial loads.

5.2 Database Criteria

The database presented in this chapter represents a large different pool of experimental studies. However, the selected sections in this study had to match certain criteria defined by AASHTO (2014) LRFD Specifications and the research goals regarding loads, geometry, and materials. The first condition regarding loads is that the axial force applied on the section should be compressive force $N \leq 0 \: kips$ (assuming negative sign for compression); the interaction diagrams in this study were generated for the axial compression forces range. In terms of geometry, the transverse steel spacing must not exceed the maximum spacing defined by AASHTO LRFD Specifications, see Section 4.4.1. The last condition is that the steel yielding strength should not exceed 100 ksi in order to have a clear yielding zone.

5.3 Comparisons Against Experimental Studies

Fourteen different sections were randomly selected from the database to be discussed in this chapter (see Table 5.1). Table 5.2 shows their material and geometrical properties. The table also shows the applied constant axial force, and moment and shear failure values. The ratio

(L$_a$/D) in the table is the ratio of the effective column length to its diameter, and it tends to relate the applied lateral force to the resulting moment according to the following relationship.

$$\frac{M}{VD} = \frac{L_a}{D}$$

Equation 5.1

Where (M) is the moment at the base of the cantilever, (V) is the applied shear force, (D) is column diameter, and (L) is the effective length of the column.

In case of a cantilever column, the effective length is the full length of the column.

Table 5.1: Selected Sections

No.	Reference	Unit
1	Arakawa, He, Arai, and Mizoguchi (1987)	No.16
2	Ang, Priestley, and Paulay (1985)	UNIT21
3	Roeder, Graff, Soderstrom, and Yoo (2001)	C1
4	Ranf, Eberhard, and Stanton (2006)	SpecimenC2
5	Zahn, Park, and Priestley (1986)	No.5
6	Pontangaroa, Priestley, and Park (1979)	Unit4
7	Nelson (2000)	Col4
8	Lehman and Moehle (2000)	No.430
9	Kunnath, El-Bahy, Taylor, and Stone (1997)	A8
10	Moyer and Kowalsky (2003)	Unit1
11	Siryo (1975)	BRI-No.3-ws22bs
12	Henry and Mahin (1999)	No.415s
13	Hamilton, Pardoen, and Kazanjy (2002)	UC3
14	Saatcioglu and Baingo (1999)	RC9

Table 5.2: Selected Sections Properties

Unit	D (in.)	Clear cover (in.)	La/D	Number of bars	Longitudinal bar diameter (in.)	fy (ksi)	Transverse bar diameter (in.)	fyt (ksi)	Spacing (in.)	f'c (ksi)	Axial force (kip)	Shear force (kip)	Moment (k.ft)
No.16	10.83	0.67	1.64	12	0.63	52.64	0.24	55.25	1.38	4.54	0	39.77	58.84
UNIT21	15.75	0.59	2	20	0.63	63.22	0.24	47.27	3.15	4.82	0	60.8	159.6
C1	16.5	2	4.7	8	0.87	62.28	0.37	59.99	2	8.79	0	26.59	171.73
SpecimenC2	20	0.57	3	10	0.62	65.98	0.18	60.03	4	8.27	259.57	62.06	310.3
No.5	15.75	0.51	4	16	0.63	48.87	0.39	67.57	5.31	4.67	124.76	32	168
Unit4	23.62	0.79	2	16	0.94	43.94	0.39	61.34	2.76	4.78	850.87	175.54	691.19
Col4	20	0.75	3	10	0.63	65.98	0.18	65.98	4.02	7.65	256.05	59.64	298.2
No.430	24	0.75	4	44	0.63	67	0.25	87.99	1.25	4.5	146.99	107.9	863.2
A8	12.01	0.49	4.5	21	0.37	64.96	0.16	62.93	0.75	4.76	49.91	16.42	73.91
Unit_1	18	0.31	5.34	12	0.75	81.99	0.37	62.99	3	4.75	52	34.86	278.88
BRI-No.3-ws22bs	9.84	1.38	2.01	8	0.37	54.38	0.23	53.07	2.48	4.59	72.39	23.08	37.85
No.415s	24	0.75	4	22	0.63	67	0.25	87.99	2.5	5.4	147.02	64.8	518.4
UC3	16	0.5	5.7	12	0.5	66.49	0.18	100.27	1.25	5.17	0	23.83	144.89
RC9	9.84	0.32	6.59	8	0.63	60.76	0.44	60.9	1.97	13.05	415.88	21.58	116.34

<u>Arakawa, He, Arai, and Mizoguchi (1987) No.16</u>
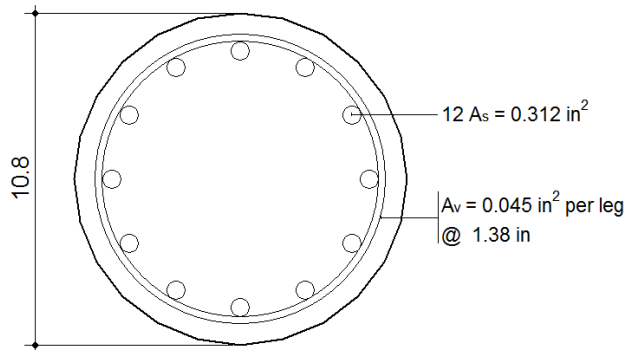
Figure 5.1: Arakawa et al. (1987) No.16 Cross Section
Note:
f_y = 52.64 ksi
f_{yt} = 55.24 ksi
f'_c = 4.54 ksi
Axial force = 0 kips
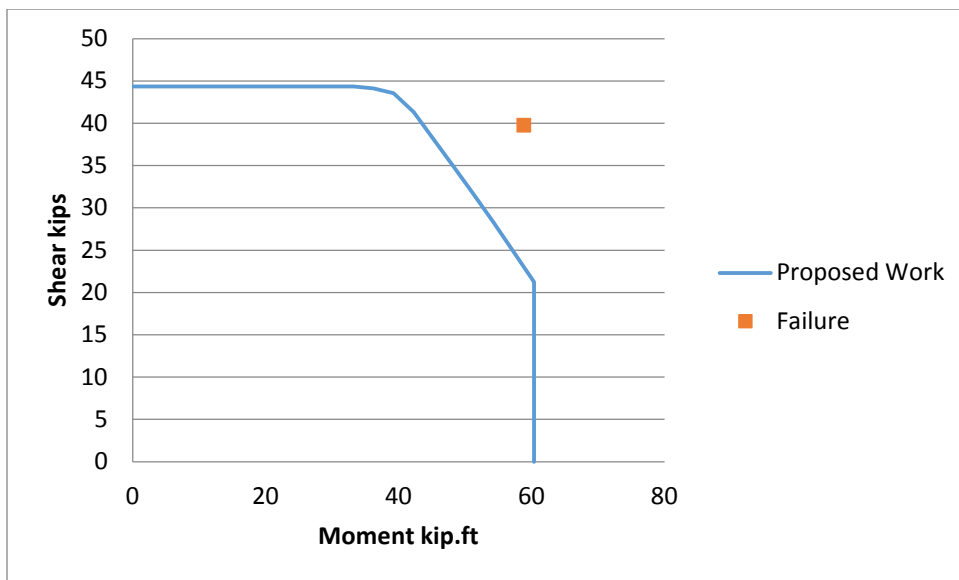
Figure 5.2: Arakawa et al. (1987) No.16 Interaction Diagram

This column was tested by Arakawa et al. (1987) with no applied axial force. The section failed due to moment-shear effect close to the inclined zone of the interaction diagram. The proposed interaction diagram is conservative and fairly accurate comparing to the failure point.

41

Ang et al. (1985) UNIT21
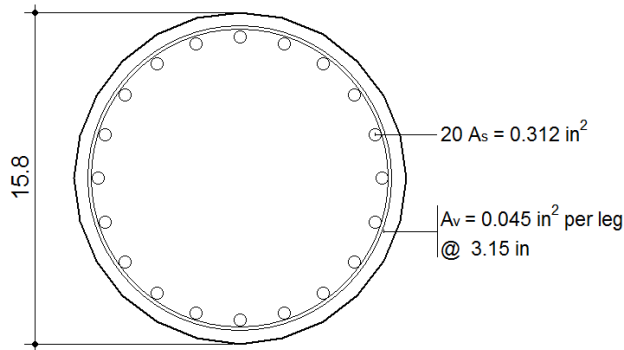
Figure 5.3: Ang et al. (1985) UNIT21 Cross Section

Note:

f_y = 63.22 ksi

f_{yt} = 47.27 ksi

f'_c = 4.82 ksi

Axial force = 0 kips
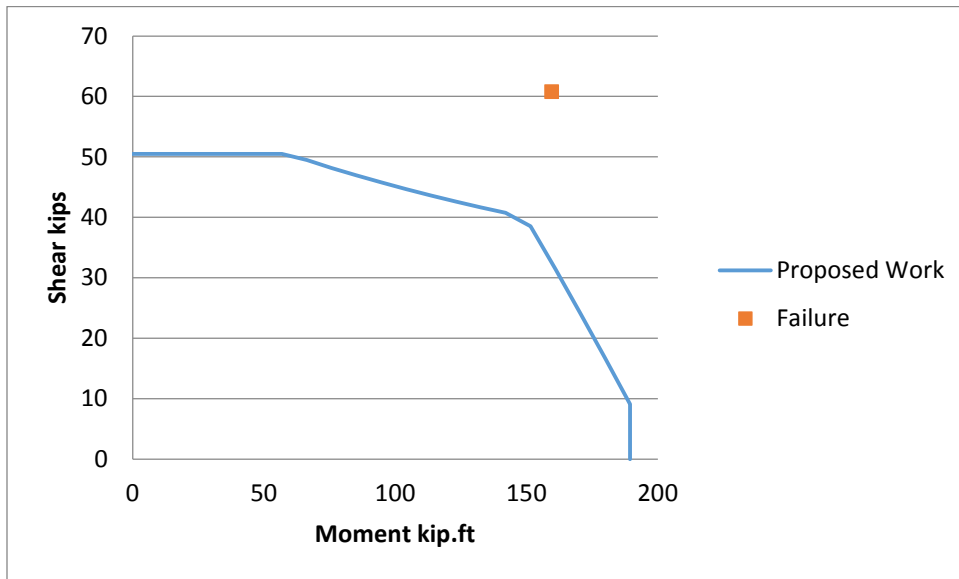
Figure 5.4: Ang et al. (1985) UNIT21 Interaction Diagram

This column was tested with no axial force. Although the transverse steel in this specimen was distributed over a larger spacing than the previous section with the same area, the larger diameter of the section managed to maintain a slightly higher pure shear value. The proposed interaction diagram in this case shows more conservativism than the previous section. This section also failed in moment-shear effect zone.

Roeder, Graff, Soderstrom, and Yoo (2001) C1
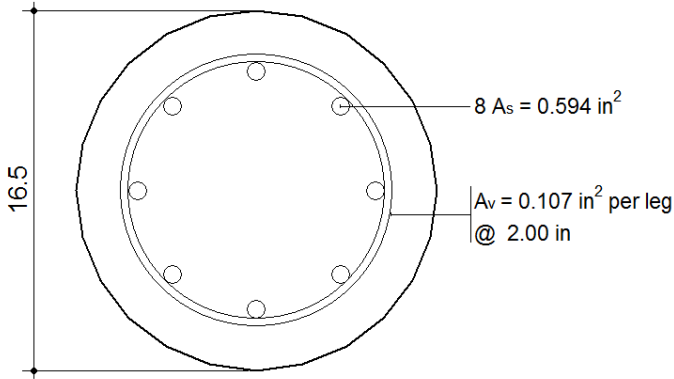
Figure 5.5: Roeder et al. (2001) C1 Cross Section
Note:
f_y = 62.88 ksi
f_{yt} = 59.99 ksi
f'_c = 8.79 ksi
Axial force = 0 kips
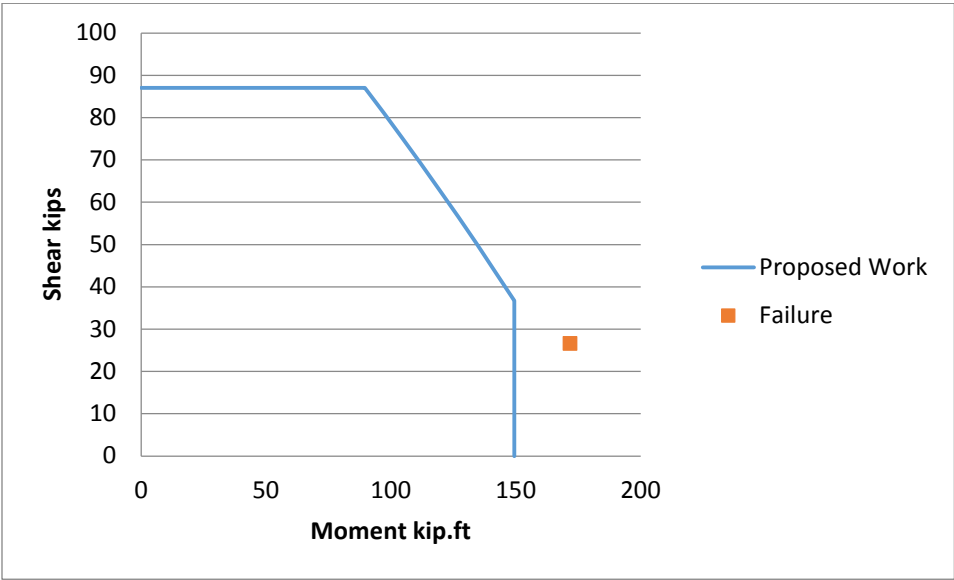
Figure 5.6: Roeder et al. (2001) C1 Interaction Diagram

The failure in this case is different than the previous cases. The section failed in the flexure zone close to the vertical curve which represents the ultimate confined flexure capacity. It is important to notice that, from the previous charts, the section diameter is one of the main keys to determine the shear capacity of the section.

43

Ranf, Eberhard, and Stanton (2006) SpecimenC2
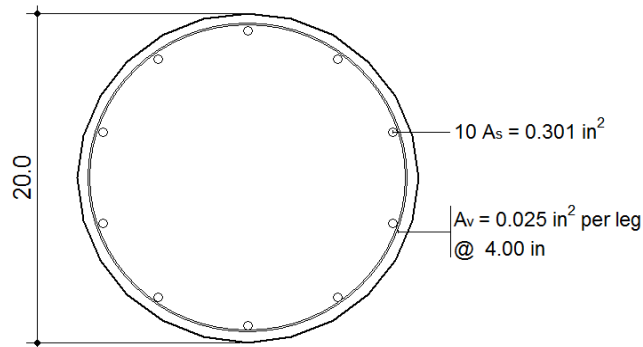
Figure 5.7: Ranf et al. (2006) SpecimenC2 Cross Section
Note:
f_y = 62.98 ksi
f_{yt} = 60.03 ksi
f'_c = 8.27 ksi
Axial force = 259.57 kips
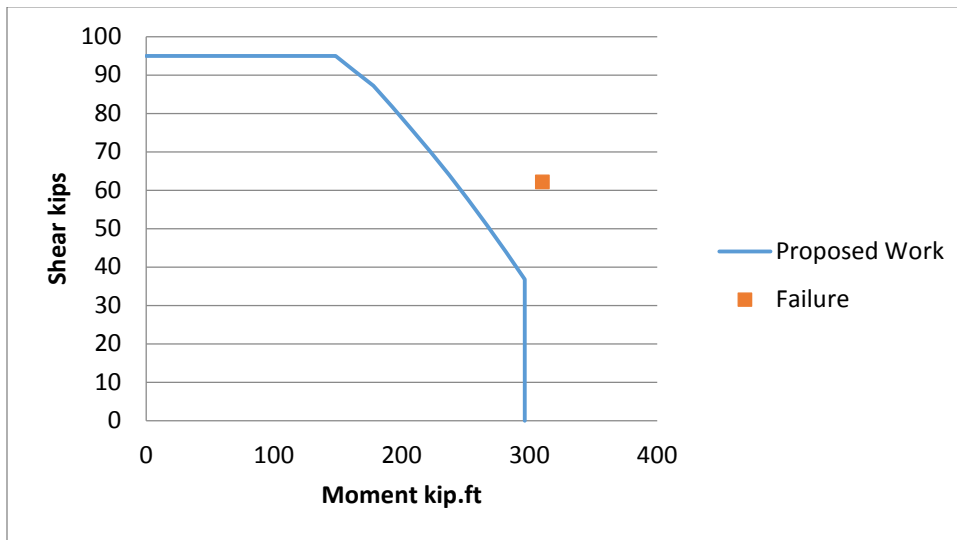
Figure 5.8: Ranf et al. (2006) SpecimenC2 Interaction Diagram

This section was tested under a constant axial force of 259.57 kips. This section has smaller transverse steel area and a larger spacing than the previous section, yet it managed to reach a slightly larger value due to the presence of the constant axial force and the larger diameter. From this chart it is important to establish a relationship between the shear force value and the axial force. The proposed interaction diagram was fairly accurate and conservative against the failure point.
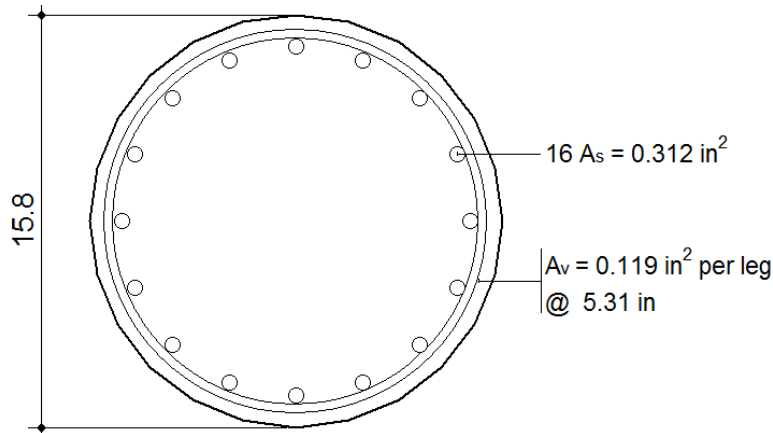
Figure 5.9: Zahn et al. (1986) No.5 Cross Section
Note:
f_y = 48.87 ksi
f_{yt} = 67.57 ksi
f'_c = 4.67 ksi
Axial force = 124.76 kips
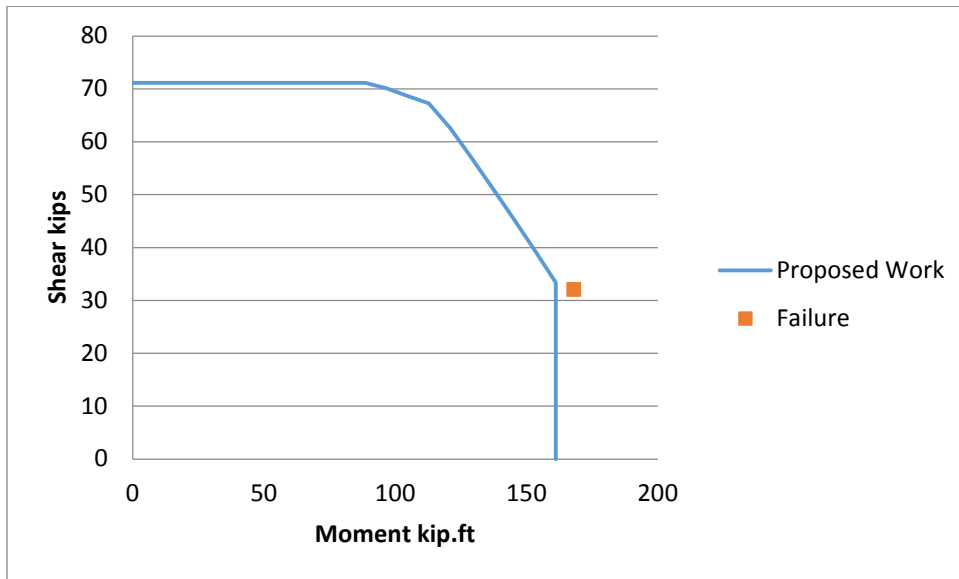
Figure 5.10: Zahn et al. (1986) No.5 Interaction Diagram

A constant axial force of 124.76 kips was applied on this section while testing against lateral displacement. The failure happened due to flexural effect as the failure point was located in the flexure zone. The proposed work showed a high accuracy against the failure point.
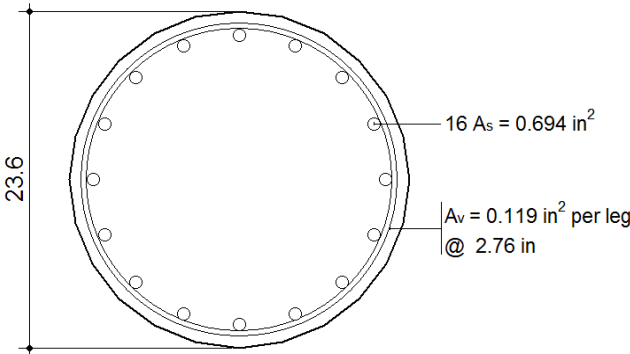
Figure 5.11: Pontangaroa et al. (1979) Unit4 Cross Section

Note:

f_y = 43.94 ksi

f_{yt} = 61.34 ksi

f'_c = 4.78 ksi

Axial force = 850.87 kips
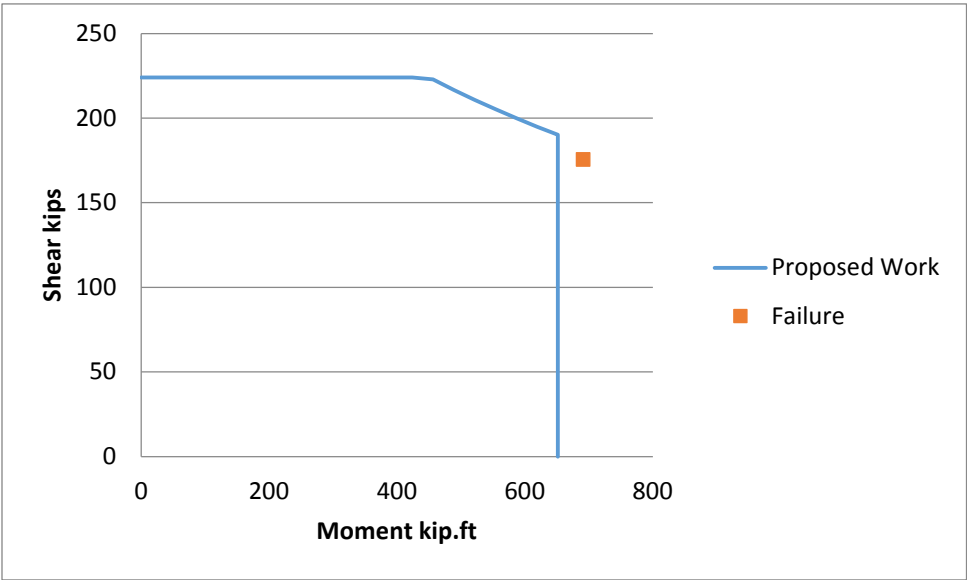
Figure 5.12: Pontangaroa et al. (1979) Unit4 Interaction Diagram

This section was tested under a relatively high constant axial force of 850.87 kips. A quick comparison between this section and the previous sections shows at least 135 kips difference in maximum shear value. This comparison presents the axial force as an important key to increase the shear capacity of the section.

Nelson (2000) Col4
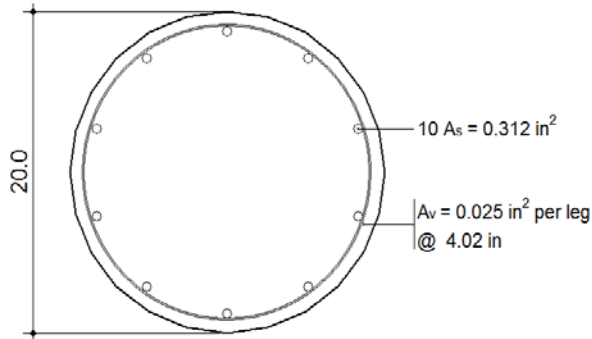
Figure 5.13: Nelson (2000) Col4 Cross Section
Note:
f_y = 65.98 ksi
f_{yt} = 65.98 ksi
f'_c = 7.65 ksi
Axial force = 256.05 kips
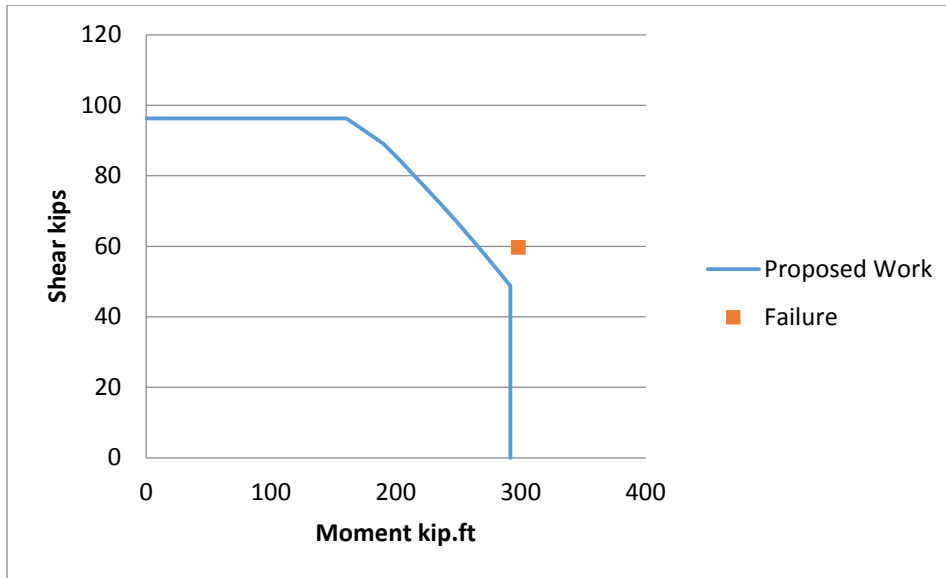
Figure 5.14: Nelson (2000) Col4 Interaction Diagram

This section was tested under 256 kips constant axial force. The interaction diagram and the failure point are similar to Ranf et al. (2006) SpecimenC2 due to the similarity in section properties and loading conditions. The proposed interaction diagram is accurate and conservative against the failure point.

Lehman and Moehle (2000) No.430
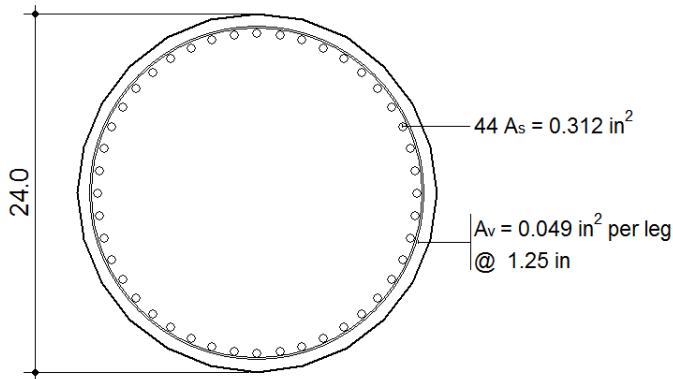
Figure 5.15: Lehman and Moehle (2000) No.430 Cross Section
Note:
$f_y = 67$ ksi
$f_{yt} = 88$ ksi
$f'_c = 4.5$ ksi
Axial force = 147 kips
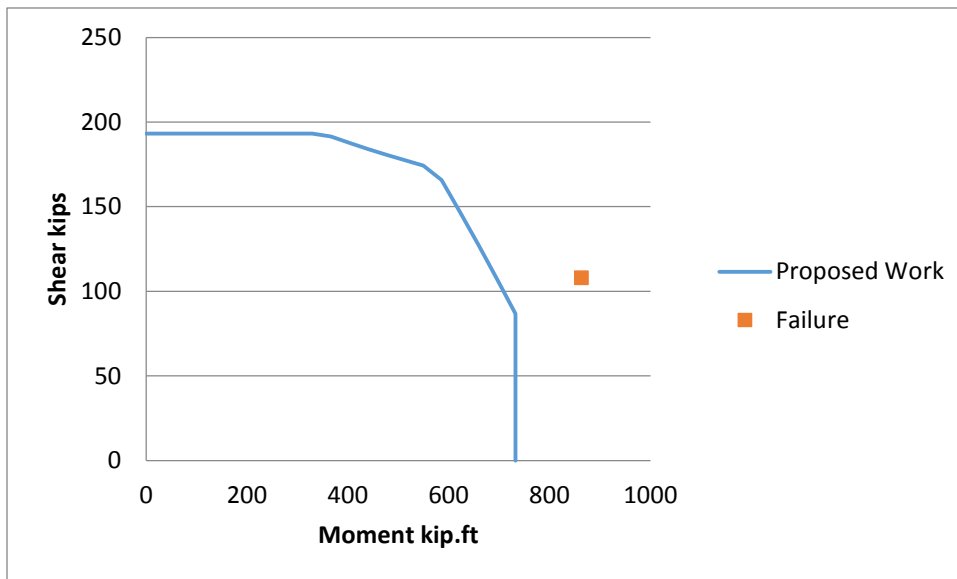
Figure 5.16: Lehman and Moehle (2000) No.430 Interaction Diagram

This section has a relatively high maximum shear value. Although this section was tested under only 147 kips, comparing to Pontangaroa et al. (1979) Unit4, the shear maximum value is almost 200 kips (Pontangaroa et al. Unit4 value is 225 kips) due to the smaller spacing and the higher transverse steel yielding strength.
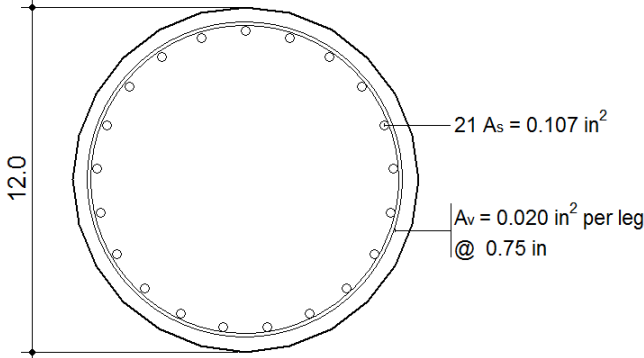
Figure 5.17: Kunnath et al. (1997) A8 Cross Section

Note:
f_y = 64.96 ksi
f_{yt} = 62.93 ksi
f'_c = 4.76 ksi
Axial force = 49.91 kips
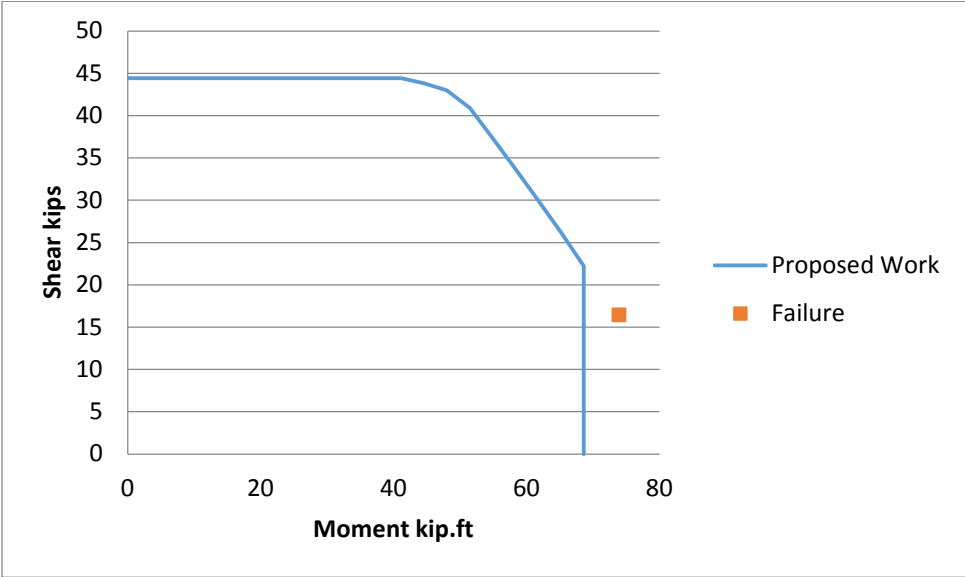
Figure 5.18: Kunnath et al. (1997) A8 Interaction Diagram

The section was tested under 49.9 kips axial force while exposed to lateral loads. It failed in the flexural zone of the interaction diagram. The predicted interaction diagram is also conservative and accurate against the failure point.

Moyer and Kowalsky (2003) Unit1
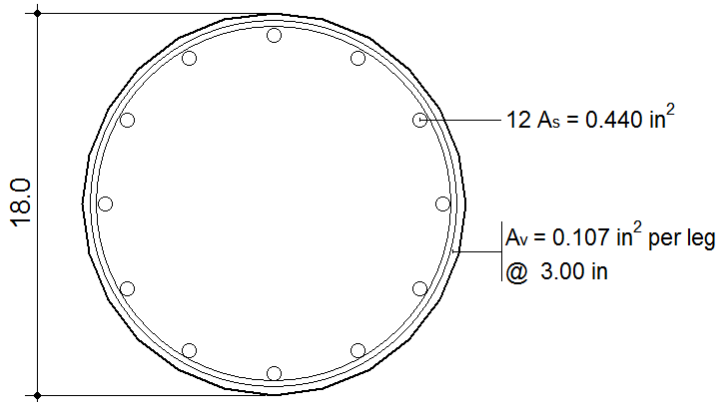
Figure 5.19: Moyer and Kowalsky (2003) Unit1 Cross Section
Note:
f_y = 82 ksi
f_{yt} = 62.99 ksi
f'_c = 4.75 ksi
Axial force = 52 kips
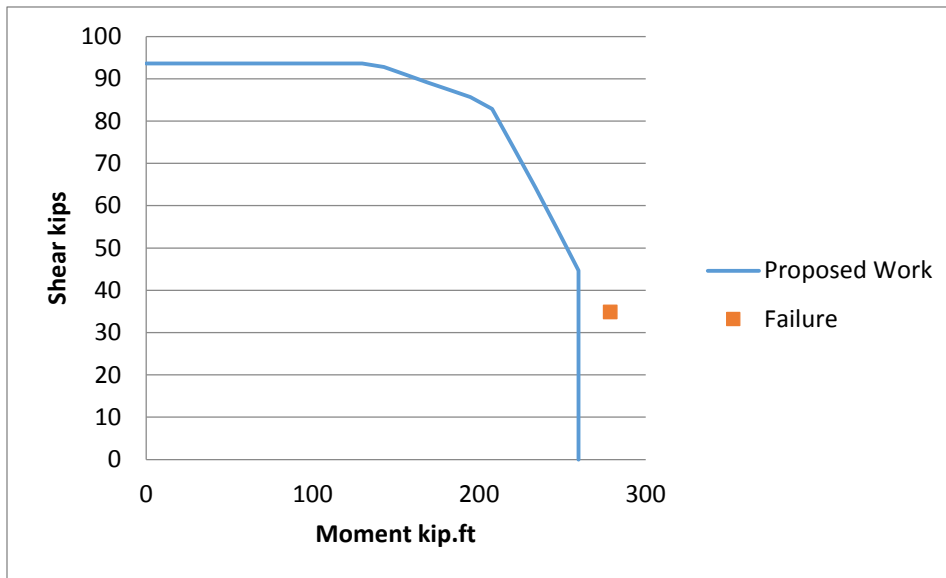
Figure 5.20: Moyer and Kowalsky (2003) Unit1 Interaction Diagram

Siryo (1975) BRI-No.3-ws22bs
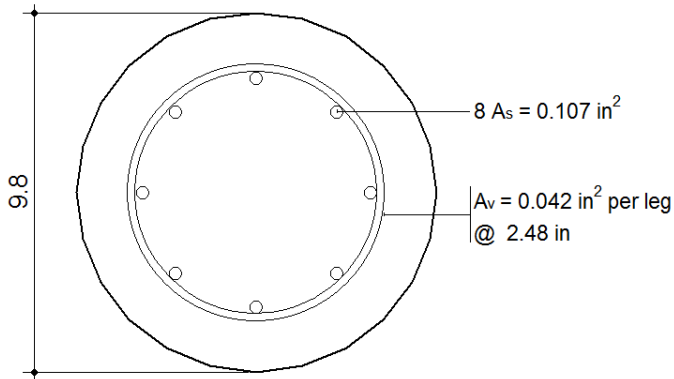
Figure 5.21: Siryo (1975) BRI-No.3-ws22bs Cross Section

Note:

f_y = 54.38 ksi

f_{yt} = 53.07 ksi

f'_c = 4.59 ksi

Axial force = 72.39 kips
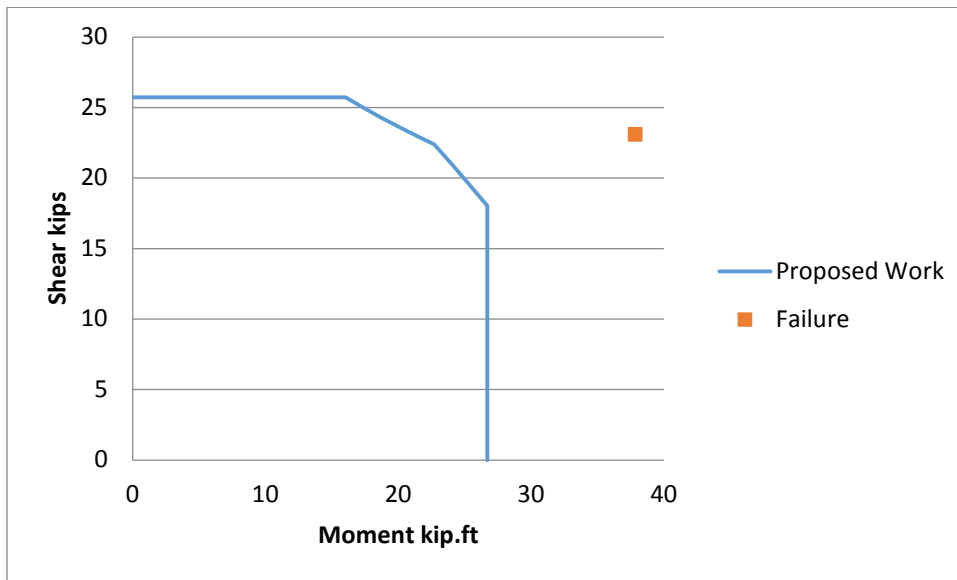
Figure 5.22: Siryo (1975) BRI-No.3-ws22bs Interaction Diagram
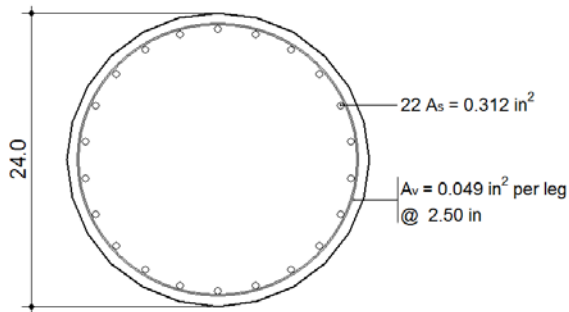
Figure 5.23: Henry and Mahin (1999) No.415s Cross Section

Note:

f_y = 67 ksi

f_{yt} = 88 ksi

f'_c = 5.4 ksi

Axial force = 147 kips
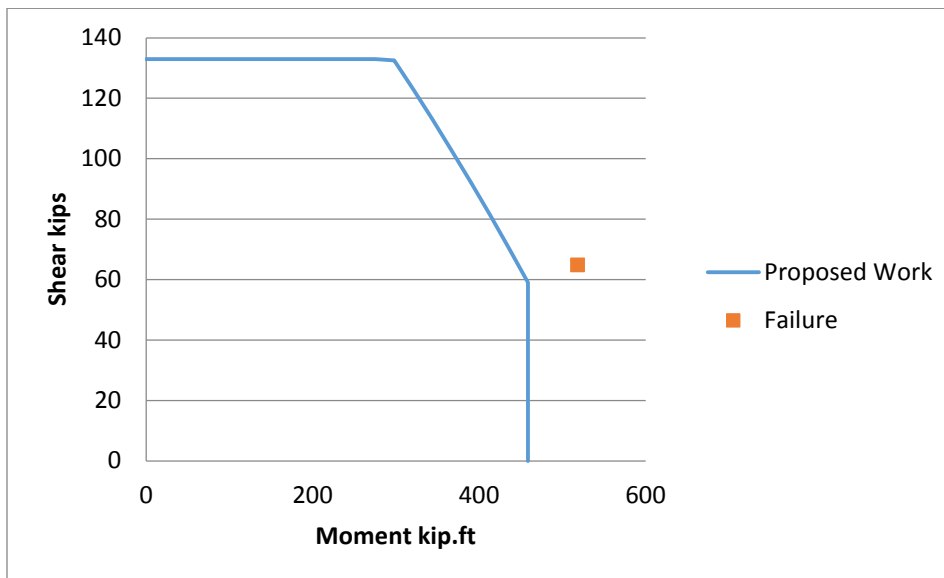
Figure 5.24: Henry and Mahin (1999) No.415s Interaction Diagram

This section was tested by Henry and Mahin (1999) under an axial force of 147 kips. Comparing this section to Lehman and Moehle (2000) No430 section, both sections have the same cross section diameter, transverse steel area, material properties, and axial load. However, the Lehman and Moehle section's maximum shear capacity was 75 kips more than the Henry and Mahin section's shear capacity because of the smaller spacing. Fifty percent smaller spacing, in

this example, provided around 30% increase in shear capacity. It is clear that spacing is one of the master keys to provide more shear strength to the section.

Hamilton, Pardoen, and Kazanjy (2002) UC3
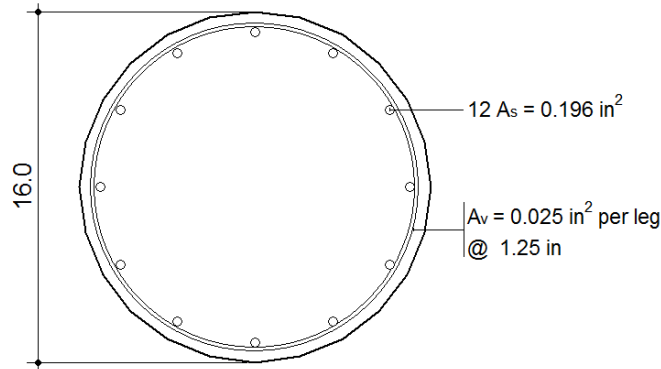
Figure 5.25: Hamilton et al. (2002) UC3 Cross Section
Note:
f_y = 66.5 ksi
f_{yt} = 100 ksi
f'_c = 5.17 ksi
Axial force = 0 kips
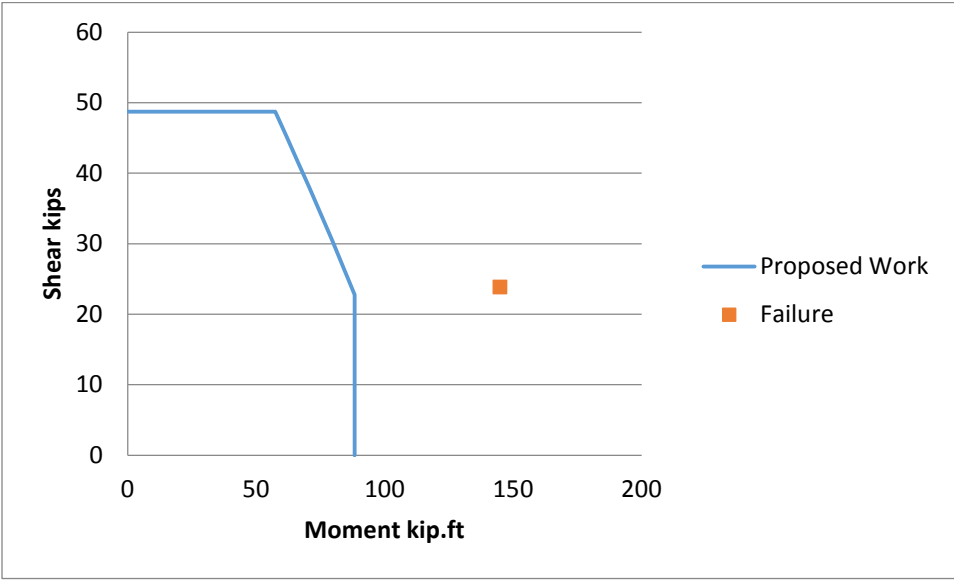
Figure 5.26: Hamilton et al. (2002) UC3 Interaction Diagram

Saatcioglu and Baingo (1999) RC9
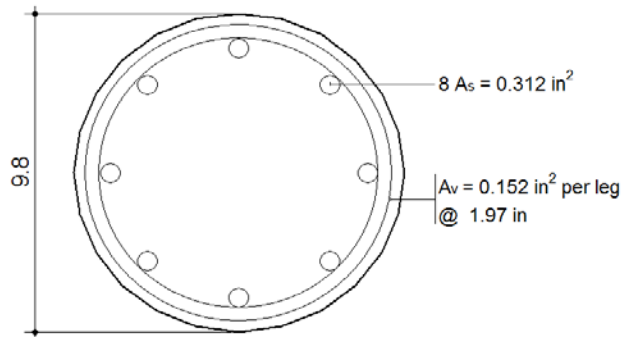
Figure 5.27: Saatcioglu and Baingo (1999) RC9 Cross Section
Note:
f_y = 60.76 ksi
f_{yt} = 60.9 ksi
f'_c = 13.05 ksi
Axial force = 415.88 kips
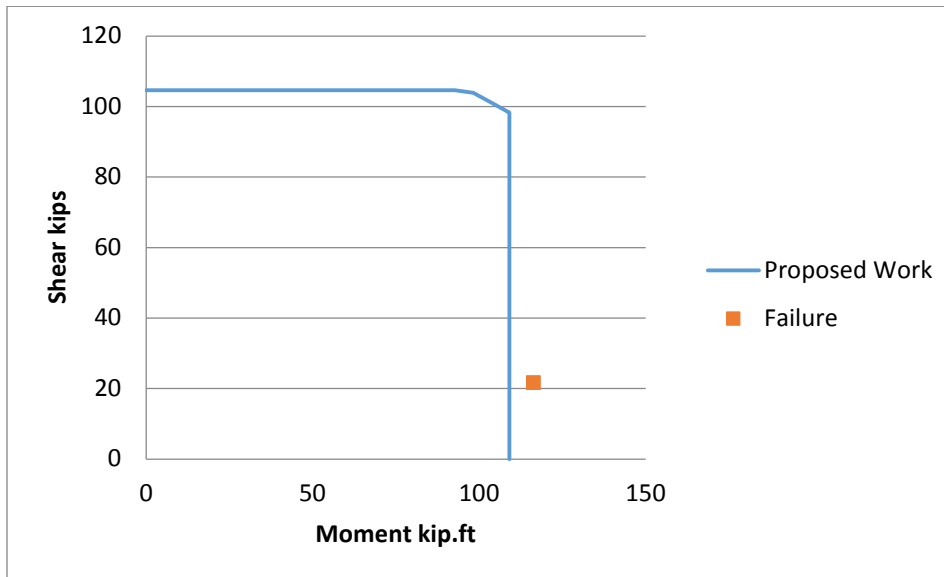
Figure 5.28: Saatcioglu and Baingo (1999) RC9 Interaction Diagram

The behavior of this interaction diagram shows the control of the limit ($V*d_v$) almost until the ultimate confined flexural capacity; this behavior indicates a high shear strength. Transverse steel area and applied axial force provide the section with a higher shear strength comparing to sections with similar properties.

54

5.4 Comparisons against Response-2000

Response 2000 is a tool developed by Professor Evan C. Bentz and made available as a freeware on the Internet. He was a key player in developing the SMCFT. This tool is based on the MCFT, and it predicts shear strength and moment-shear interaction diagrams at specific levels of axial loads. In this section, a comparison takes place between the interaction diagrams generated by Response-2000 for AASHTO (1999) based on the MCFT and the present formulation based on the equations of AASHTO (2014) using the SMCFT to examine the similarities and differences in moment-shear interaction diagrams of circular reinforced-concrete columns. Table 5.1 shows the properties of the selected cross sections examined in this chapter.

Ang et al. (1985) UNIT21
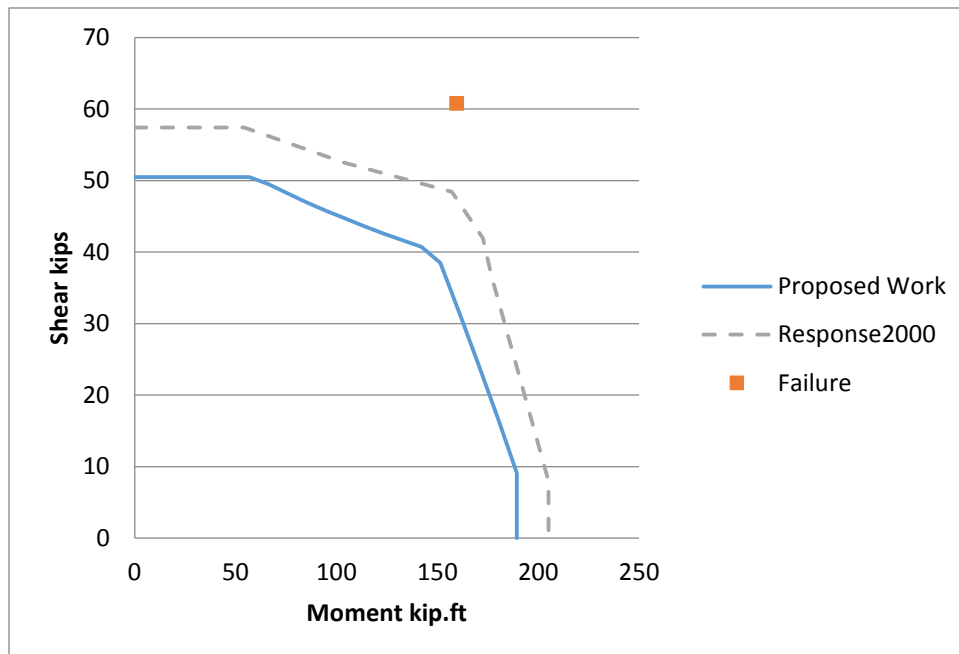
Figure 5.29: Ang et al. (1985) UNIT21 Proposed Interaction Diagram vs. Response 2000

Both predicted interaction diagrams are conservative, and Response 2000 showed a higher accuracy than the proposed work against the experimental failure point.

Roeder et al. (2001) C1
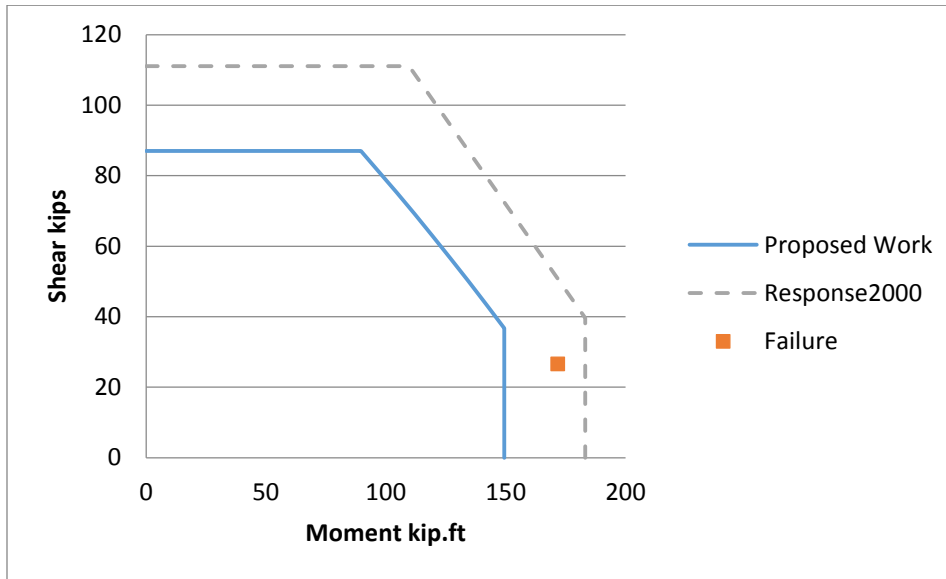
Figure 5.30: Roeder et al. (2001) C1 Proposed Interaction Diagram vs. Response 2000

In this case, the failure point locates between the two interaction diagrams. The proposed work is more accurate and conservative, while the Response 2000 interaction diagram is less accurate and less conservative.

Ranf et al. (2006) SpecimenC2
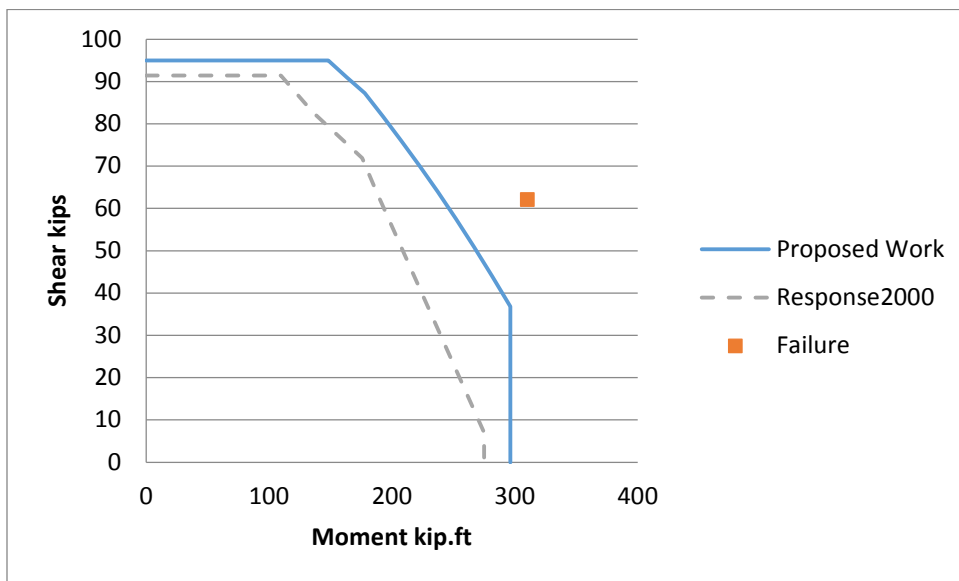
Figure 5.31: Ranf et al. (2006) SpecimenC2 Proposed Interaction Diagram vs. Response 2000

Both interaction diagrams are conservative. The proposed interaction diagram shows more accuracy than Response 2000 against the failure point.

Zahn et al. (1986) No.5
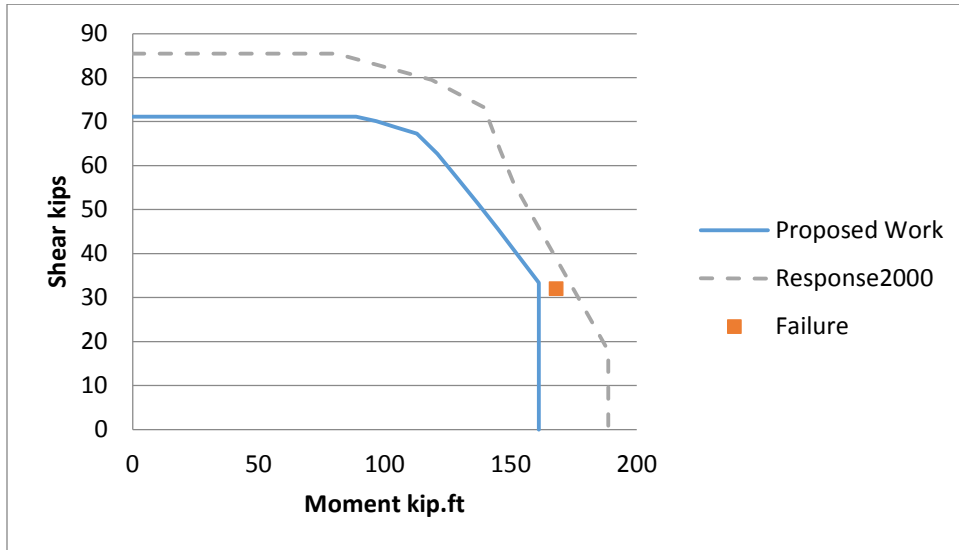
Figure 5.32: Zahn et al. (1986) No.5 Proposed Interaction Diagram vs. Response 2000

Response 2000 interaction diagram is not accurate and not conservative. The proposed interaction diagram shows a better agreement against the experimental point.

Pontangaroa et al. (1979) Unit4
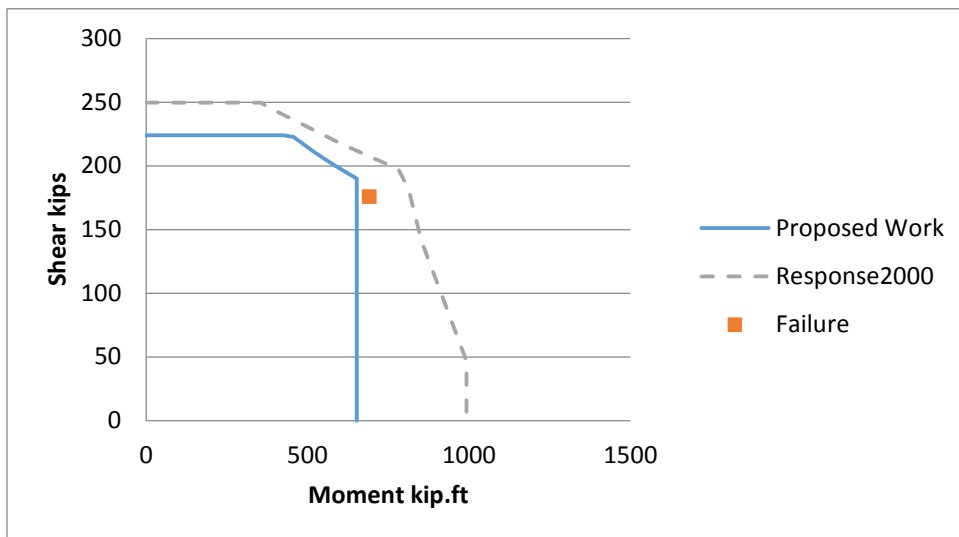
Figure 5.33: Pontangaroa et al. (1979) Unit4 Proposed Interaction Diagram vs. Response 2000

In this case, the pure moment calculations show a large difference between the two interaction diagrams. The failure point is located just outside the proposed interaction diagram. Response 2000 overestimated the moment capacity of the section, causing the failure point to locate inside its interaction diagram.

Nelson (2000) Col4
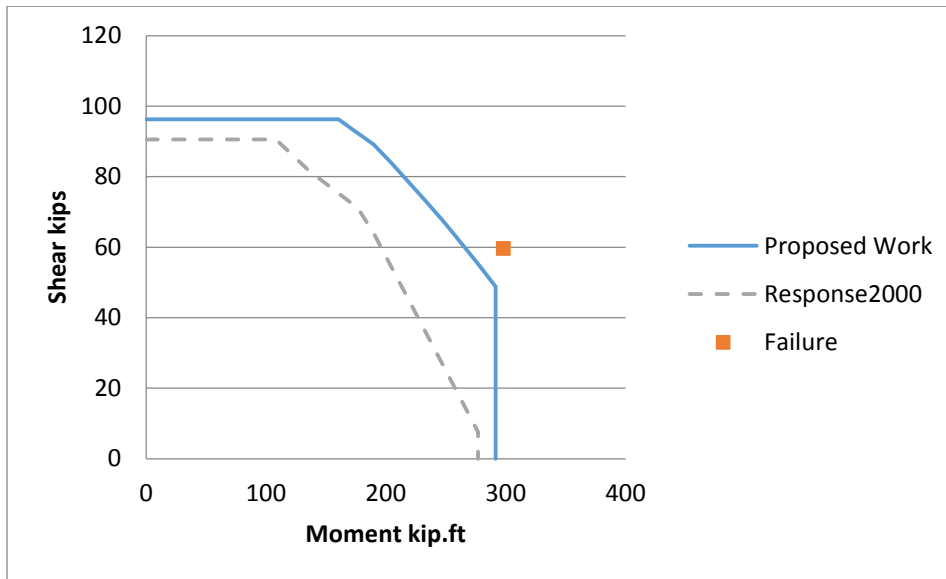
Figure 5.34: Nelson (2000) Col4 Proposed Interaction Diagram vs. Response 2000

Both predicted interaction diagrams are conservative. The proposed interaction diagram accurately estimated the failure envelope of the section, and the failure point locates just outside the interaction diagram. Response 2000 underestimated the section strength by almost 100 kip.ft.

<u>Lehman and Moehle (2000) No.430</u>
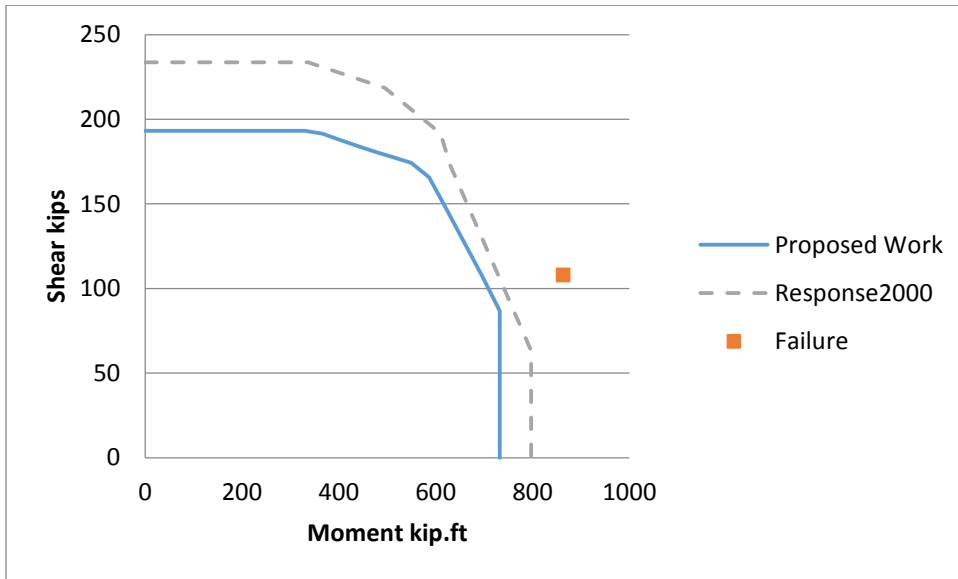
Figure 5.35: Lehman and Moehle (2000) No.430 Proposed Interaction Diagram vs. Response 2000

In this case, both interaction diagrams were conservative. Response 2000 showed a slightly better prediction of the failure point than the proposed interaction diagram.

<u>Kunnath et al. (1997) A8</u>
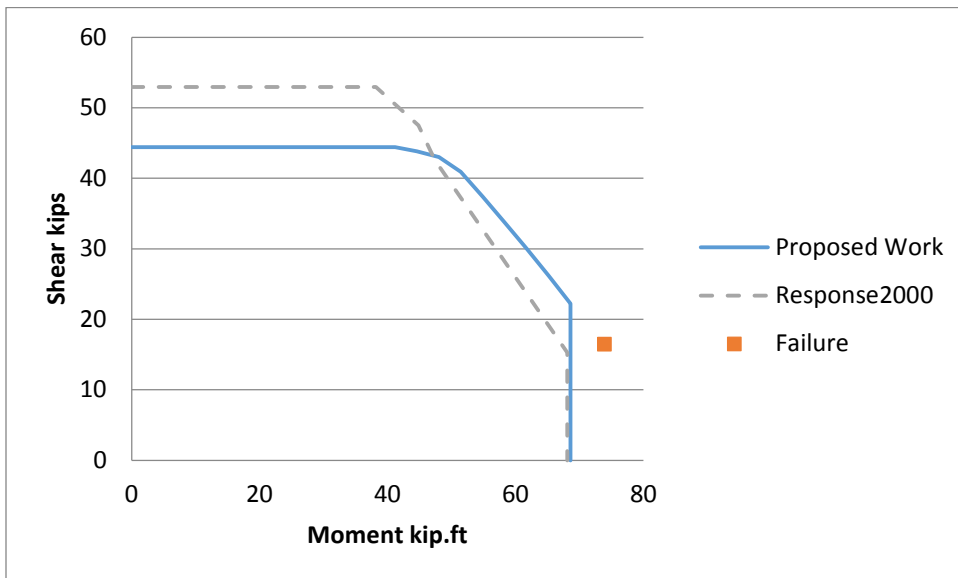
Figure 5.36: Kunnath et al. (1997) A8 Proposed Interaction Diagram vs. Response 2000

Both interaction diagrams were fairly accurate in predicting the failure point.

Moyer and Kowalsky (2003) Unit1
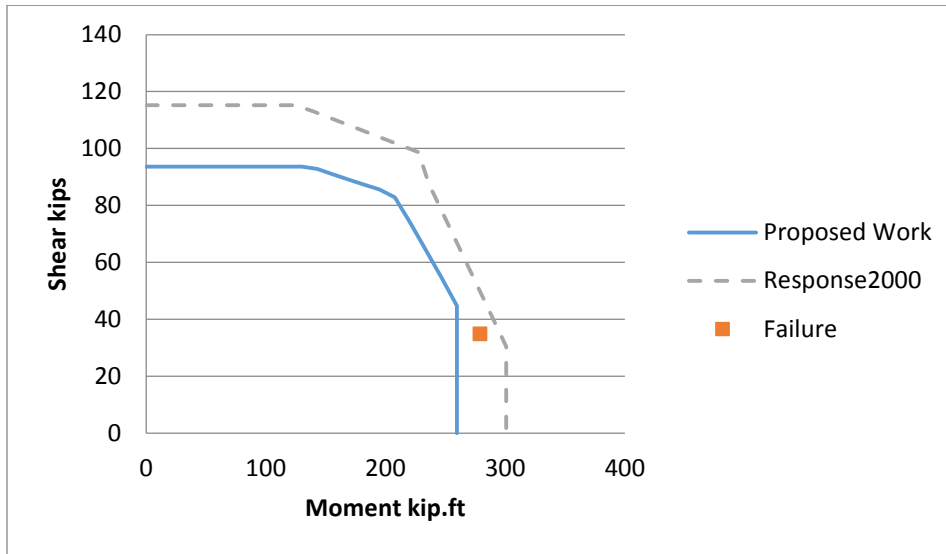
Figure 5.37: Moyer and Kowalsky (2003) Unit1 Proposed Interaction Diagram vs. Response 2000

The failure point locates between the two interaction diagrams. Response 2000 overestimated section capacity. The proposed interaction diagram managed to accurately predict the section behavior.

Saatcioglu and Baingo (1999) RC9
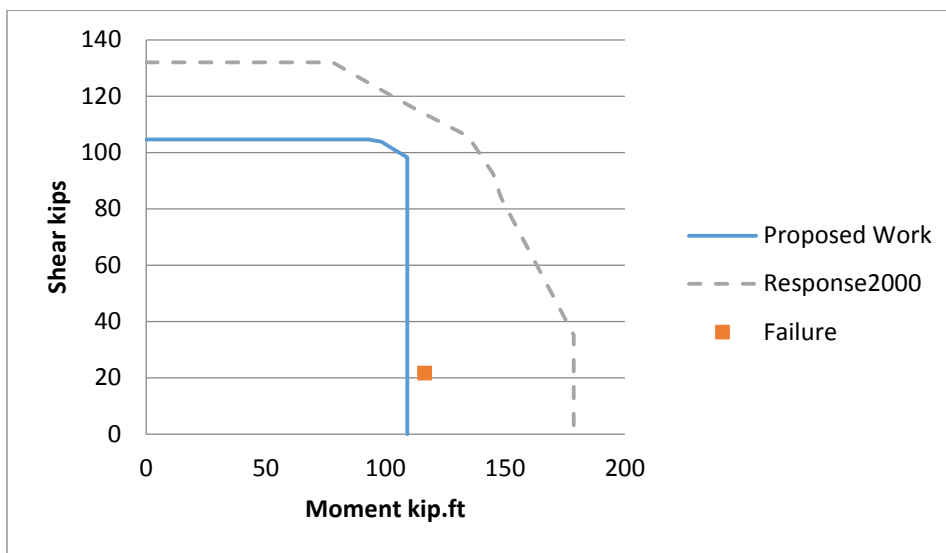
Figure 5.38: Saatcioglu and Baingo (1999) RC9 Proposed Interaction Diagram vs. Response 2000

In this case, Response 2000 failed to estimate the flexural capacity of the section, shifting the interaction diagram away from the failure point. On the other hand, the proposed interaction diagram was conservative and accurate in predicting the failure envelope of the section.

In this section, different circular columns and bridge piers were analyzed using the present AASHTO (2014) formulation to generate the 2D moment-shear interaction diagrams at a constant axial force. The resulting diagrams are compared against the corresponding experimental axial force-shear-moment failure point to examine the accuracy of the procedure, see Table 5.1. In most of the cases, the failure point locates just outside the generated interaction diagram, indicating that this diagram is accurate and conservative enough. As for some cases like Hamilton et al. (2002) Unit UC3, it is evident that the experimental points are also outside the diagrams while the diagrams are more conservative compared to the other specimens that seem to match the experimental data point very well. It may be concluded from the different experiments that were dominated by shear failure, bending moment failure, and a combination thereof that the present AASHTO (2014) procedure examined here for circular bridge piers is accurate enough when compared to the experiments.

The next step was to examine a head-to-head comparison between the present formulation and the AASHTO (1999) interaction diagrams developed by the well-known software Response 2000 using the same assumptions, limits, and overall equations. For this purpose, ten specimens were selected. Based on the diagrams discussed in this section, it can be concluded that the present diagrams are more conservative than those of Response 2000 in moment-dominated failure, indicating that Response 2000 predictions in this region are erroneous. This is due to the fact that at zero shear force, the moment values indicated by the present diagrams are the very ultimate values of confined analysis of moment-axial compression computed by Abd El-Fattah et al. (2011). The fact that Response 2000 moment values exceed this limit indicates an error in that program's results. Mapping the experimental data points on both interaction diagrams supports this finding and indicates the accuracy of the present formulation over that of Response 2000.

5.5 Database

This section provides a tabulated database of the cross sections used to analyze, compare, and predict the proposed interaction diagram procedure. Chapter 7 provides full results of this database, based on the proposed calculation in the same order shown in the tables. The parameters presented in the tables are the parameters needed to predict the interaction diagram based on the proposed procedures.

Table 5.3: Arakawa et al. (1987) Sections

Unit	D (in.)	Clear cover (in.)	L_a/D	Number of bars	Longitudinal bar diameter (in.)	fy (ksi)	Transverse bar diameter (in.)	fyt (ksi)	Spacing (in.)	f'c (ksi)	Axial force (kip)	Shear force (kip)	Moment (k.ft)
UNIT1	10.83	0.67	1.1	12	0.63	53.07	0.24	53.36	3.94	4.18	0	39.65	39.37
UNIT2	10.83	0.67	1.1	12	0.63	53.07	0.24	53.36	1.97	4.25	0	45.82	45.49
UNIT4	10.83	0.67	1.1	12	0.63	53.07	0.24	53.36	3.94	4.33	48.33	44.01	43.7
UNIT6	10.83	0.67	1.1	12	0.63	53.07	0.24	53.36	1.97	4.15	48.33	50.65	50.29
UNIT8	10.83	0.67	1.1	12	0.63	53.07	0.24	53.36	1.38	4.56	48.33	48.53	48.18
UNIT9	10.83	0.67	1.1	16	0.63	53.07	0.24	53.36	1.97	4.43	48.33	51.26	50.89
UNIT10	10.83	0.67	1.1	8	0.63	53.07	0.24	53.36	1.97	4.38	48.33	57.15	56.74
UNIT12	10.83	0.67	1.1	12	0.63	53.07	0.24	53.36	3.94	4.04	96.66	43.15	42.84
UNIT13	10.83	0.67	1.1	12	0.63	53.07	0.24	53.36	1.97	4.43	96.66	53.6	53.22
UNIT14	10.83	0.67	1.1	12	0.63	53.07	0.24	53.36	1.38	4.54	96.66	62.74	62.29
UNIT15	10.83	0.67	1.64	12	0.63	52.64	0.24	55.25	2.95	4.64	0	40.38	59.77
UNIT16	10.83	0.67	1.64	12	0.63	52.64	0.24	55.25	1.38	4.54	0	39.77	58.87
UNIT17	10.83	0.67	1.1	12	0.63	52.64	0.24	55.25	2.95	4.54	48.33	55.43	55.03
UNIT19	10.83	0.67	1.64	12	0.63	52.64	0.24	55.25	2.95	4.53	48.33	41.92	62.05
UNIT20	10.83	0.67	1.64	12	0.63	52.64	0.24	55.25	1.38	4.25	48.33	47.71	70.62
UNIT21	10.83	0.67	2.19	12	0.63	52.64	0.24	55.25	2.95	4.43	48.33	34.67	68.53
UNIT23	15.75	0.43	2	12	0.63	63.22	0.47	48.14	6.3	4.69	48.33	47.7	125.22
UNIT24	10.83	0.67	1.1	12	0.63	52.64	0.24	55.25	2.95	4.51	96.66	52.61	52.23
UNIT25	10.83	0.67	1.64	12	0.63	52.64	0.24	55.25	2.95	4.31	96.66	45.24	66.96
UNIT26	10.83	0.67	2.19	12	0.63	52.64	0.24	55.25	2.95	4.49	96.66	39.15	77.38
UNIT27	10.83	0.67	1.64	12	0.63	52.64	0.24	55.25	2.95	2.75	96.66	39.58	58.59
UNIT28	10.83	0.67	1.64	12	0.63	52.64	0.24	55.25	2.95	5.99	96.66	51.88	76.79

Table 5.4: Calderone, Lehman, and Moehle (2001) Sections

Unit	D (in.)	Clear cover (in.)	L_a/D	Number of bars	Longitudinal bar diameter (in.)	fy (ksi)	Transverse bar diameter (in.)	fyt (ksi)	Spacing (in.)	f'c (ksi)	Axial force (kip)	Shear force (kip)	Moment (k.ft)
No.328	24	1	3	28	0.75	63.99	0.25	87.99	1	5.01	204.98	124.76	748.56
No.828	24	1	8	28	0.75	63.99	0.25	87.99	1	5.01	204.98	45.63	730.08
No.1028	24	1	10	28	0.75	63.99	0.25	87.99	1	5.01	204.98	42.8	856

Table 5.5: Henry and Mahin (1999) Sections

Unit	D (in.)	Clear cover (in.)	L_a/D	Number of bars	Longitudinal bar diameter (in.)	fy (ksi)	Transverse bar diameter (in.)	fyt (ksi)	Spacing (in.)	f'c (ksi)	Axial force (kip)	Shear force (kip)	Moment (k.ft)
No.415p	24	0.75	4	22	0.63	66.99	0.25	87.99	1.25	5.4	294.04	74.19	593.52
No.415s	24	0.75	4	22	0.63	66.99	0.25	87.99	2.5	5.4	147.02	64.8	518.4

Table 5.6: Hamilton et al. (2002) Sections

Unit	D (in.)	Clear cover (in.)	L_a/D	Number of bars	Longitudinal bar diameter (in.)	fy (ksi)	Transverse bar diameter (in.)	fyt (ksi)	Spacing (in.)	f'c (ksi)	Axial force (kip)	Shear force (kip)	Moment (k.ft)
UC13	16	0.32	2.58	14	0.5	66.49	0.18	100.27	6.75	5.04	0	32.21	110.81
UC14	16	0.32	2.58	14	0.5	66.49	0.18	100.27	6.75	5.04	0	36.96	127.15
UC15	16	0.32	2.58	12	0.5	66.49	0.18	100.27	2.5	5.14	0	39.24	134.99
UC1	16	0.5	4.57	12	0.5	66.49	0.18	100.27	1.25	5.3	0	15.81	96.34
UC2	16	0.5	4.57	12	0.5	66.49	0.18	100.27	1.25	5.3	0	16.96	103.35
UC3	16	0.5	4.57	12	0.5	66.49	0.18	100.27	1.25	5.17	0	23.83	145.21

Table 5.7: Cheok and Stone (1986) Sections

Unit	D (in.)	Clear cover (in.)	L_a/D	Number of bars	Longitudinal bar diameter (in.)	fy (ksi)	Transverse bar diameter (in.)	fyt (ksi)	Spacing (in.)	f'c (ksi)	Axial force (kip)	Shear force (kip)	Moment (k.ft)
NIST-Full-scale Flexure	59.84	2	6.02	25	1.69	68.88	0.63	71.49	3.5	5.2	1000.36	290.76	8728.54
NIST-Full-scale-shear	59.84	1.75	3.01	25	1.69	68.88	0.75	63.08	2.13	4.98	1000.36	737.79	11074.13

Table 5.8: Chai, Priestley, and Seible (1991) Sections

Unit	D (in.)	Clear cover (in.)	L_a/D	Number of bars	Longitudinal bar diameter (in.)	fy (ksi)	Transverse bar diameter (in.)	fyt (ksi)	Spacing (in.)	f'c (ksi)	Axial force (kip)	Shear force (kip)	Moment (k.ft)
CCS1	24.02	0.55	2	26	0.75	45.71	0.25	46.13	5	5.01	135.96	124.2	497.22
Test3	24	0.66	6	26	0.75	45.69	0.25	50.99	5	4.73	399.92	55.74	668.88
UNIT1	24	0.55	6	26	0.75	45.7	0.25	51	5	5.54	400	48.5	582

Table 5.9: Siryo (1975) Sections

Unit	D (in.)	Clear cover (in.)	L_a/D	Number of bars	Longitudinal bar diameter (in.)	fy (ksi)	Transverse bar diameter (in.)	fyt (ksi)	Spacing (in.)	f'c (ksi)	Axial force (kip)	Shear force (kip)	Moment (k.ft)
BRI-No.2	9.84	1.4	1.5	4	0.38	57.86	0.35	51.48	1.97	3.85	41.36	27.96	34.4
BRI-No.3-ws22bs	9.84	1.38	2.01	8	0.37	54.38	0.23	53.07	2.48	4.59	72.39	23.08	38.05
BRI-No.3-ws27bs	9.84	1.4	2.01	8	0.63	50.03	0.35	48.51	1.65	4.59	72.39	33.25	54.81
ws21bs	9.84	1.4	1	8	0.37	54.38	0.35	48.51	1.3	3.85	72.39	41.32	33.89
ws25bs	9.84	1.34	1	8	0.5	55.39	0.35	48.51	1.81	3.85	36.19	41.59	34.11
ws26bs	9.84	1.38	2.01	8	0.5	55.39	0.15	56.05	1.46	4.59	36.19	23.52	38.77

Table 5.10: Kowalesky and Priestley (2000) Sections

Unit	D (in.)	Clear cover (in.)	L_a/D	Number of bars	Longitudinal bar diameter (in.)	fy (ksi)	Transverse bar diameter (in.)	fyt (ksi)	Spacing (in.)	f'c (ksi)	Axial force (kip)	Shear force (kip)	Moment (k.ft)
FL1	17.99	1	8.01	30	0.63	69.17	0.37	64.53	2.99	5.31	400.14	42.04	504.83
FL2	17.99	1.06	8.01	30	0.63	69.17	0.25	63.37	2.01	5.8	400.14	39.28	471.69
FL3	17.99	1.06	8.01	30	0.63	69.17	0.25	64.53	2.99	5.6	400.14	44.38	532.93

Table 5.11: Hose, Seible, and Priestley (1997) Section and Elsanadedy (2002) Section

Unit	D (in.)	Clear cover (in.)	L_a/D	Number of bars	Longitudinal bar diameter (in.)	fy (ksi)	Transverse bar diameter (in.)	fyt (ksi)	Spacing (in.)	f'c (ksi)	Axial force (kip)	Shear force (kip)	Moment (k.ft)
SRPH1	24.02	0.91	6	20	0.87	65.98	0.37	60.03	2.24	5.96	400.14	81.75	981.82
UnitCS-A1	24	0.75	2	20	0.75	43.41	0.25	30.51	5	5.35	145	102.1	408.4

Table 5.12: Moyer and Kowalsky (2003) Sections

Unit	D (in.)	Clear cover (in.)	L_a/D	Number of bars	Longitudinal bar diameter (in.)	fy (ksi)	Transverse bar diameter (in.)	fyt (ksi)	Spacing (in.)	f'c (ksi)	Axial force (kip)	Shear force (kip)	Moment (k.ft)
Unit_1	18	0.31	5.34	12	0.75	81.99	0.37	62.99	3	4.75	52	34.86	279.23
Unit_2	18	0.31	5.34	12	0.75	81.99	0.37	62.99	3	4.96	52	35.8	286.76
Unit_3	18	0.31	5.34	12	0.75	81.99	0.37	62.99	3	4.6	52	43.08	345.08
Unit_4	18	0.31	5.34	12	0.75	81.99	0.37	62.99	3	4.92	52	35.32	282.92

Table 5.13: Ng, Lam, and Kwan (2010) Sections

Unit	D (in.)	Clear cover (in.)	L_a/D	Number of bars	Longitudinal bar diameter (in.)	fy (ksi)	Transverse bar diameter (in.)	fyt (ksi)	Spacing (in.)	f'c (ksi)	Axial force (kip)	Shear force (kip)	Moment (k.ft)
No.2	9.84	0.34	5.37	10	0.51	44.23	0.17	38.14	0.55	5.09	3.8	8.23	36.24
No.3	9.84	0.32	3.73	10	0.47	42.63	0.17	30.02	0.39	4.79	123.64	17.56	53.71

Table 5.14: Kunnath et al. (1997) Sections

Unit	D (in.)	Clear cover (in.)	L_a/D	Number of bars	Longitudinal bar diameter (in.)	fy (ksi)	Transverse bar diameter (in.)	fyt (ksi)	Spacing (in.)	f'c (ksi)	Axial force (kip)	Shear force (kip)	Moment (k.ft)
A2	12.01	0.49	4.5	21	0.37	64.96	0.16	62.93	0.75	4.21	44.96	16.63	74.9
A3	12.01	0.49	4.5	21	0.37	64.96	0.16	62.93	0.75	4.21	44.96	16.93	76.25
A4	12.01	0.49	4.5	21	0.37	64.96	0.16	62.93	0.75	5.15	49.91	16.97	76.43
A5	12.01	0.49	4.5	21	0.37	64.96	0.16	62.93	0.75	5.15	49.91	20.86	93.95
A6	12.01	0.49	4.5	21	0.37	64.96	0.16	62.93	0.75	5.15	49.91	17.26	77.74
A7	12.01	0.49	4.5	21	0.37	64.96	0.16	62.93	0.75	4.76	49.91	17.75	79.95
A8	12.01	0.49	4.5	21	0.37	64.96	0.16	62.93	0.75	4.76	49.91	16.42	73.96
A9	12.01	0.49	4.5	21	0.37	64.96	0.16	62.93	0.75	4.72	49.91	16.86	75.94
A10	12.01	0.49	4.5	21	0.37	64.96	0.16	62.93	0.75	3.92	44.96	16.69	75.17
A11	12.01	0.49	4.5	21	0.37	64.96	0.16	62.93	0.75	3.92	44.96	16.3	73.42
A12	12.01	0.49	4.5	21	0.37	64.96	0.16	62.93	0.75	3.92	44.96	16.25	73.19

Table 5.15: Lehman and Moehle (2000) Sections

Unit	D (in.)	Clear cover (in.)	L_a/D	Number of bars	Longitudinal bar diameter (in.)	fy (ksi)	Transverse bar diameter (in.)	fyt (ksi)	Spacing (in.)	f'c (ksi)	Axial force (kip)	Shear force (kip)	Moment (k.ft)
No.415	24	0.75	4	22	0.63	66.99	0.25	87.99	1.25	4.5	146.99	64.07	512.56
No.815	24	0.75	8	22	0.63	66.99	0.25	87.99	1.25	4.5	146.99	33.94	543.04
No.1015	24	0.75	10	22	0.63	66.99	0.25	87.99	1.25	4.5	146.99	22.82	456.4
No.407	24	0.75	4	11	0.63	66.99	0.25	87.99	1.25	4.5	146.99	40.46	323.68
No.430	24	0.75	4	44	0.63	66.99	0.25	87.99	1.25	4.5	146.99	107.9	863.2

Table 5.16: Lim and McLean (1991) Sections

Unit	D (in.)	Clear cover (in.)	L_a/D	Number of bars	Longitudinal bar diameter (in.)	fy (ksi)	Transverse bar diameter (in.)	fyt (ksi)	Spacing (in.)	f'c (ksi)	Axial force (kip)	Shear force (kip)	Moment (k.ft)
Con1	5.98	0.33	7.51	8	0.5	64.96	0.15	89.9	0.87	5.01	33.94	4.28	16.02
Con2	5.98	0.33	3.76	8	0.5	64.96	0.15	89.9	0.87	5.01	33.94	9.3	17.43
Con3	5.98	0.33	3.76	8	0.5	64.96	0.15	89.9	0.87	5.01	49.46	9.67	18.12

Table 5.17: Munro, Park, and Priestley (1976) Section and Iwasaki et al. (1986) Section

Unit	D (in.)	Clear cover (in.)	L_a/D	Number of bars	Longitudinal bar diameter (in.)	fy (ksi)	Transverse bar diameter (in.)	fyt (ksi)	Spacing (in.)	f'c (ksi)	Axial force (kip)	Shear force (kip)	Moment (k.ft)
No.1	19.69	0.64	5.46	20	0.72	44.23	0.31	56.41	1.34	5.8	5.93	31.1	278.63
I30	22.2	1.38	1.78	40	0.51	46.84	0.35	37.47	8.9	5.77	0	91.37	300.89

Table 5.18: McDaniel (1997) Sections

Unit	D (in.)	Clear cover (in.)	L_a/D	Number of bars	Longitudinal bar diameter (in.)	fy (ksi)	Transverse bar diameter (in.)	fyt (ksi)	Spacing (in.)	f'c (ksi)	Axial force (kip)	Shear force (kip)	Moment (k.ft)
UNITS-1	24	0.64	2	20	0.63	65.83	0.19	29	4	4.33	4.23	91.15	364.6
UNITS1-2	24	0.64	2	20	0.63	65.83	0.19	29	4	3.89	4.23	74.7	298.8
UNITS2	24	0.64	2	20	0.63	63.46	0.19	29	4	4.53	4.23	74.7	298.8

Table 5.19: Jaradat (1996) Sections

Unit	D (in.)	Clear cover (in.)	L_a/D	Number of bars	Longitudinal bar diameter (in.)	fy (ksi)	Transverse bar diameter (in.)	fyt (ksi)	Spacing (in.)	f'c (ksi)	Axial force (kip)	Shear force (kip)	Moment (k.ft)
SpecimenS1	10	1.44	2	8	0.5	53.81	0.15	30.51	3.85	4.21	19	17.84	29.74
SpecimenS3	10	1.56	2	8	0.38	52.11	0.15	30.51	3.85	3.81	17	17.34	28.9

Table 5.20: Nelson (2000) Sections

Unit	D (in.)	Clear cover (in.)	L_a/D	Number of bars	Longitudinal bar diameter (in.)	fy (ksi)	Transverse bar diameter (in.)	fyt (ksi)	Spacing (in.)	f'c (ksi)	Axial force (kip)	Shear force (kip)	Moment (k.ft)
Col1	20	0.75	3	10	0.63	65.98	0.18	65.98	4.02	8.15	325.96	69.32	346.6
Col2	20	0.75	3	10	0.63	65.98	0.18	65.98	4.02	8.17	279.43	65.95	329.75
Col3	20	0.75	3	10	0.63	65.98	0.18	65.98	4.02	8.27	256.05	61.89	309.45
Col4	20	0.75	3	10	0.63	65.98	0.18	65.98	4.02	7.65	256.05	59.64	298.2

Table 5.21: Priestley et al. (1994) Sections

Unit	D (in.)	Clear cover (in.)	L_a/D	Number of bars	Longitudinal bar diameter (in.)	fy (ksi)	Transverse bar diameter (in.)	fyt (ksi)	Spacing (in.)	f'c (ksi)	Axial force (kip)	Shear force (kip)	Moment (k.ft)
NR1	24.02	0.5	1.5	12	0.5	66.99	0.25	52.35	3	4.35	113.07	94.05	282.39
NR2	24.02	0.5	1.5	24	0.5	66.99	0.25	52.35	5	4.35	113.07	132.04	396.46

Table 5.22: Petrovski and Ristic (1984) Sections

Unit	D (in.)	Clear cover (in.)	L_a/D	Number of bars	Longitudinal bar diameter (in.)	fy (ksi)	Transverse bar diameter (in.)	fyt (ksi)	Spacing (in.)	f'c (ksi)	Axial force (kip)	Shear force (kip)	Moment (k.ft)
M1E1	12.09	1.3	6.23	12	0.47	34.8	0.24	34.8	2.95	5.63	32.6	7.55	47.39
M1E2	12.09	1.3	6.23	12	0.47	34.8	0.24	34.8	2.95	5.25	57.1	8.31	52.16
M2E1	12.09	1.3	2.94	12	0.47	34.8	0.24	34.8	1.42	5.21	32.6	19.32	57.23
M2E2	12.09	1.3	2.92	12	0.47	34.8	0.24	34.8	1.42	4.99	57.1	20.9	61.49

Table 5.23: Zahn et al. (1986) Sections

Unit	D (in.)	Clear cover (in.)	L_a/D	Number of bars	Longitudinal bar diameter (in.)	fy (ksi)	Transverse bar diameter (in.)	fyt (ksi)	Spacing (in.)	f'c (ksi)	Axial force (kip)	Shear force (kip)	Moment (k.ft)
No.5	15.75	0.51	4	16	0.63	48.87	0.39	67.57	5.31	4.67	124.76	32	168
No.6	15.75	0.51	4	16	0.63	48.87	0.39	67.57	2.95	3.92	467.58	39.37	206.7

Table 5.24: Pontangaroa et al. (1979) Sections

Unit	D (in.)	Clear cover (in.)	L_a/D	Number of bars	Longitudinal bar diameter (in.)	fy (ksi)	Transverse bar diameter (in.)	fyt (ksi)	Spacing (in.)	f'c (ksi)	Axial force (kip)	Shear force (kip)	Moment (k.ft)
Unit1	23.62	0.79	2	16	0.94	43.94	0.39	43.5	2.95	4.12	431.62	154.47	608.1
Unit4	23.62	0.79	2	16	0.94	43.94	0.39	61.34	2.76	4.78	850.87	175.54	691.05
No.5A	23.62	0.79	2	16	0.94	44.52	0.63	40.6	2.17	4.72	760.95	182.48	718.37
No.5B	23.62	0.79	2	16	0.94	44.52	0.63	40.6	2.17	4.72	1521.9	210.65	829.26

Table 5.25: Watson and Park (1994) Sections

Unit	D (in.)	Clear cover (in.)	L_a/D	Number of bars	Longitudinal bar diameter (in.)	fy (ksi)	Transverse bar diameter (in.)	fyt (ksi)	Spacing (in.)	f'c (ksi)	Axial force (kip)	Shear force (kip)	Moment (k.ft)
No.10	15.75	0.51	4	12	0.63	68.73	0.31	53.94	3.31	5.8	596.17	47.72	250.53
No.11	15.75	0.51	4	12	0.63	68.73	0.39	49.01	2.24	5.66	813.78	46.41	243.66

Table 5.26: Ranf et al. (2006) Sections

Unit	D (in.)	Clear cover (in.)	L_a/D	Number of bars	Longitudinal bar diameter (in.)	fy (ksi)	Transverse bar diameter (in.)	fyt (ksi)	Spacing (in.)	f'c (ksi)	Axial force (kip)	Shear force (kip)	Moment (k.ft)
SpecimenS1	20	0.57	3	10	0.62	65.98	0.18	60.03	4	5.28	165.62	48.31	241.55
SpecimenC2	20	0.57	3	10	0.62	65.98	0.18	60.03	4	8.27	259.57	62.06	310.3
SpecimenC3R	20	0.57	3	10	0.62	65.98	0.18	60.03	4	7.65	240.07	59.99	299.95
SpecimenS3	20	0.57	3	10	0.62	65.98	0.18	60.03	4	8.16	256.11	59.87	299.35

Table 5.27: Yalcin (1997) Section and Yarandi (2007) Section

Unit	D (in.)	Clear cover (in.)	L_a/D	Number of bars	Longitudinal bar diameter (in.)	fy (ksi)	Transverse bar diameter (in.)	fyt (ksi)	Spacing (in.)	f'c (ksi)	Axial force (kip)	Shear force (kip)	Moment (k.ft)
SpecimenBR-C1	24.02	2.17	2.44	12	0.98	64.53	0.39	61.63	11.81	6.53	404.46	126.45	617.6
SpecimenCR-C	23.62	1.77	2.5	12	0.77	67.43	0.25	71.2	11.81	5.08	311.43	95.23	468.62

Table 5.28: Roeder et al. (2001) Sections

Unit	D (in.)	Clear cover (in.)	L_a/D	Number of bars	Longitudinal bar diameter (in.)	fy (ksi)	Transverse bar diameter (in.)	fyt (ksi)	Spacing (in.)	f'c (ksi)	Axial force (kip)	Shear force (kip)	Moment (k.ft)
C1	16.5	2	4.7	8	0.87	62.28	0.37	59.99	2	8.79	0	26.59	171.84
C2	16.5	2	4.7	8	0.87	62.28	0.37	59.99	2	9.08	0	27.21	175.85
C3	16.5	2	4.7	8	0.87	62.28	0.39	59.99	2	10.1	0	30.69	198.34
C4	16.5	2	4.7	8	0.87	62.28	0.39	59.99	2	10.1	221.99	38.28	247.39
C5	16.5	2	4.7	8	0.87	71.29	0.39	59.99	2	10.1	221.99	41.29	266.84
C6	16.5	2	4.7	8	0.87	73.37	0.39	59.99	2	10.1	221.99	40.83	263.87
C7	16.5	2	4.7	8	0.87	73.37	0.39	59.99	2	10.1	221.99	39.92	257.99
C8	16.5	2	4.7	8	0.87	71.29	0.39	59.99	2	10.1	221.99	44.59	288.17

Table 5.29: Sritharan, Priestley, and Seible (2001) Sections

Unit	D (in.)	Clear cover (in.)	L_a/D	Number of bars	Longitudinal bar diameter (in.)	fy (ksi)	Transverse bar diameter (in.)	fyt (ksi)	Spacing (in.)	f'c (ksi)	Axial force (kip)	Shear force (kip)	Moment (k.ft)
IC1	23.62	1	3.01	14	0.87	64.96	0.37	62.5	3.82	4.56	89.92	97.48	577.54
B105IC2	23.62	1	3.01	14	0.87	64.96	0.37	62.5	3.82	5.02	89.92	96.79	573.46
IC3	23.62	1	3.01	14	0.87	62.93	0.37	62.93	2.52	4.79	89.92	103.48	613.09

Table 5.30: Stone and Cheok (1989) Sections

Unit	D (in.)	Clear cover (in.)	L_a/D	Number of bars	Longitudinal bar diameter (in.)	fy (ksi)	Transverse bar diameter (in.)	fyt (ksi)	Spacing (in.)	f'c (ksi)	Axial force (kip)	Shear force (kip)	Moment (k.ft)
NIST-Model-N1	9.84	0.33	3.01	25	0.28	64.67	0.12	63.95	0.35	3.5	26.98	14.41	35.57
NIST-Model-N2	9.84	0.33	3.01	25	0.28	64.67	0.12	63.95	0.35	3.35	53.73	16.51	40.75
NIST-Model-N3	9.84	0.33	6.01	25	0.28	64.67	0.11	69.02	0.55	3.69	26.98	7.17	35.34
NIST-Model-N4	9.84	0.33	3.01	25	0.28	64.67	0.12	63.95	0.35	3.54	26.98	14.1	34.81
NIST-Model-N5	9.84	0.33	3.01	25	0.28	64.67	0.12	63.95	0.35	3.53	53.73	17.21	42.48
NIST-Model-N6	9.84	0.33	6.01	25	0.28	64.67	0.11	63.95	0.55	3.38	26.98	6.67	32.88

Table 5.31: Vu, Priestley, Seible, and Benzoni (1998) Sections

Unit	D (in.)	Clear cover (in.)	L_a/D	Number of bars	Longitudinal bar diameter (in.)	fy (ksi)	Transverse bar diameter (in.)	fyt (ksi)	Spacing (in.)	f'c (ksi)	Axial force (kip)	Shear force (kip)	Moment (k.ft)
NH1	18	0.79	2	20	0.63	62	0.37	62.38	2.36	5.56	433.41	139.38	417.91
NH3	18	0.79	2	20	0.63	62	0.37	62.38	2.36	5.72	218.06	124	371.8
NH4	18	0.79	2	30	0.75	67.89	0.5	63	1.77	5.08	191.08	221.45	663.99
NH6	18	0.79	2	30	0.75	70.5	0.5	63	1.57	5.08	430.27	249.3	747.49

Table 5.32: Wong (1990) Sections

Unit	D (in.)	Clear cover (in.)	L_a/D	Number of bars	Longitudinal bar diameter (in.)	fy (ksi)	Transverse bar diameter (in.)	fyt (ksi)	Spacing (in.)	f'c (ksi)	Axial force (kip)	Shear force (kip)	Moment (k.ft)
UnitNo.2	15.75	0.59	2	20	0.63	68.88	0.24	49.3	2.56	5.37	411.38	109.99	288.73
UnitNo.1	15.75	0.59	2	20	0.63	61.34	0.39	43.5	2.36	5.51	203.89	103.69	272.19
UnitNo.3	15.75	0.59	2	20	0.63	68.88	0.39	43.5	2.36	5.37	407.56	130.07	341.44

Table 5.33: Ang et al. (1985) Sections

Unit	D (in.)	Clear cover (in.)	L_a/D	Number of bars	Longitudinal bar diameter (in.)	fy (ksi)	Tranverse bar diameter (in.)	fyt (ksi)	Spacing (in.)	f'c (ksi)	Axial force (kip)	Shear force (kip)	Moment (k.ft)
1	15.75	0.59	2	20	0.63	63.22	0.24	47.56	2.36	5.44	0	72.25	189.66
2	15.75	0.59	2	20	0.63	42.92	0.24	47.56	2.36	5.4	0	49.61	130.23
3	15.75	0.59	2.5	20	0.63	63.22	0.24	47.56	2.36	5.22	0	62.09	203.71
4	15.75	0.59	2	20	0.63	63.22	0.39	45.82	6.5	4.44	0	65.01	170.66
5	15.75	0.59	2	20	0.63	63.22	0.24	47.56	1.57	4.51	0	74.39	195.28
6	15.75	0.59	1.5	20	0.63	63.22	0.24	47.56	2.36	4.37	0	88.04	173.3
7	15.75	0.59	2	20	0.63	64.96	0.24	53.94	3.15	4.28	0	63.09	165.62
8	15.75	0.59	2	20	0.63	64.96	0.24	53.94	1.18	4.17	162.08	104.54	274.42
9	15.75	0.59	2.5	20	0.63	64.96	0.24	53.94	1.18	4.53	0	101.037	266.15
10	15.75	0.59	2	20	0.63	64.96	0.47	48.14	4.72	4.34	176.24	101.39	240.24
11	15.75	0.59	2	20	0.63	64.96	0.24	53.94	2.36	4.15	168.82	91.52	233.13
12	15.75	0.59	1.5	20	0.63	64.96	0.24	53.94	1.17	5.25	80.7	118.44	259.85
13	15.75	0.59	2	20	0.63	63.22	0.24	47.27	1.18	4.89	102.28	98.99	186.69
14	15.75	0.43	2	9	0.94	61.48	0.24	47.27	2.36	5.05	0	71.12	135.93
15	15.75	0.59	2	12	0.63	63.22	0.24	47.27	2.36	4.85	0	51.78	219.66
16	15.75	0.59	2	20	0.63	63.22	0.24	47.27	2.36	4.98	94.42	83.68	239.9
17	15.75	0.59	2.5	20	0.63	63.22	0.24	47.27	2.36	5.08	96.89	73.12	297.92
18	15.75	0.59	2	20	0.63	63.22	0.24	47.27	2.36	4.99	98.91	113.49	193.57
19	15.75	0.59	1.5	20	0.63	63.22	0.24	47.27	3.15	5.33	97.11	98.34	251.26
20	15.75	0.59	1.75	20	0.63	69.89	0.24	47.27	3.15	4.82	181.41	109.4	159.6
21	15.75	0.59	2	20	0.63	63.22	0.24	47.27	3.15	4.49	0	60.8	168.08
22	15.75	0.59	2	20	0.63	63.22	0.39	44.95	8.66	4.69	0	64.03	196.22
23	15.75	0.59	2	20	0.63	63.22	0.47	48.14	6.3	4.8	0	74.75	200.92
24	15.75	0.59	2	20	0.63	63.22	0.39	44.95	4.33	0	0	76.54	0

Chapter 6: Software Development

6.1 Introduction

The proposed procedure was built into the KDOT Column Expert software in order to compute the full domain moment-shear-axial force interaction diagram for circular reinforced-concrete column sections (Rasheed, Abd El-Fattah, Esmaeily, Jones, & Hurst, 2012). KDOT Column Expert is an object oriented program written within the framework of the visual C# language. This software can predict the steel confined and unconfined moment-axial force capacity for circular and rectangular sections. By adding shear analysis to the software, KDOT Column Expert can predict the full domain of the sections under the three major loads: moment-axial-shear force combinations. In this chapter, input interface and output interface are discussed for circular sections for the cases where shear is a key design of the load combinations.

6.2 Input Interface

The input data is divided into four subsections. The geometrical properties are the first subsection, including section diameter, clear cover, number of bars, number of longitudinal and transverse bars, and spacing. The second subsection is the concrete properties, including the concrete compressive strength and its corresponding strain, as well as the maximum strain. The third and fourth subsections are for the longitudinal and transverse steel properties. Steel properties are Young's modulus and yielding strength of the steel. The user also has the option to choose the transverse steel order between the two main orders, spiral and hoops. Figure 6.1 shows the input properties interface of the section.
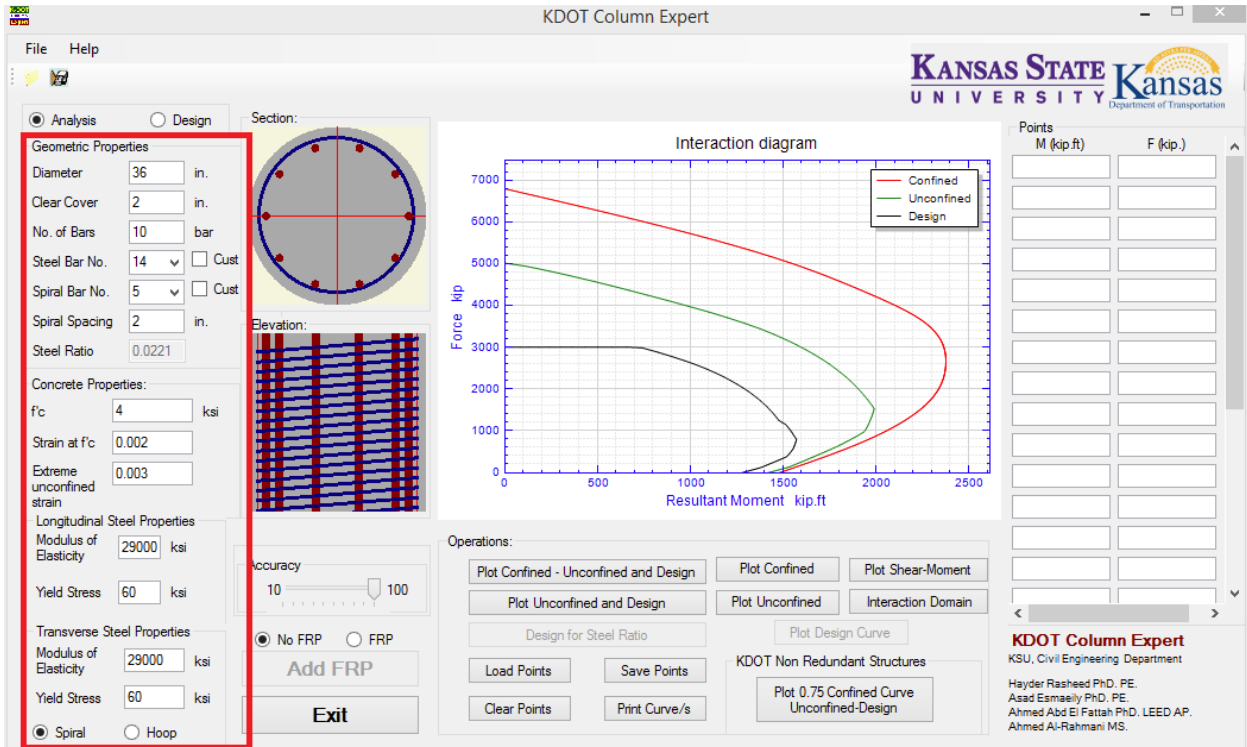
Figure 6.1: KDOT Column Expert Input Interface

The custom check box beside the steel bar textbox is to give the user the option to define the steel bar diameter if the bar diameter is not within the US rebar size charts, see Figure 6.2.
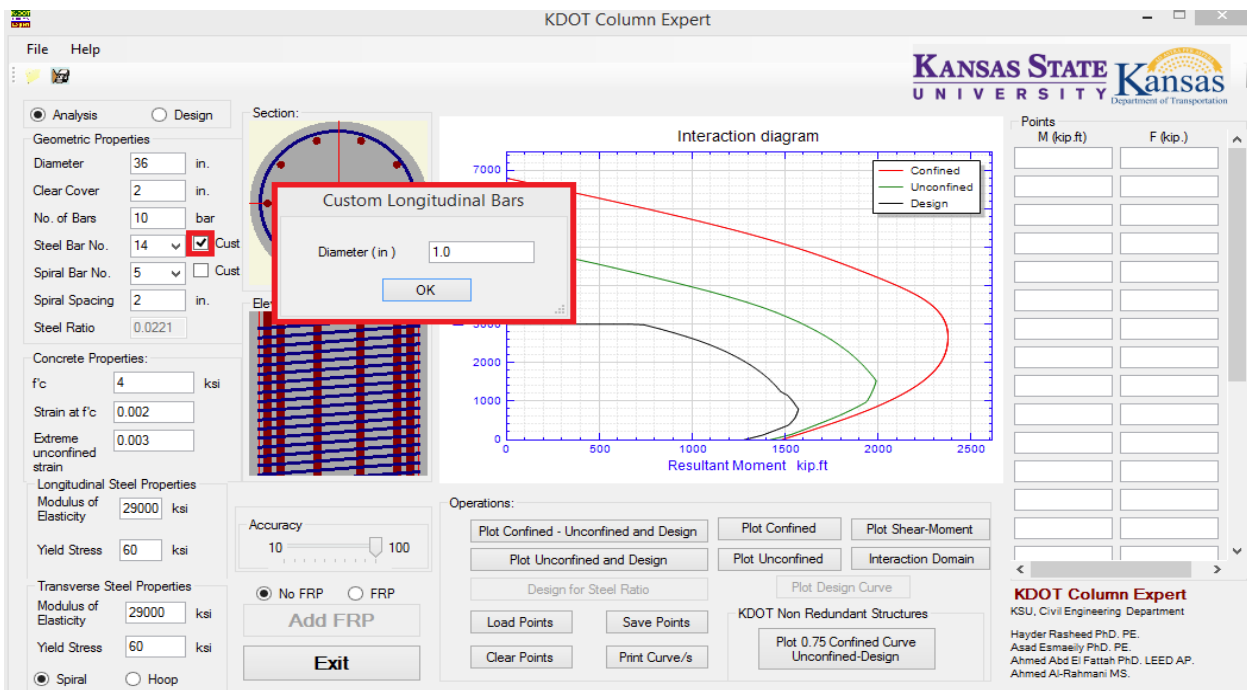
Figure 6.2: KDOT Column Expert Custom Bars Input

6.3 Output Interface

The default output interaction diagram is the moment versus axial force with zero shear value, see Figure 6.1. It shows the steel confined (red curve) and unconfined (green curve) section capacities.

In order to account for the shear calculations, the "Plot Shear-Moment" button was added. This button generates the interaction diagram for moment and shear force at a constant axial force defined by the user, see Figure 6.3. Figure 6.4 shows the final output of the "Plot Shear-Moment" button for constant axial force. The full domain could be generated using the "Interaction Domain" button, where the calculation in "Plot Shear-Moment" is repeated for a series of axial forces up to the maximum confined axial load capacity. Figure 6.5 shows the full domain of moment-axial force-shear force combination.
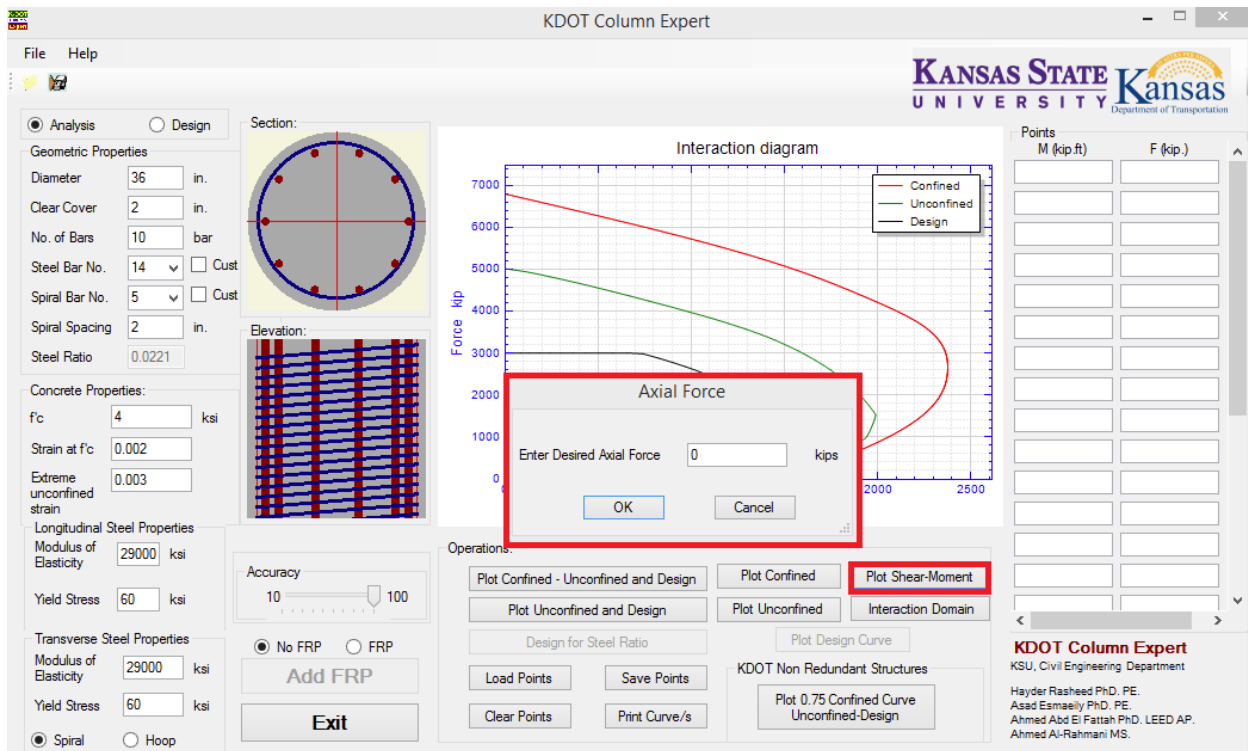
Figure 6.3: KDOT Column Expert Axial Force Input

Figure 6.4: KDOT Column Expert 2D Moment-Shear Interaction Diagram

Figure 6.5: KDOT Column Expert 3D Domain

In the case of sections having transverse steel less than the minimum transverse steel defined by AASHTO (2014) LRFD Bridge Construction Specifications, the user is asked to provide a value of maximum aggregate size; see Figures 6.6 and 6.7.
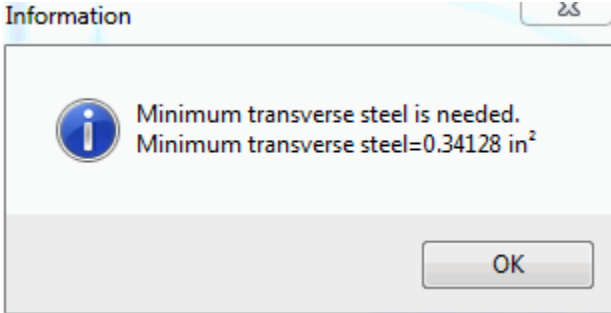
Figure 6.6: Minimum Transverse Steel
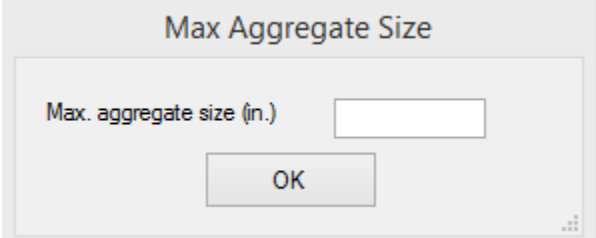
Figure 6.7: Maximum Aggregate Size Input

There are three cases in which AASHTO (2014) LRFD Specifications consider the section invalid, and will ask to change the properties of the section. In KDOT Column Expert, the user is notified to change the section properties if any of these cases matched. The first case occurs if the transverse steel spacing exceeded the maximum; in this case the message shown in Figure 6.8 appears and the analysis stops.
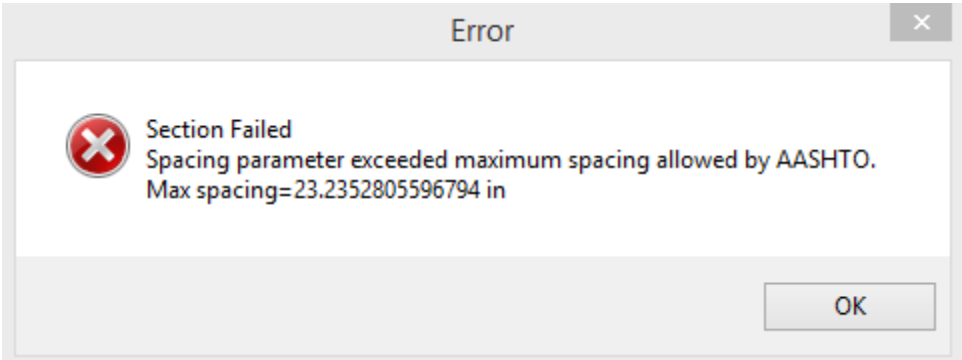
Figure 6.8: Maximum Spacing Error Message

The second case is to make sure that the section has enough longitudinal steel to resist cracks in the case of sections having transverse steel less than the minimum transverse steel defined by AASHTO (2014) LRFD Specifications. Figure 6.9 shows the KDOT Column Expert message to the user in this case.
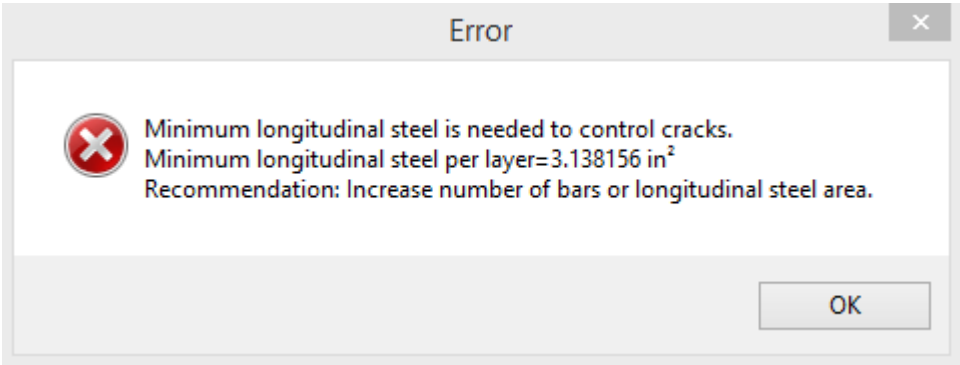
Figure 6.9: Lack of Longitudinal Steel Error

The third case is to confirm that the transverse steel yielding strength is less than 100 ksi. This limit is established to have a clear yielding zone in the steel stress-strain curve. If the transverse steel yielding strength exceeded 100 ksi, the yielding zone vanishes. Figure 6.10 shows the KDOT Column Expert message to the user in this case.
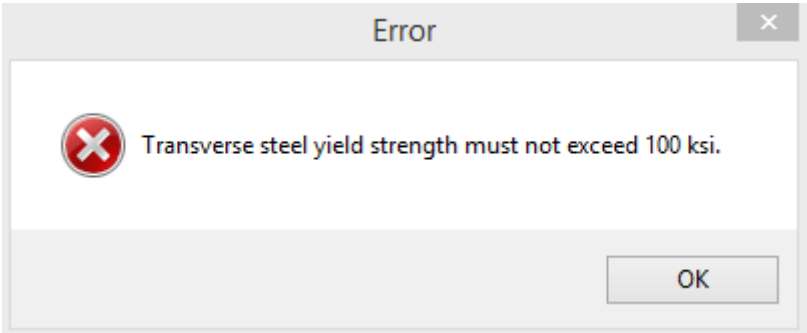
Figure 6.10: Transverse Steel Exceeded 100 ksi Error

Chapter 7: Complete Database Comparisons of AASHTO LRFD Approach

This chapter provides the interaction diagrams for the full database discussed in Chapter 5 based on the AASHTO (2014) LRFD Bridge Construction Specifications approach. In this chapter, the calculated interaction diagram is represented as a solid line, while the reported experimental failure point is represented as a square mark.
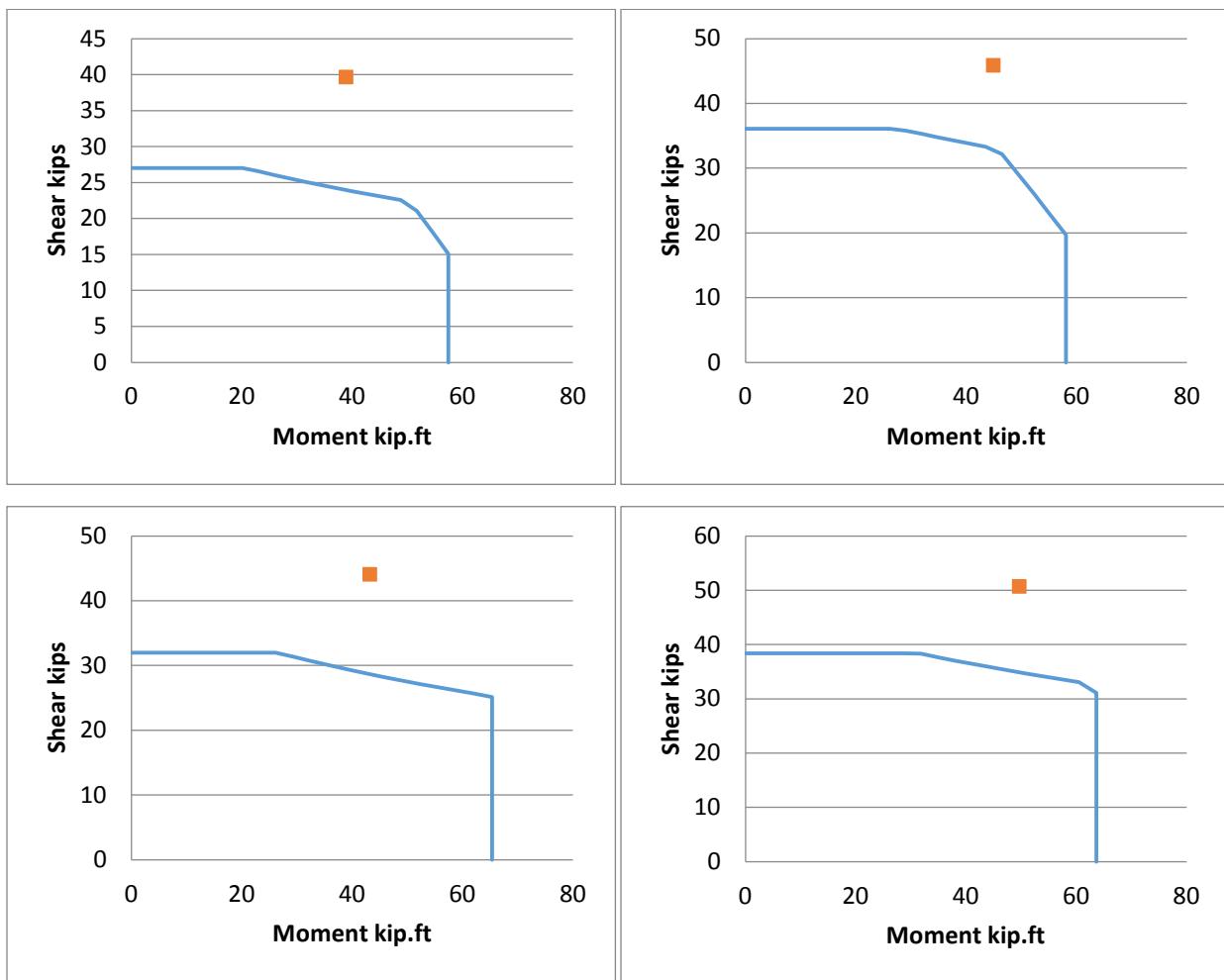
Figure 7.1: Arakawa et al. (1987) Interaction Diagrams (UNITs 1, 2, 4, and 6; Table 5.3)
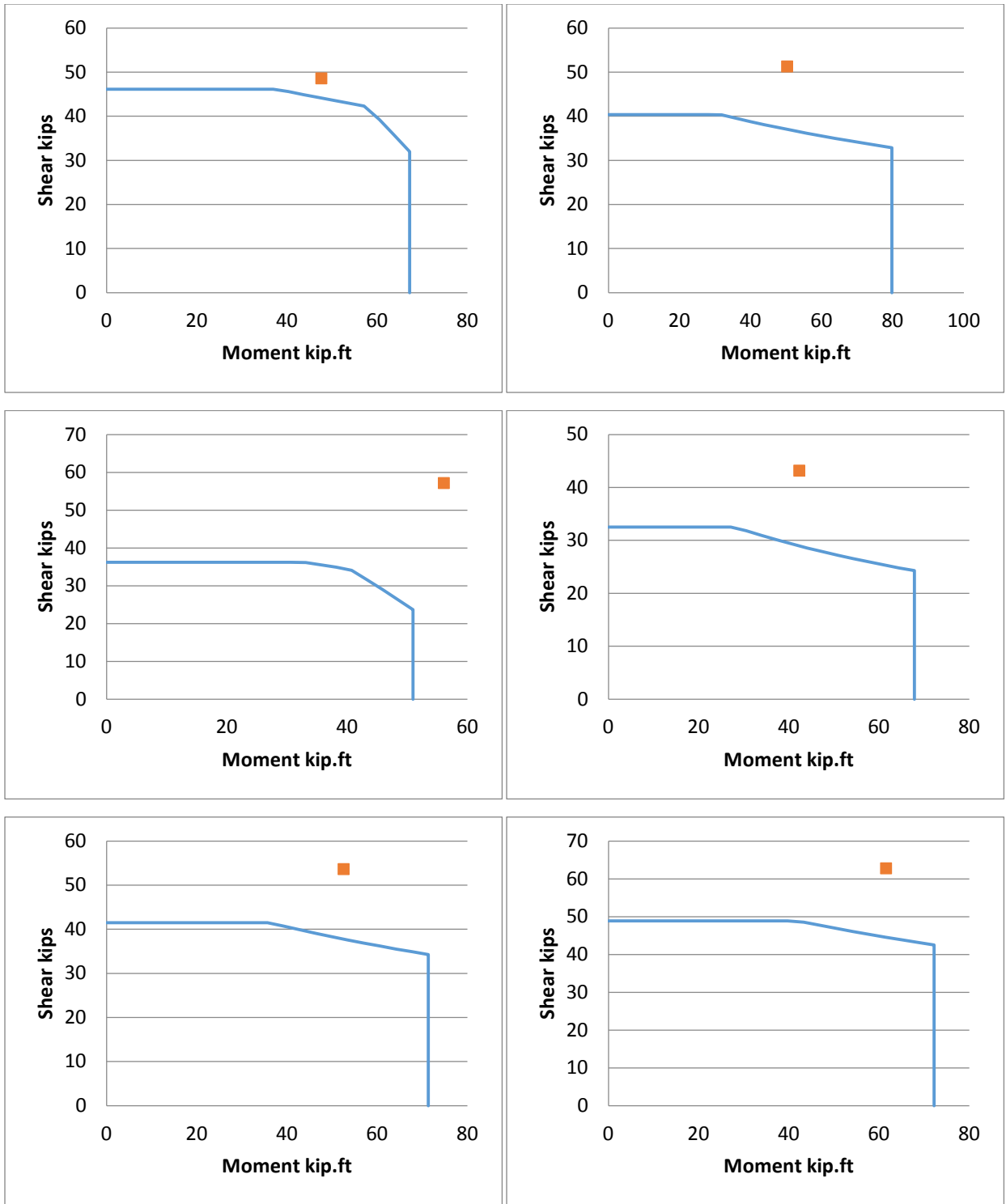
Figure 7.2: Arakawa et al. (1987) Interaction Diagrams (UNITs 8, 9, 10, 12, 13, and 14; Table 5.3)
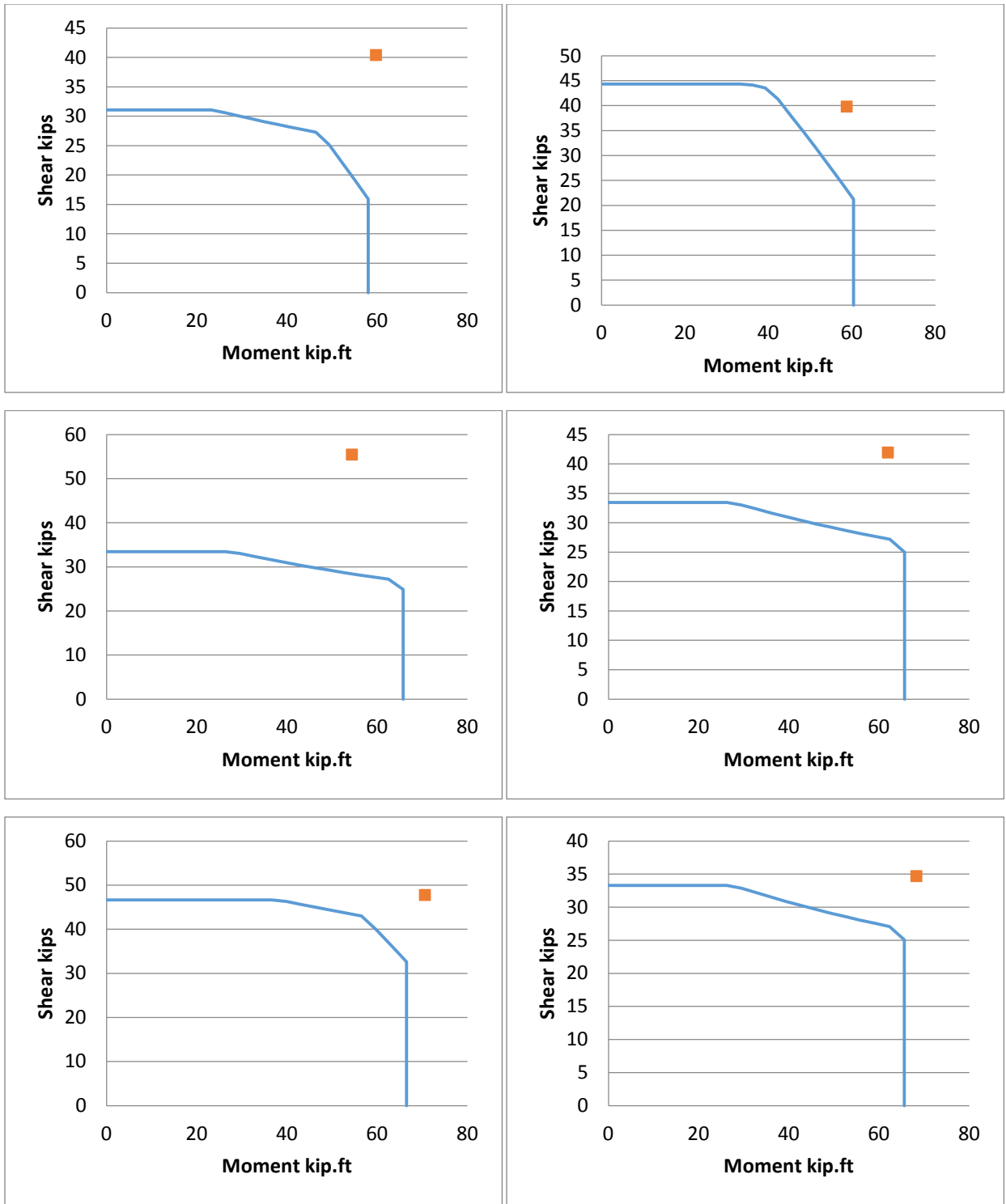
Figure 7.3: Arakawa et al. (1987) Interaction Diagrams (UNITs 15, 16, 17, 19, 20, and 21; Table 5.3)

83
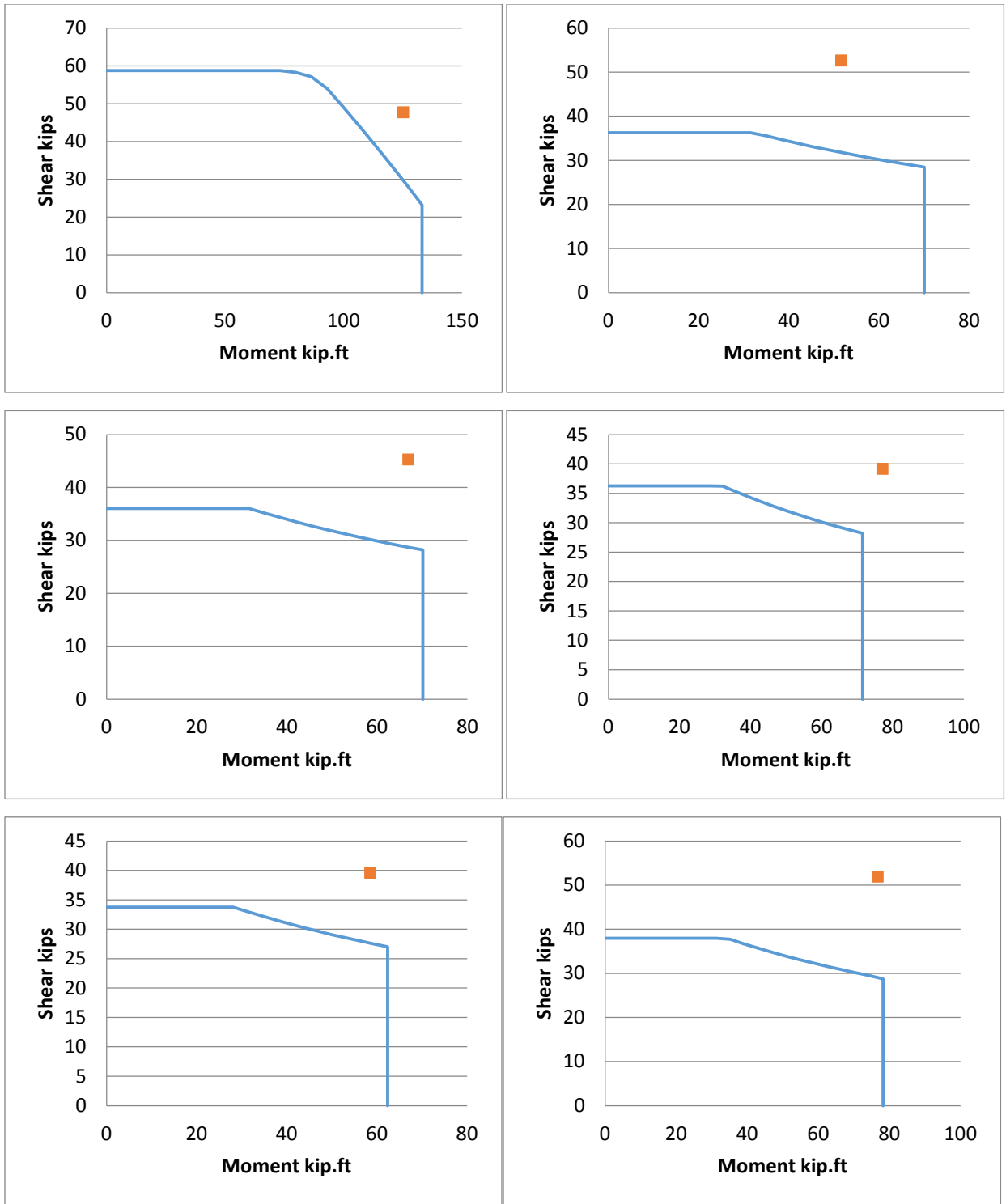
Figure 7.4: Arakawa et al. (1987) Interaction Diagrams (UNITs 23, 24, 25, 26, 27, and 28; Table 5.3)

84
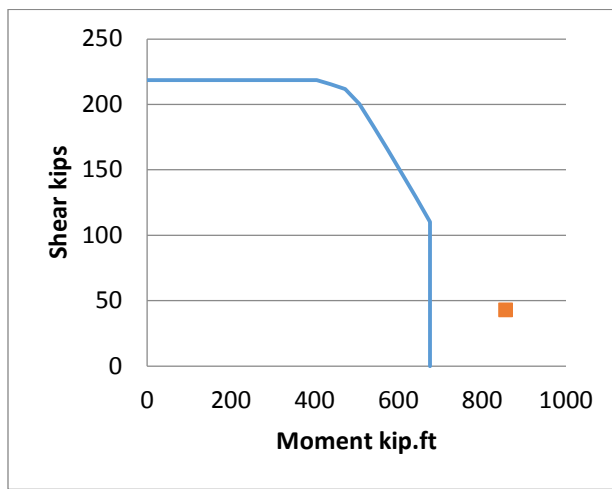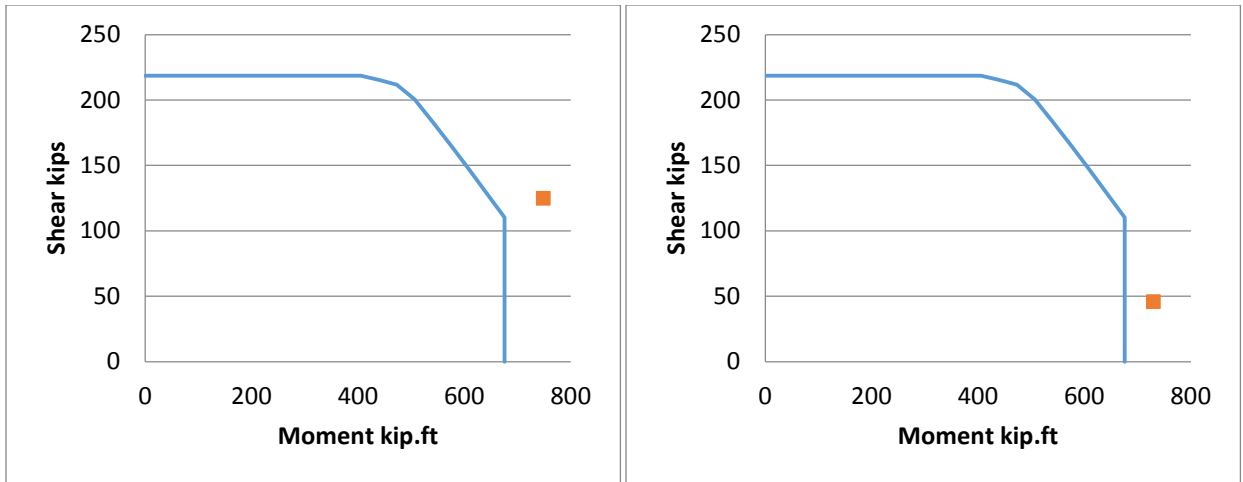
Figure 7.5: Calderone et al. (2001) Interaction Diagrams (Table 5.4)
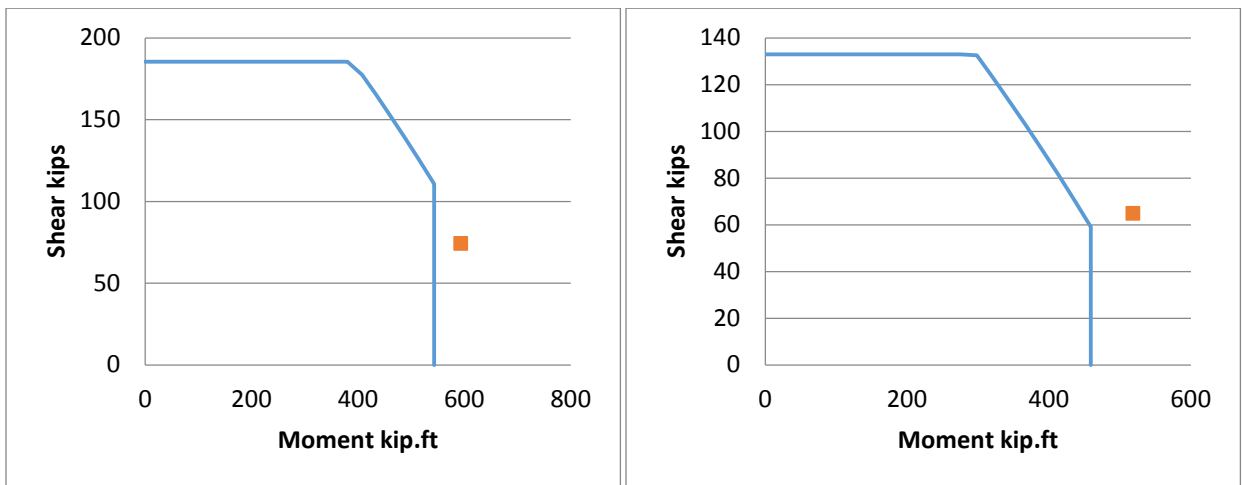
Figure 7.6: Henry and Mahin (1999) Interaction Diagrams (Table 5.5)

85
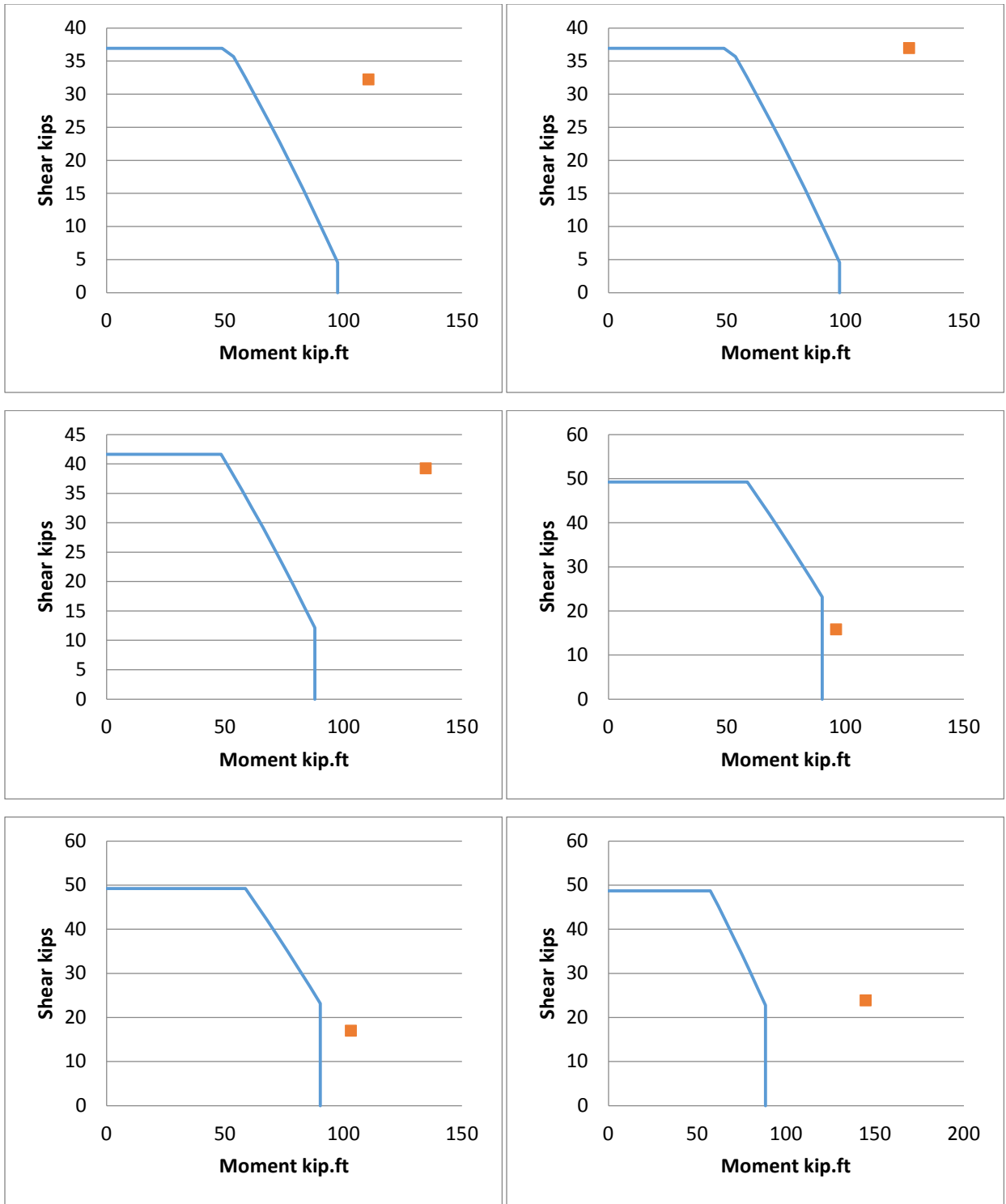
Figure 7.7: Hamilton et al. (2002) Interaction Diagrams (Table 5.6)
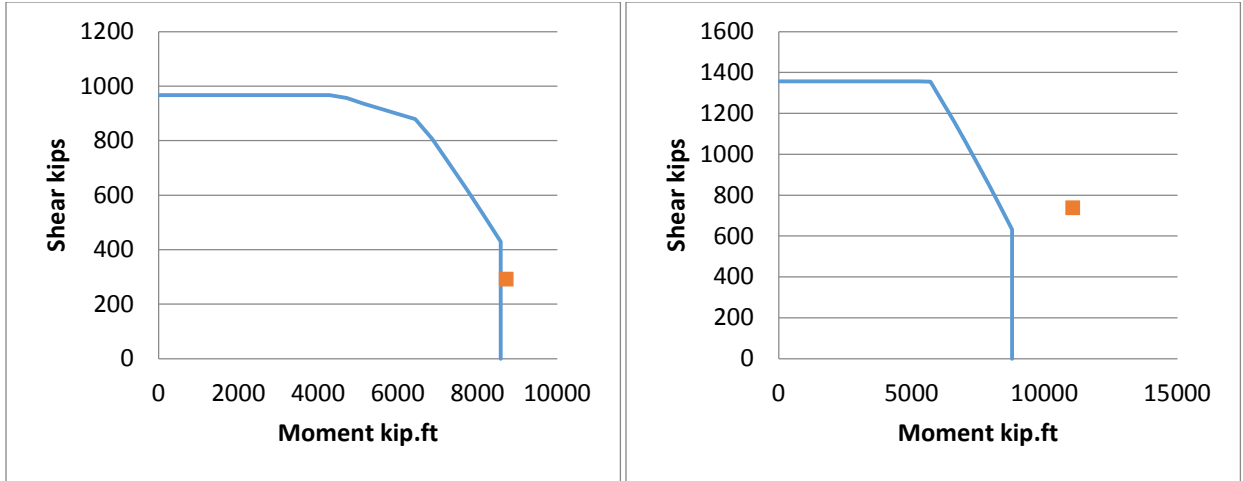
Figure 7.8: Cheok and Stone (1986) Interaction Diagrams (Table 5.7)
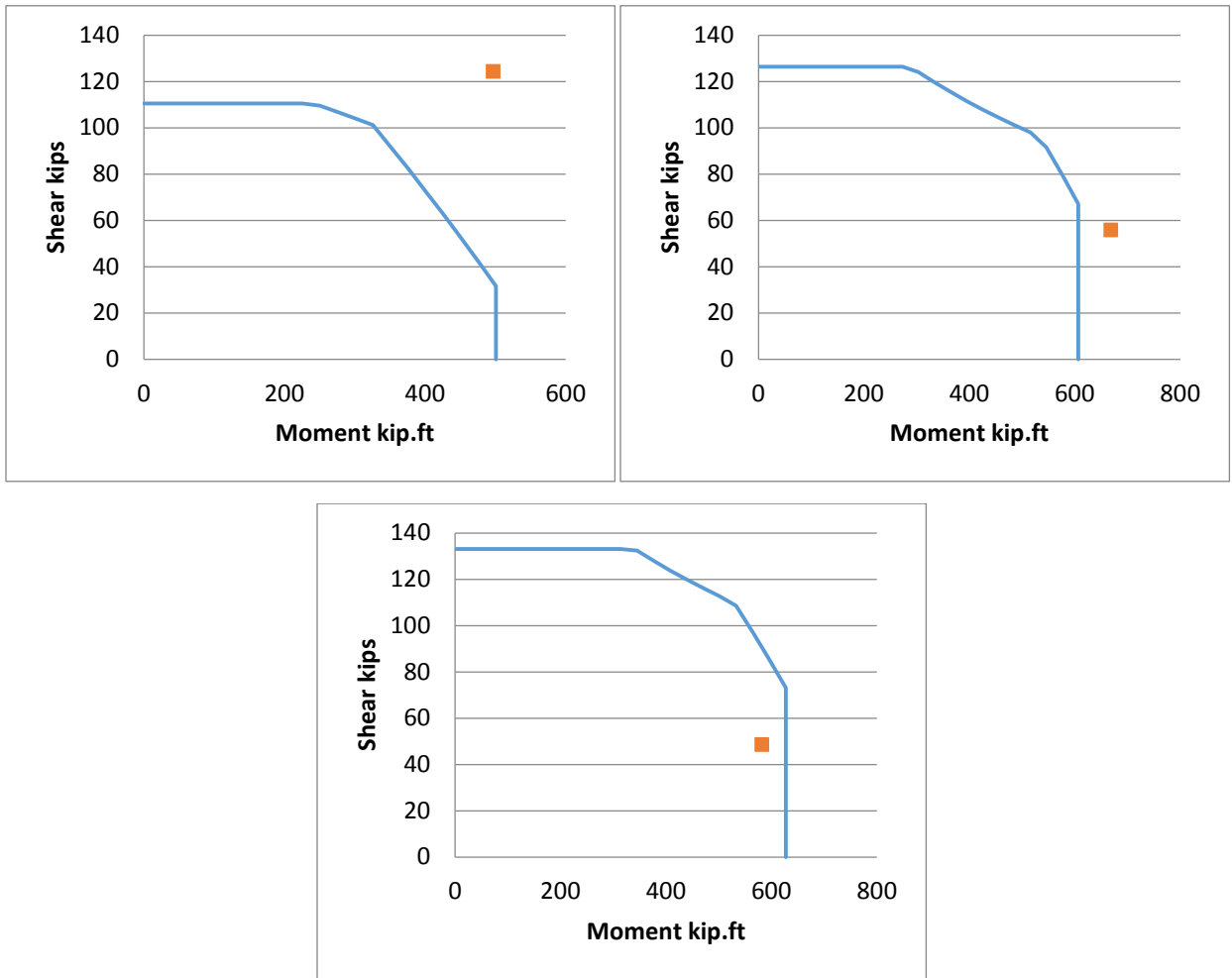
Figure 7.9: Chai et al. (1991) Interaction Diagrams (Table 5.8)
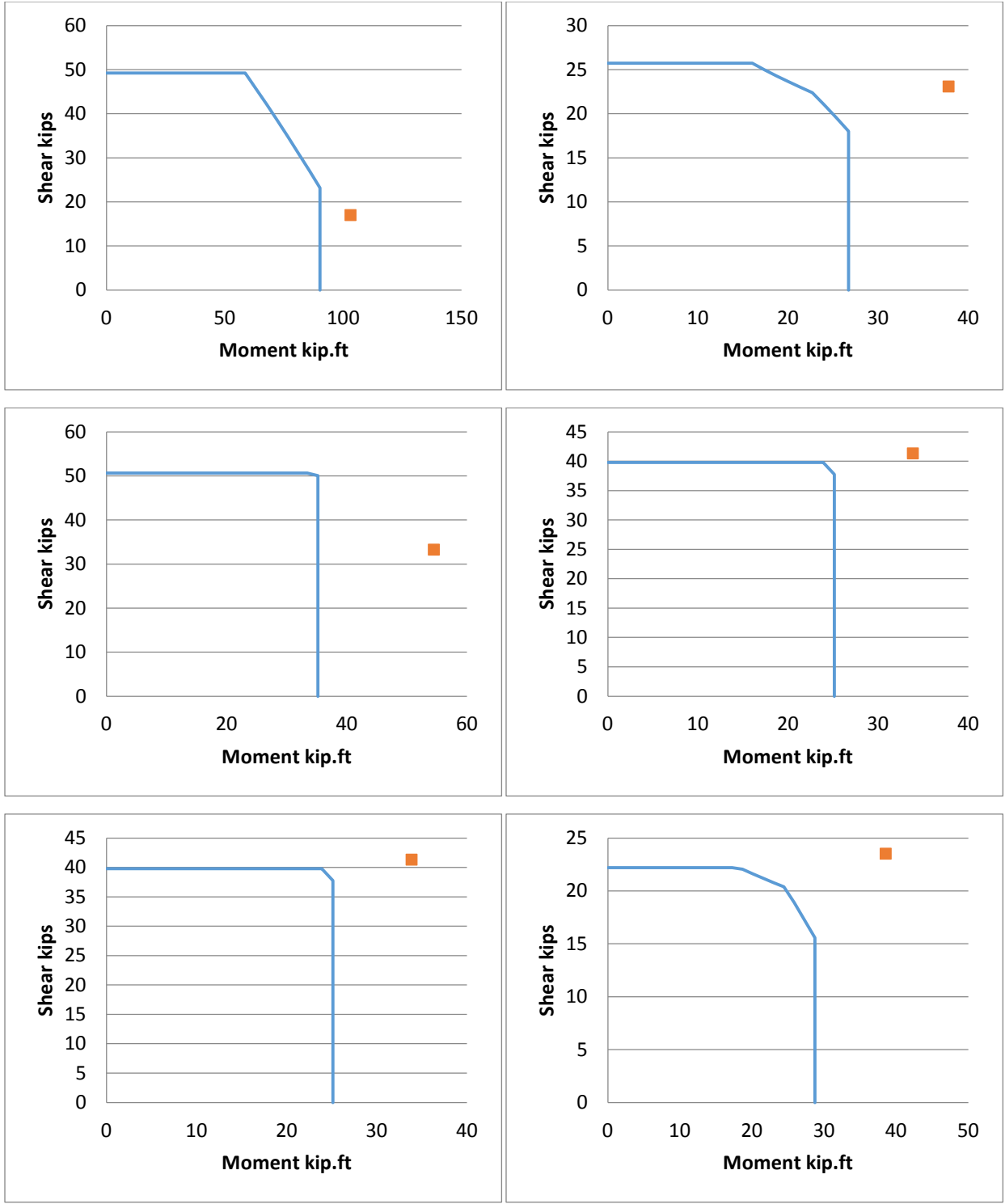
Figure 7.10: Siryo (1975) Interaction Diagrams (Table 5.9)
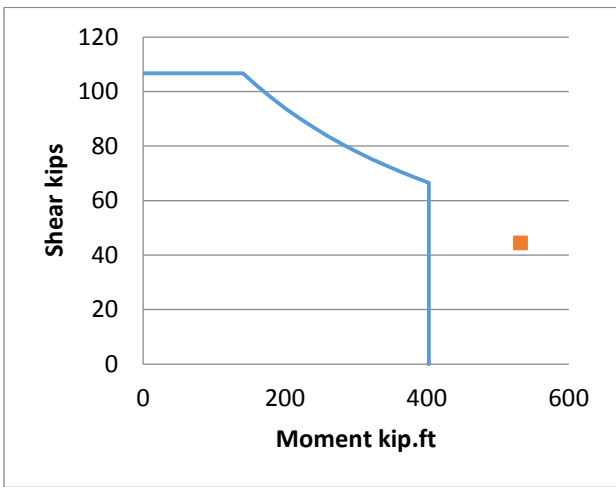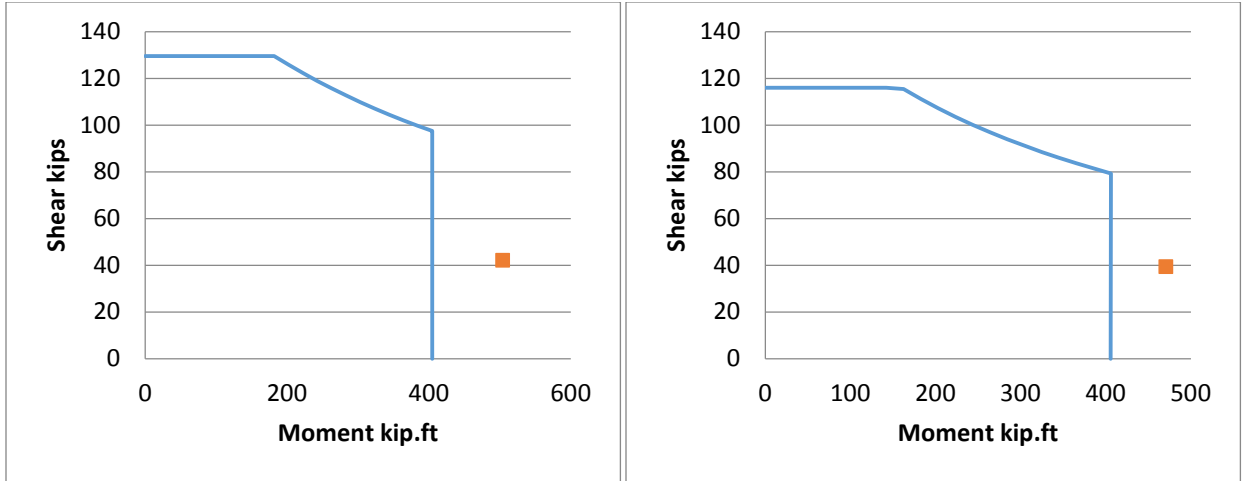
Figure 7.11: Kowalsky and Priestley (2000) Interaction Diagrams (Table 5.10)
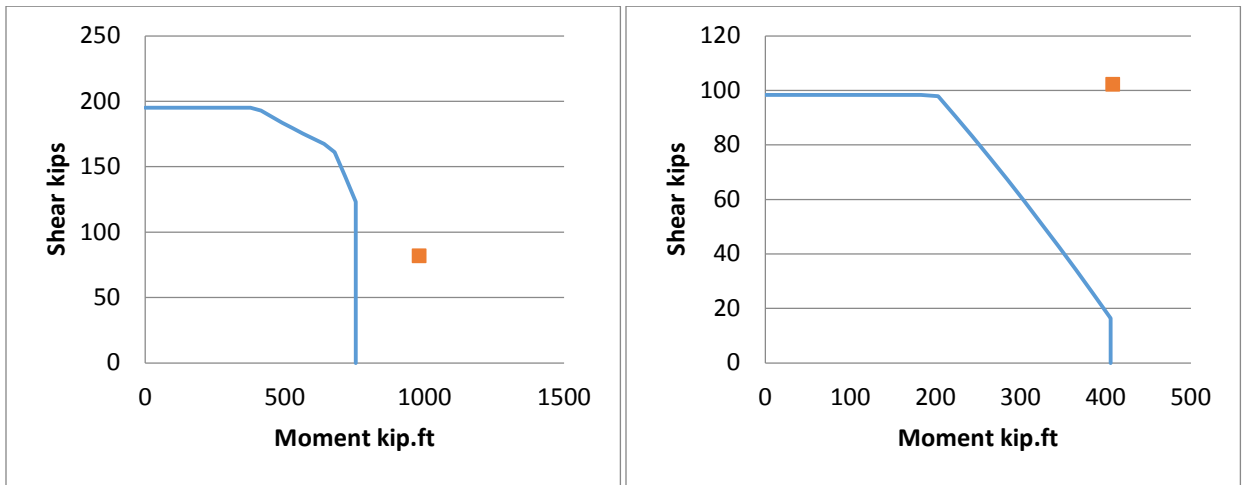
Figure 7.12: Hose et al. (1997; left) and Elsanadedy (2002; right) Interaction Diagrams (Table 5.11)
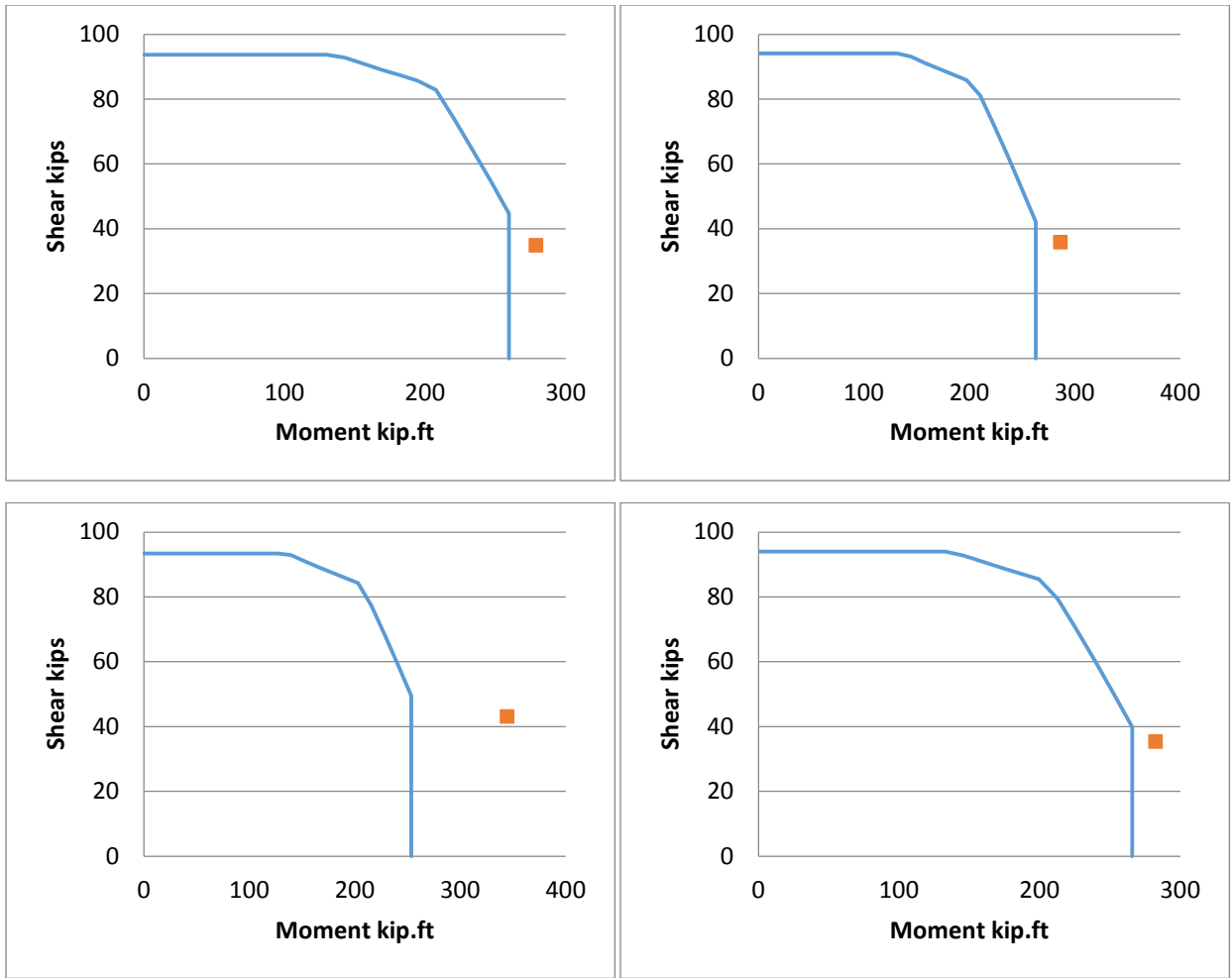
Figure 7.13: Moyer and Kowalsky (2003) Interaction Diagrams (Table 5.12)
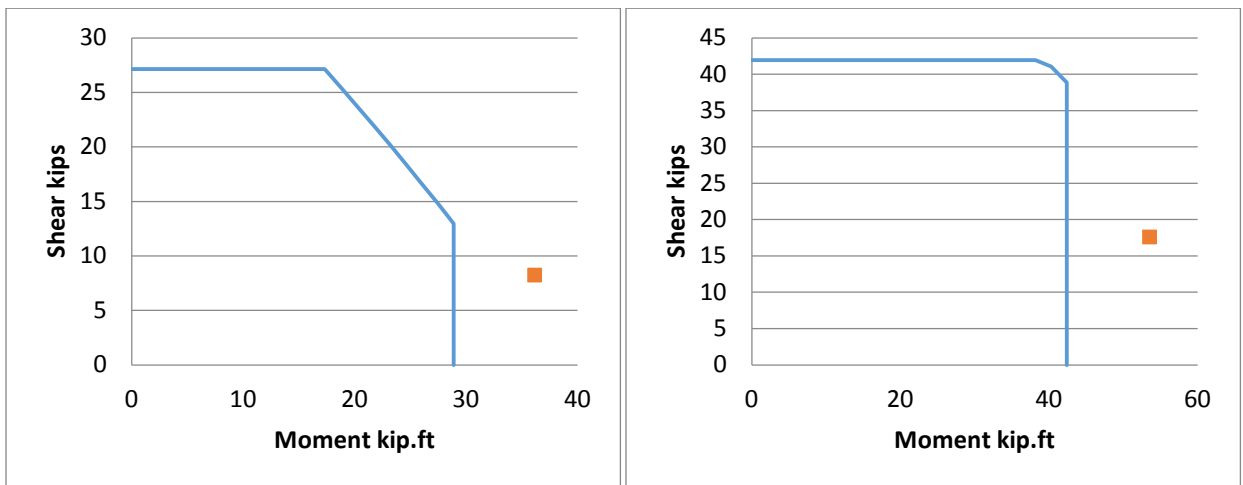
Figure 7.14: Ng et al. (2010) Interaction Diagrams (Table 5.13)
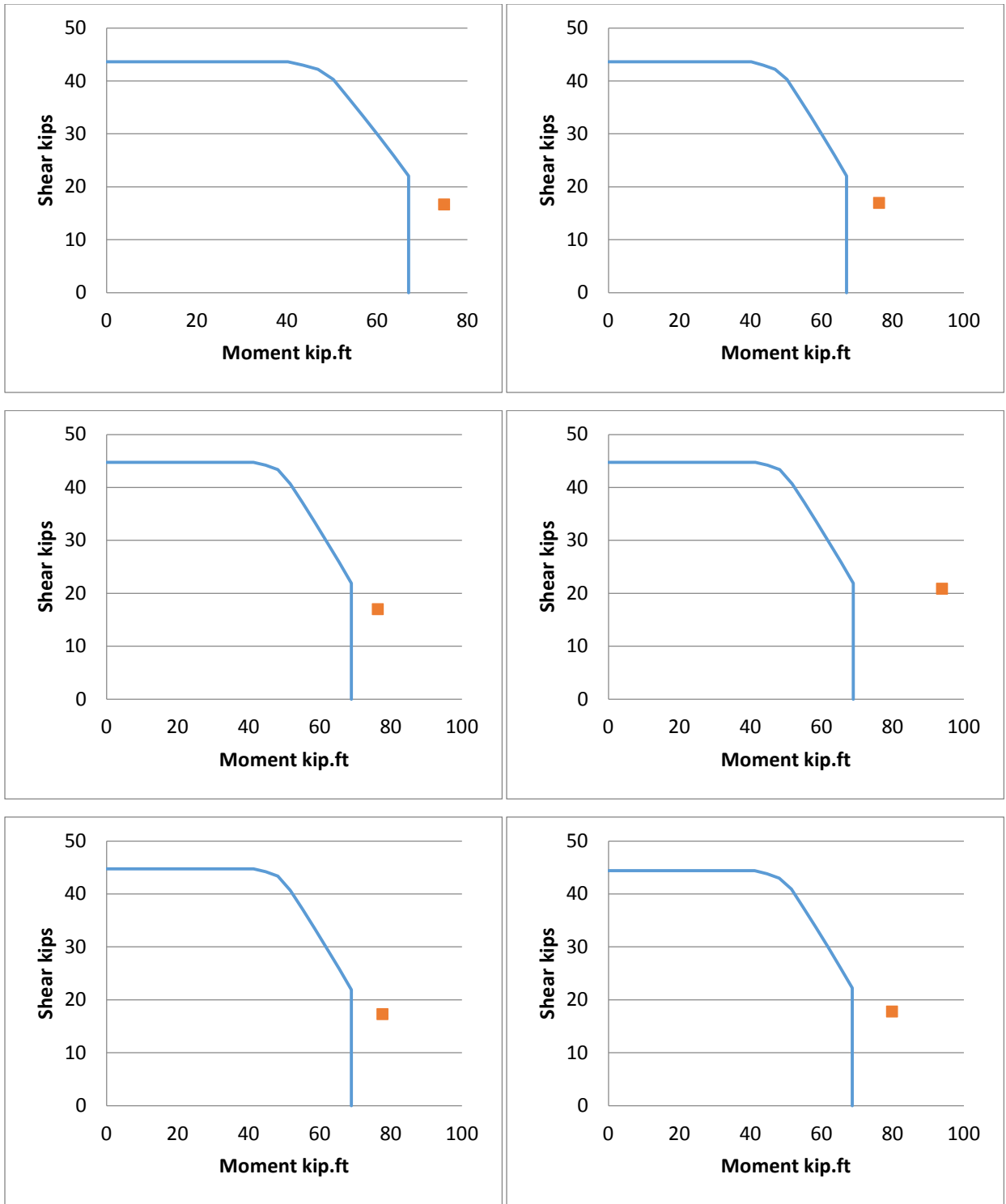
Figure 7.15: Kunnath et al. (1997) Interaction Diagrams (UNITs A2-A7; Table 5.14)
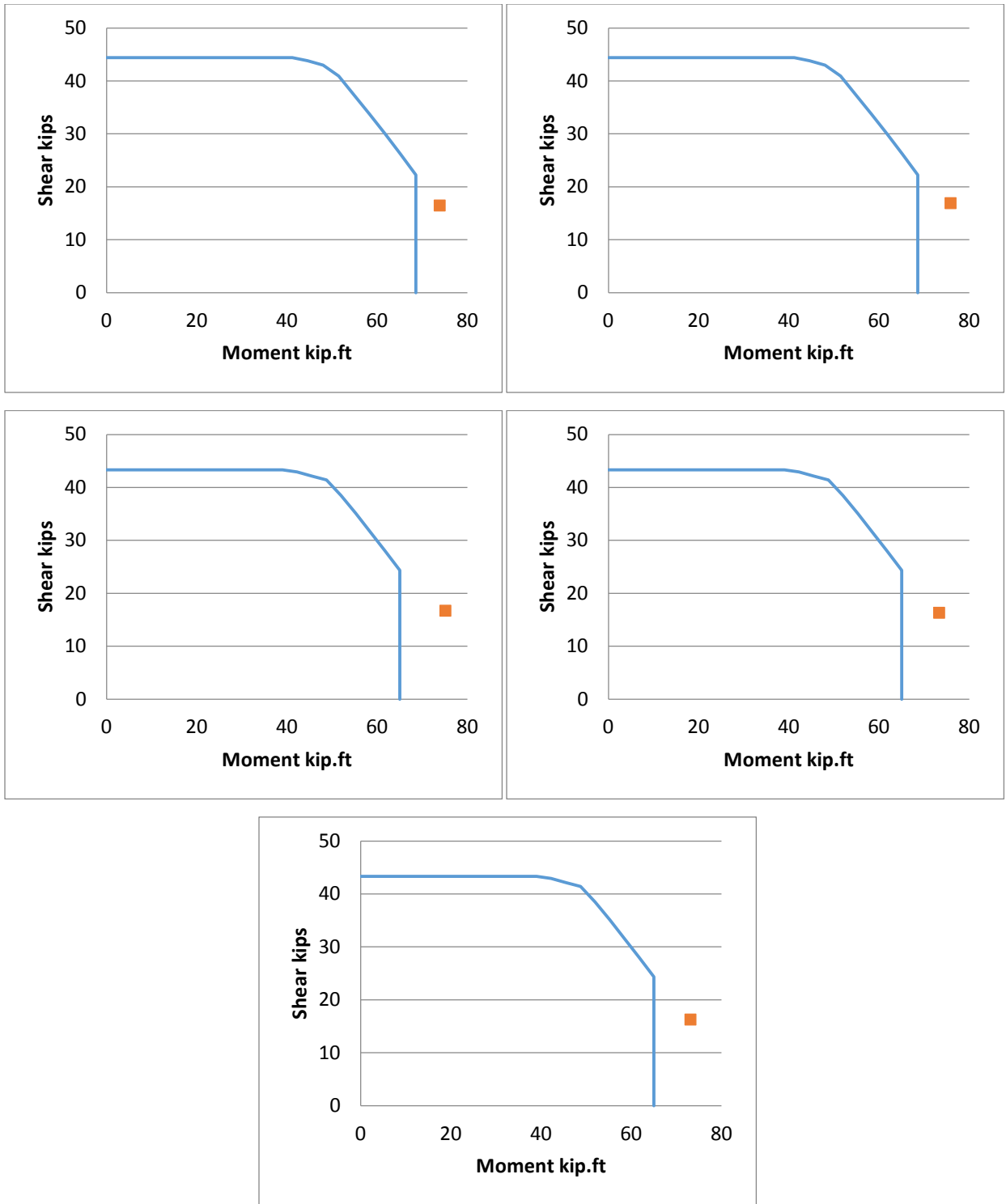
Figure 7.16: Kunnath et al. (1997) Interaction Diagrams (UNITs A8-A12; Table 5.14)
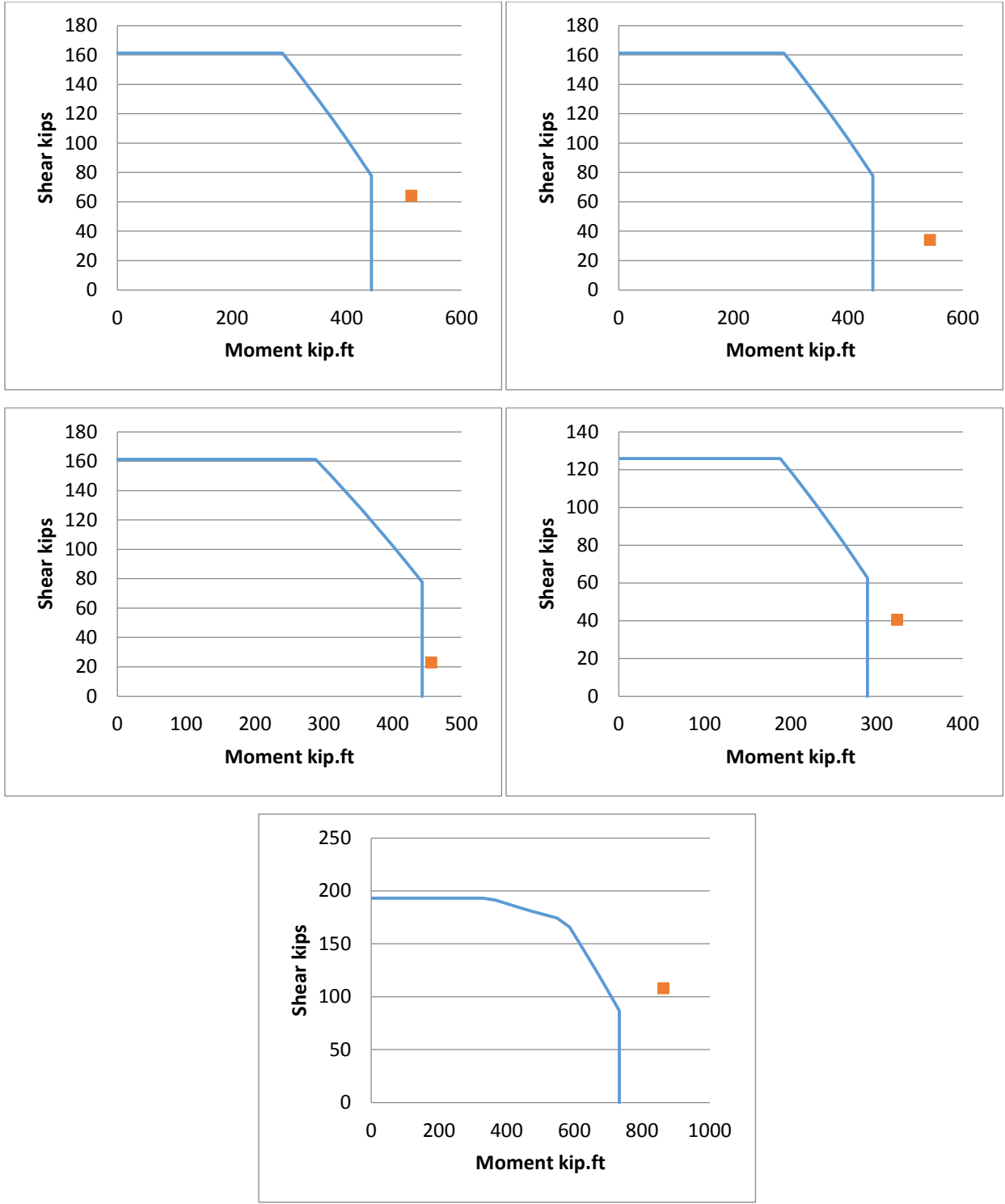
Figure 7.17: Lehman and Moehle (2000) Interaction Diagrams (Table 5.15)
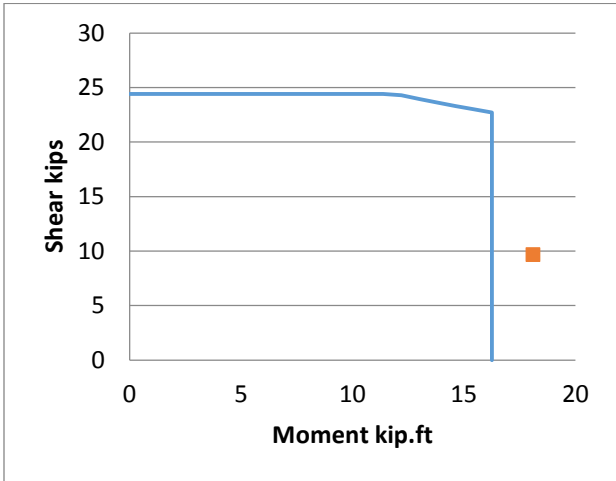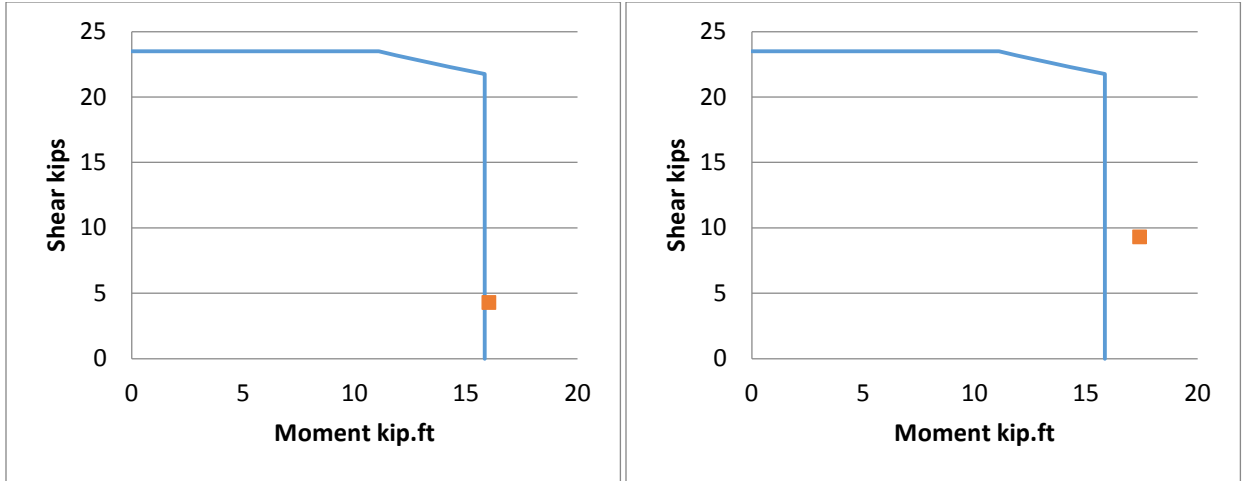
Figure 7.18: Lim and McLean (1991) Interaction Diagrams (Table 5.16)
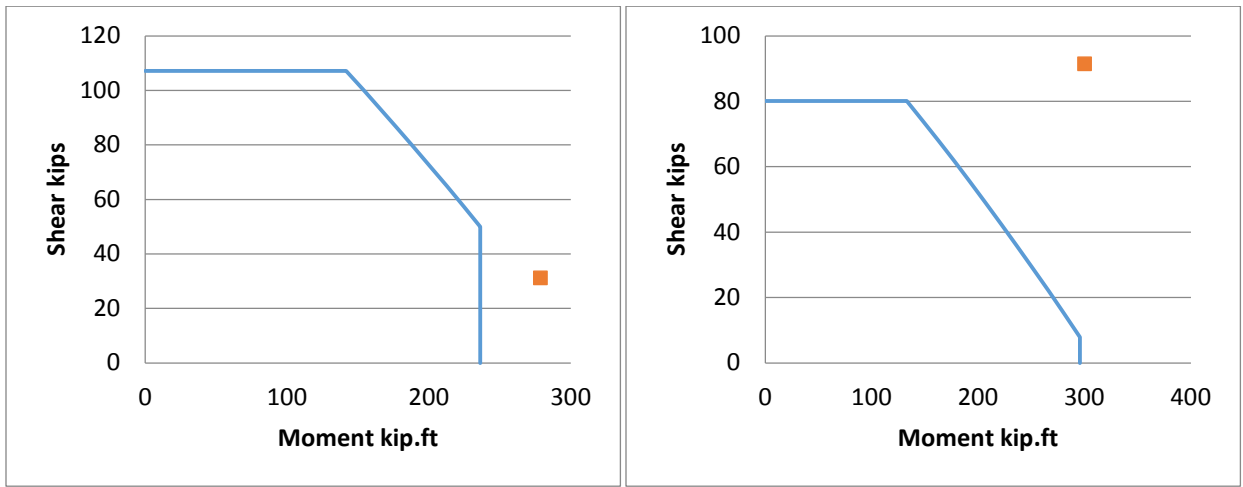
Figure 7.19: Munro et al. (1976; left) and Iwasaki et al. (1986; right) Interaction Diagrams (Table 5.17)
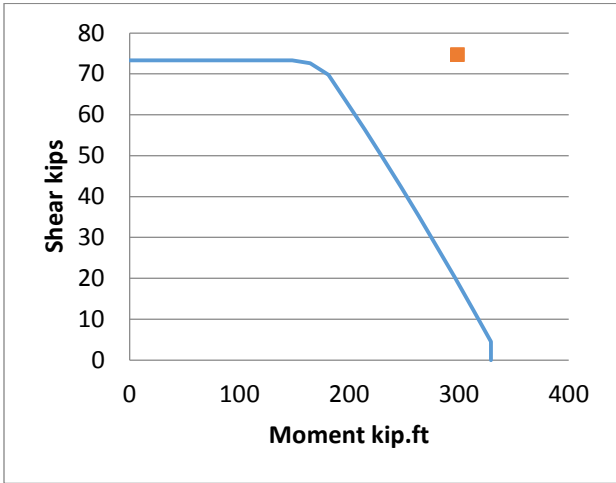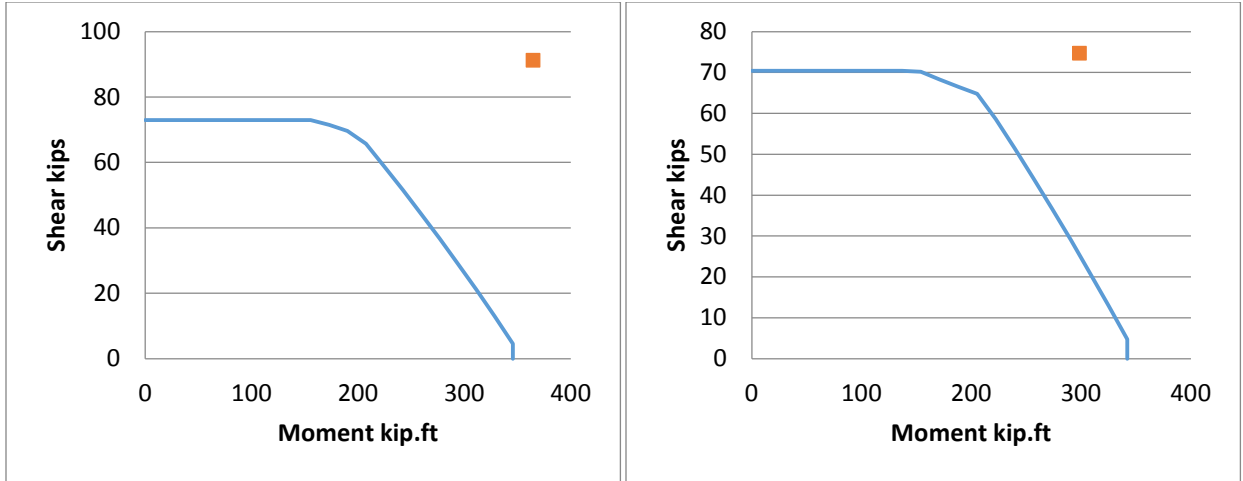
Figure 7.20: McDaniel (1997) Interaction Diagrams (Table 5.18)
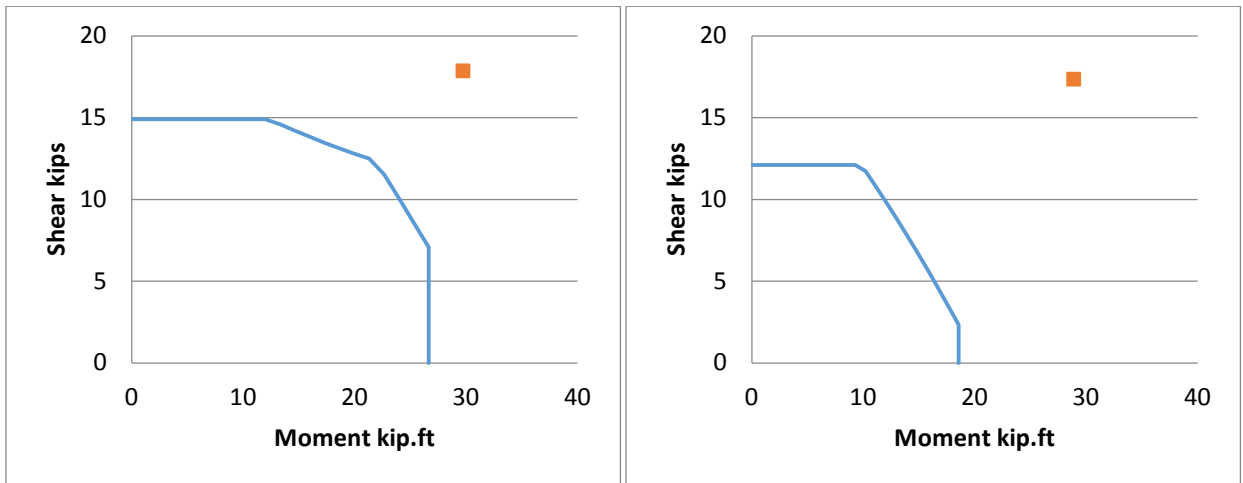
Figure 7.21: Jaradat (1996) Interaction Diagrams (Table 5.19)

95
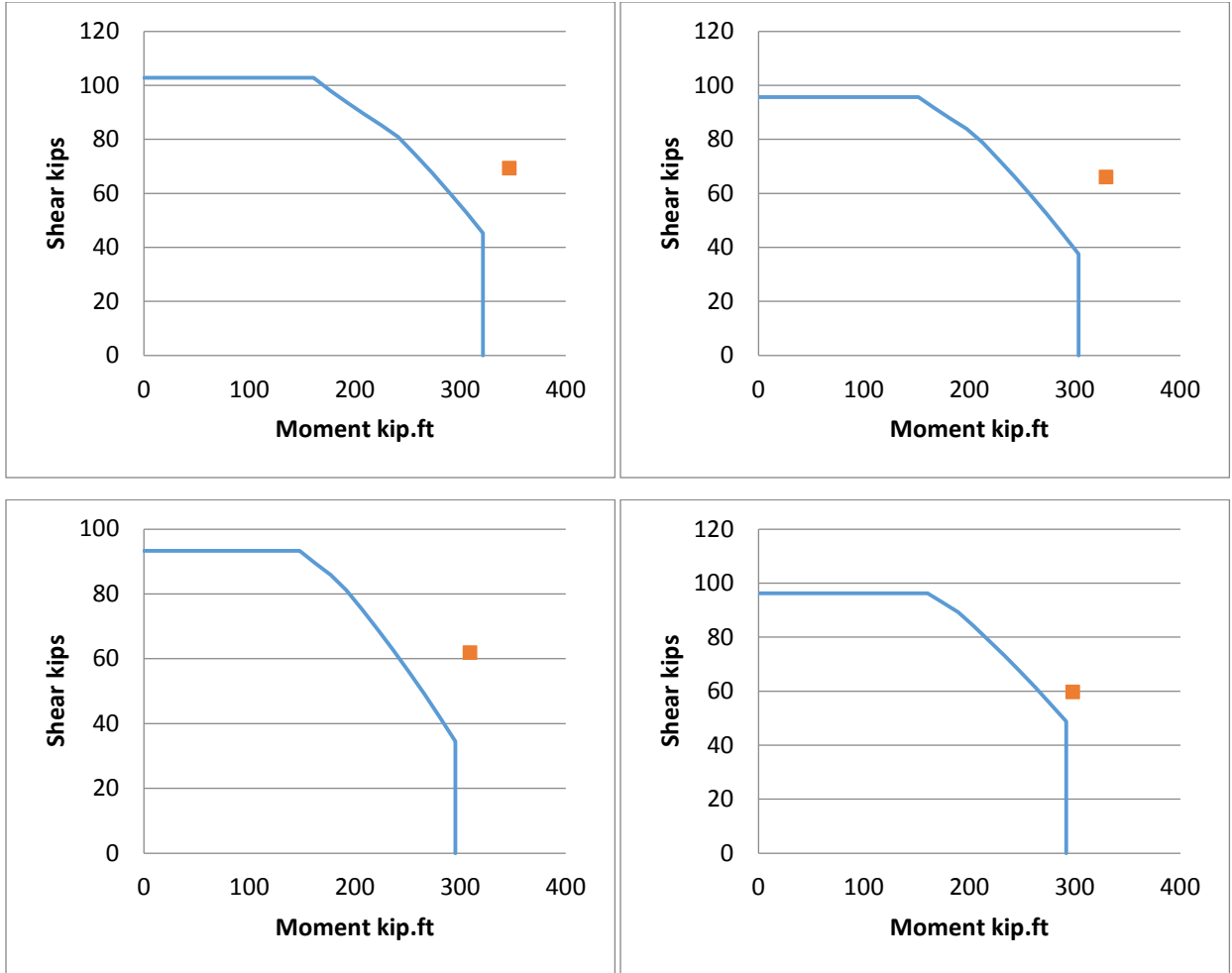
Figure 7.22: Nelson (2000) Interaction Diagrams (Table 5.20)
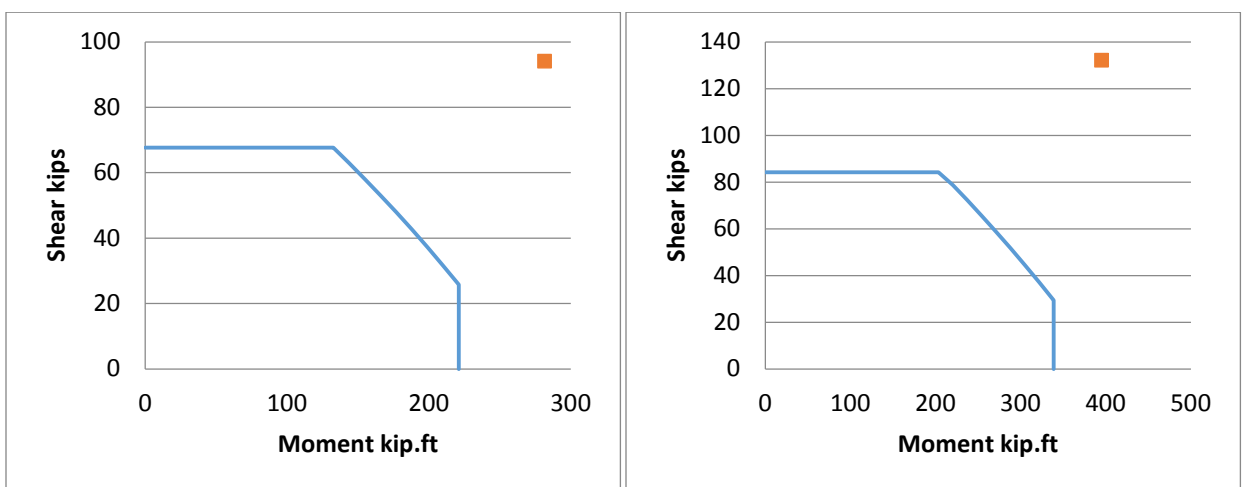
Figure 7.23: Priestley et al. (1994) Interaction Diagrams (Table 5.21)
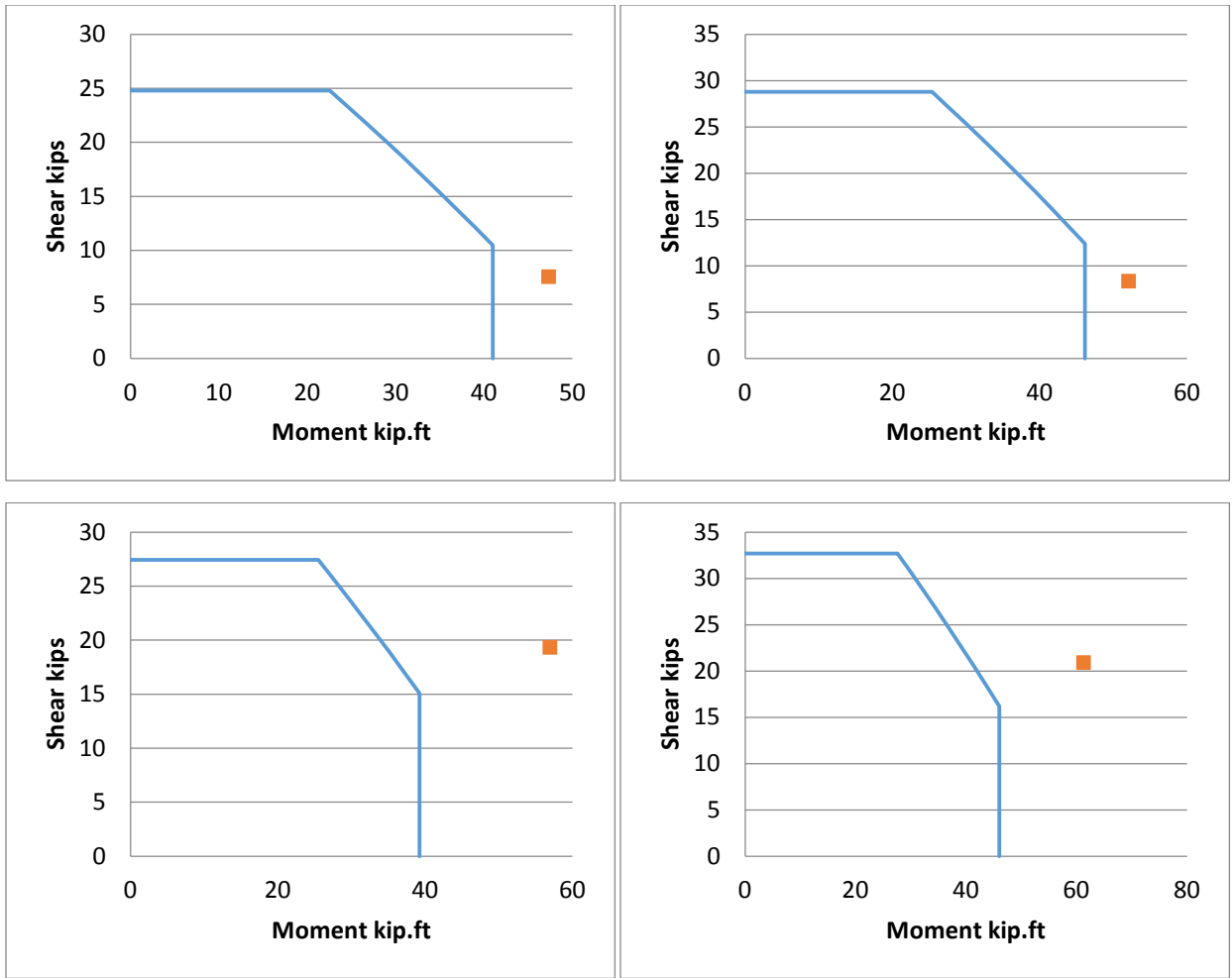
Figure 7.24: Petrovski and Ristic (1984) Interaction Diagrams (Table 5.22)
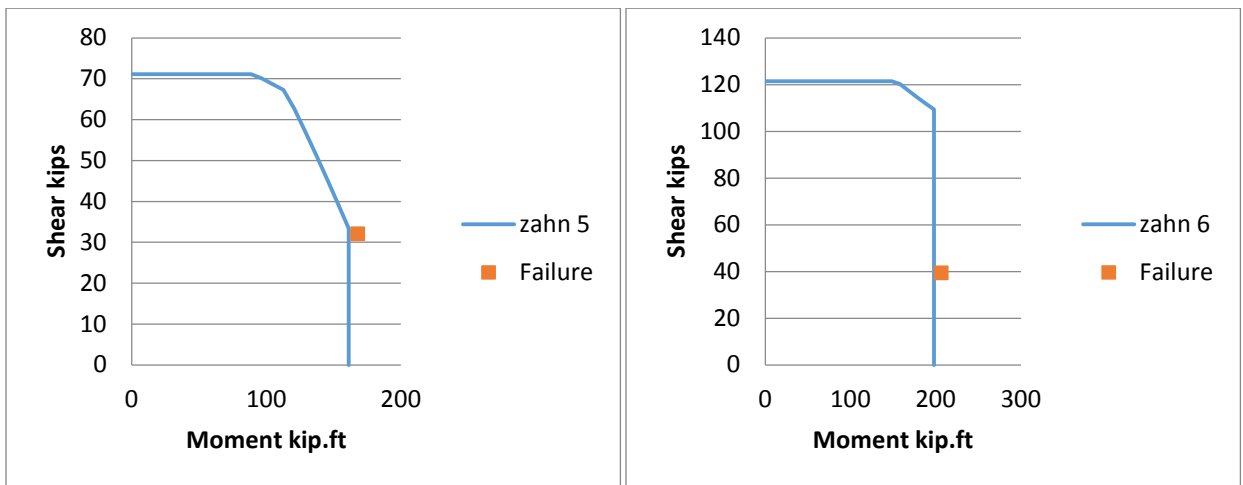
Figure 7.25: Zahn et al. (1986) Interaction Diagrams (Table 5.23)
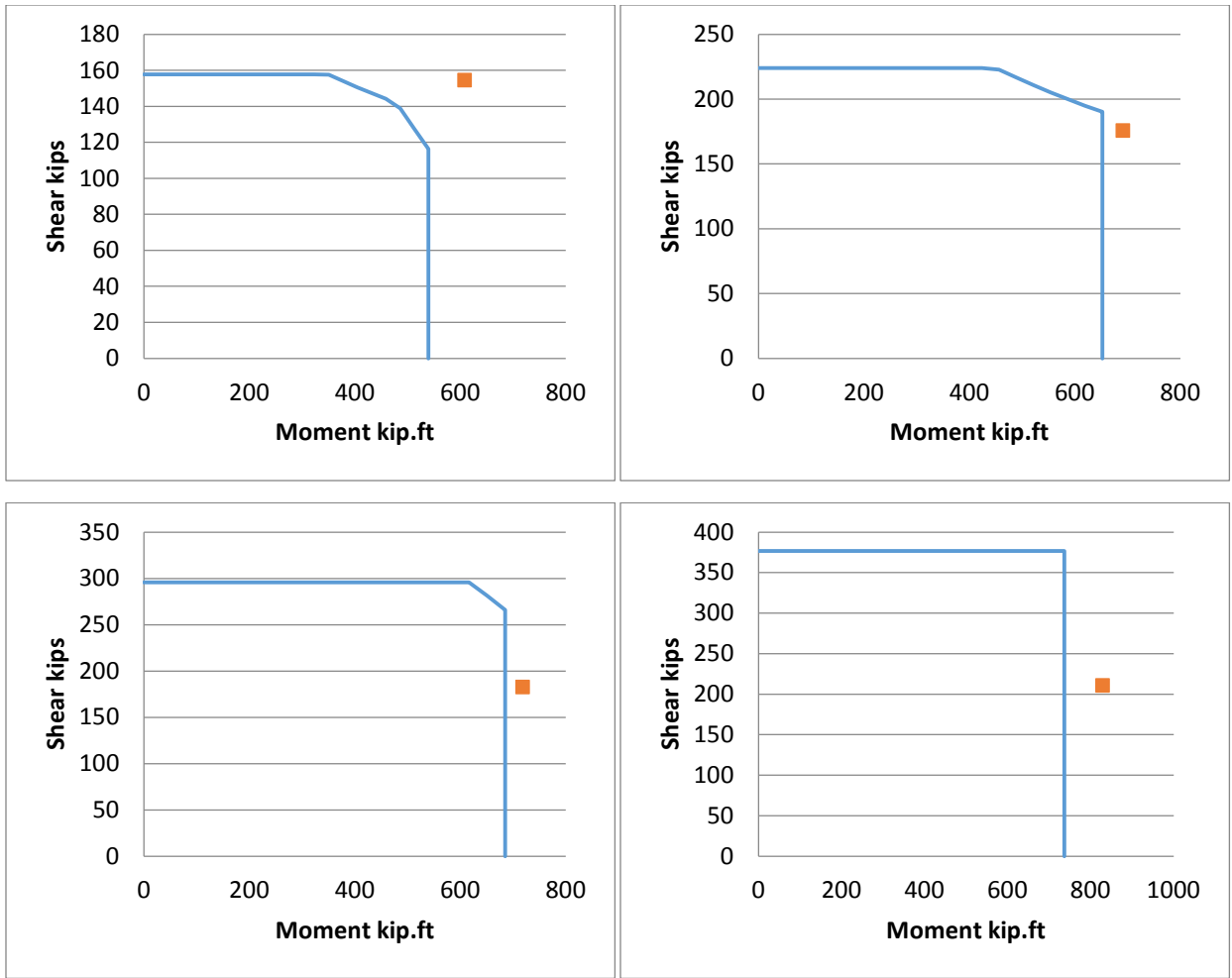
Figure 7.26: Pontangaroa et al. (1979) Interaction Diagrams (Table 5.24)
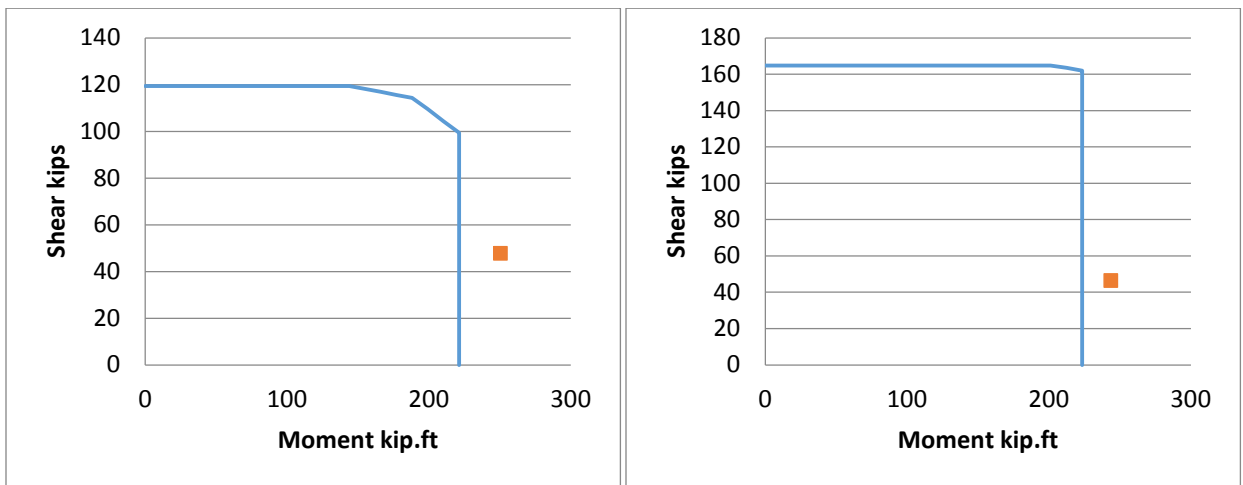
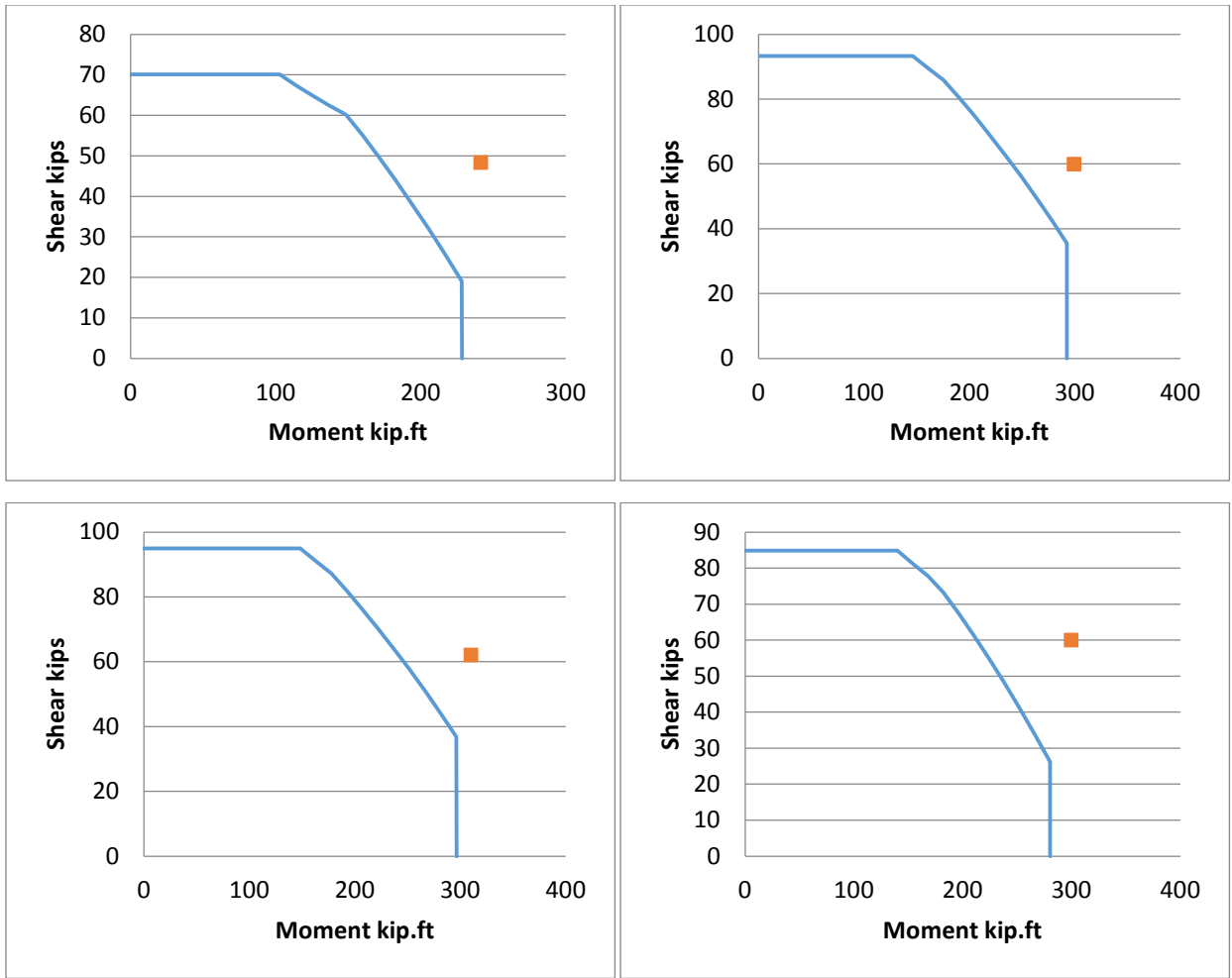**Figure 7.27: Watson and Park (1994) Interaction Diagrams (Table 5.25)**

Figure 7.28: Ranf et al. (2006) Interaction Diagrams (Table 5.26)
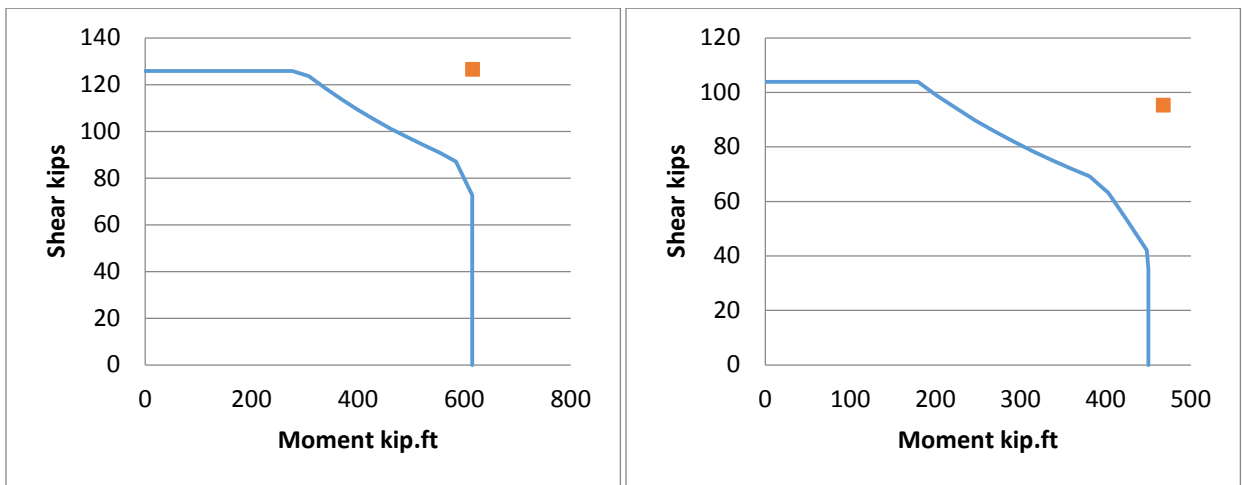

Figure 7.29: Yalcin (1997; left) and Yarandi (2007; right) Interaction Diagrams (Table 5.27)
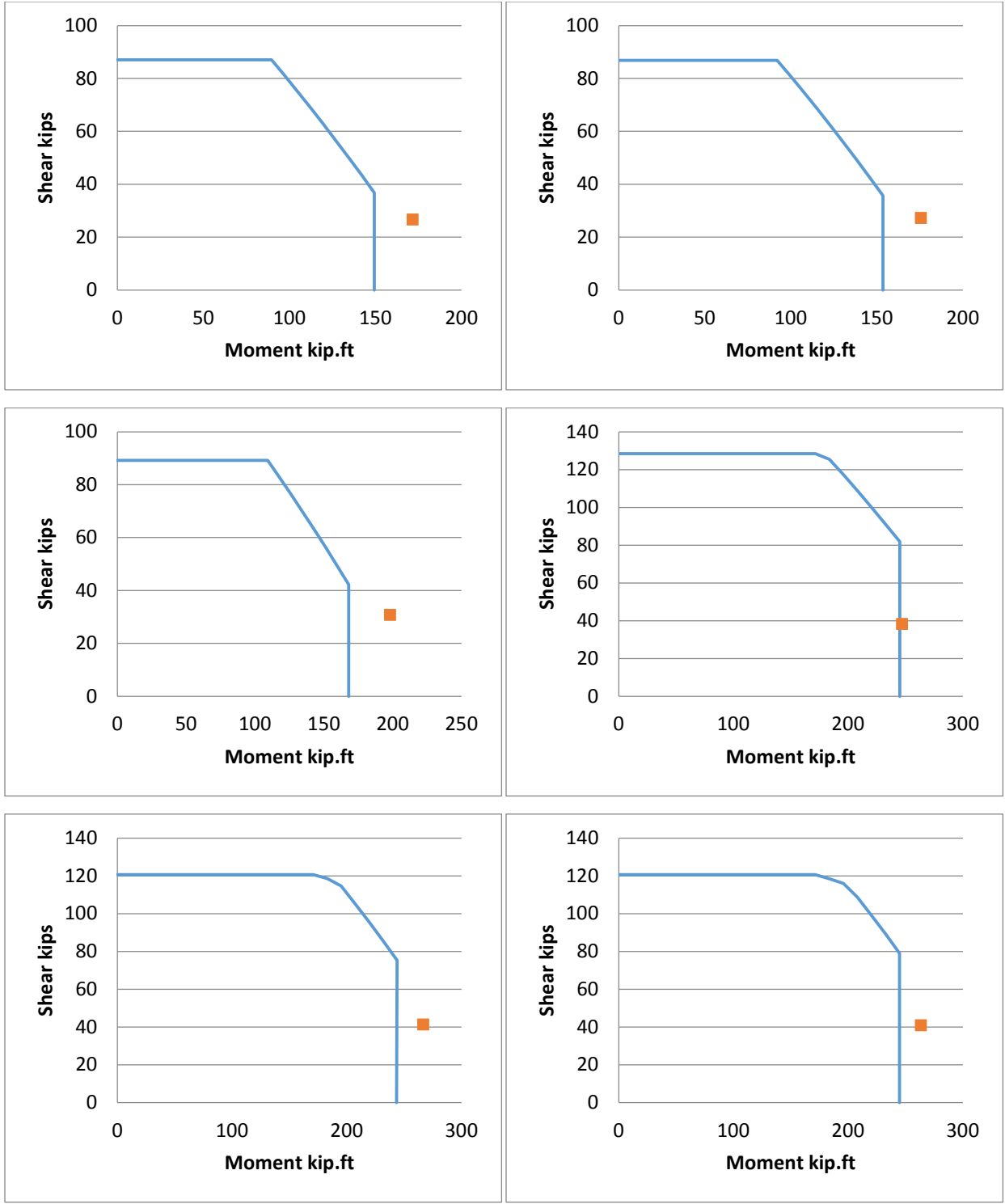
Figure 7.30: Roeder et al. (2001) Interaction Diagrams (Units C1-C6; Table 5.28)
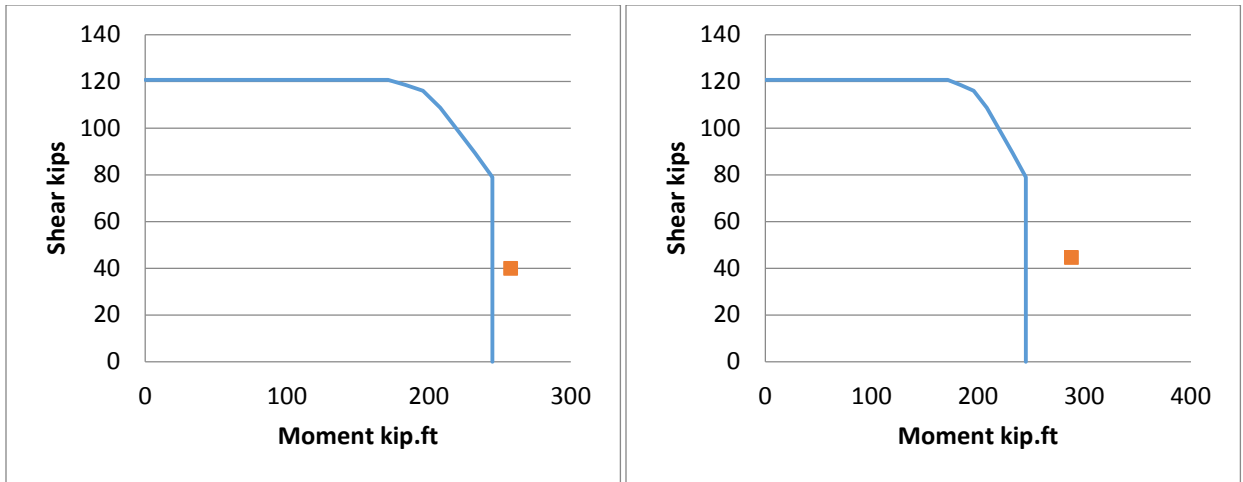
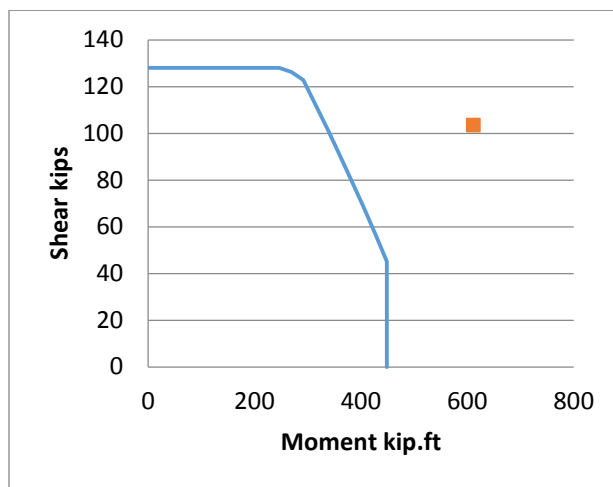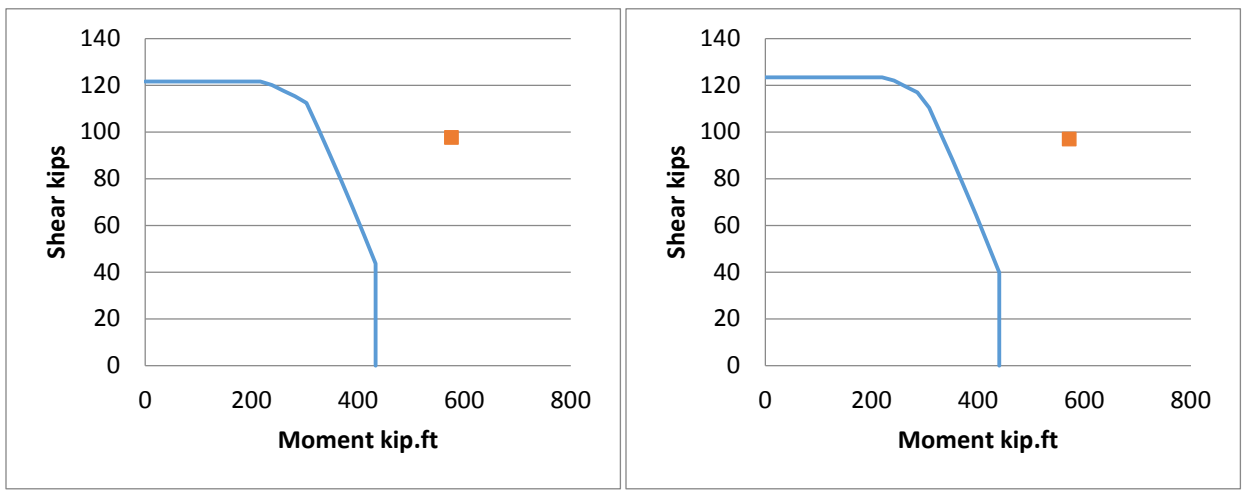**Figure 7.31: Roeder et al. (2001) Interaction Diagrams (Units C7, C8; Table 5.28)**

Figure 7.32: Sritharan et al. (2001) Interaction Diagrams (Table 5.29)
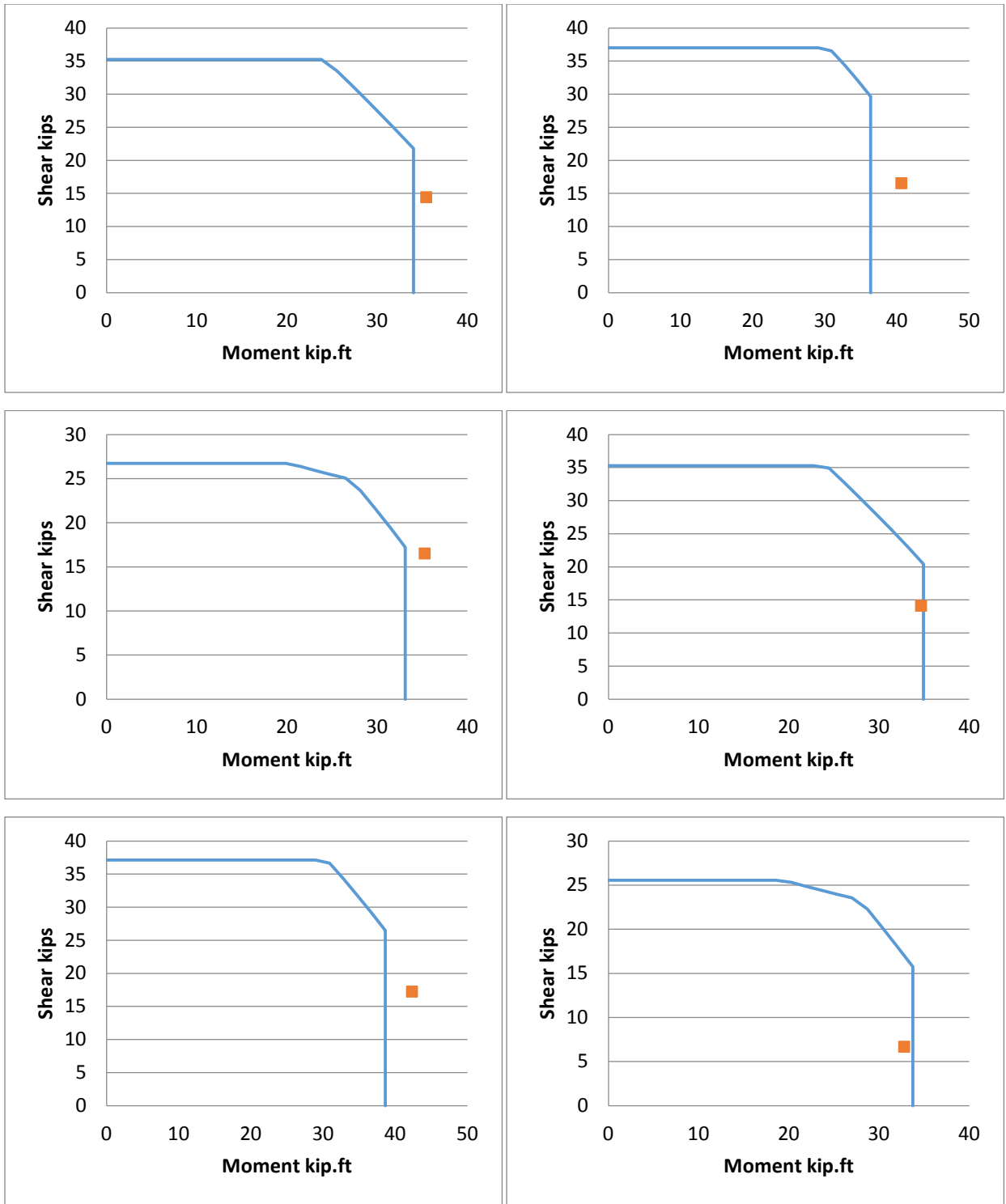
101

Figure 7.33: Stone and Cheok (1989) Interaction Diagrams (Table 5.30)
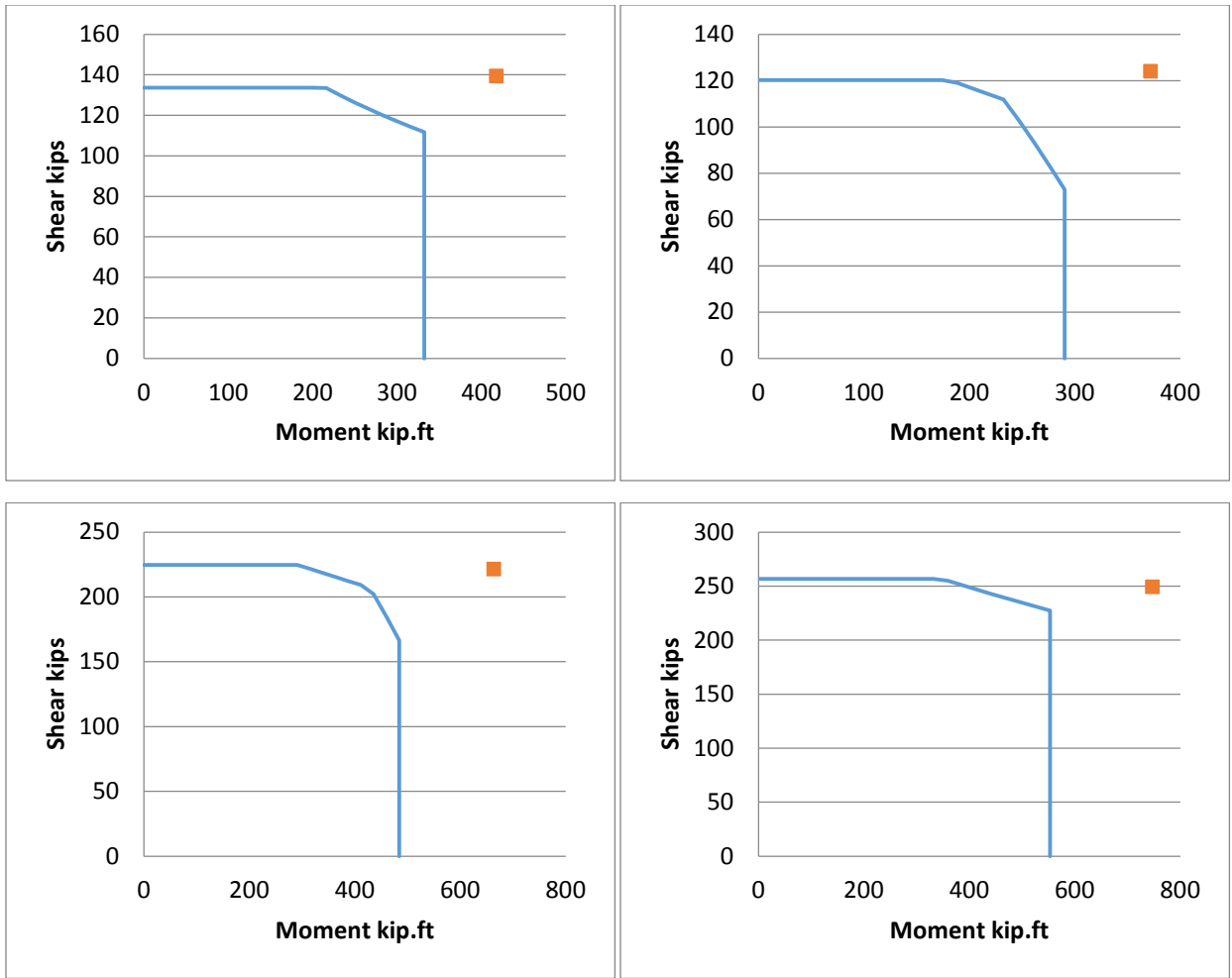
Figure 7.34: Vu et al. (1998) Interaction Diagrams (Table 5.31)

Figure 7.35: Wong (1990) Interaction Diagrams (Table 5.32)

Figure 7.36: Ang et al. (1985) Interaction Diagrams (UNITs 1-6; Table 5.33)

105

Figure 7.37: Ang et al. (1985) Interaction Diagrams (UNITs 7-12; Table 5.33)

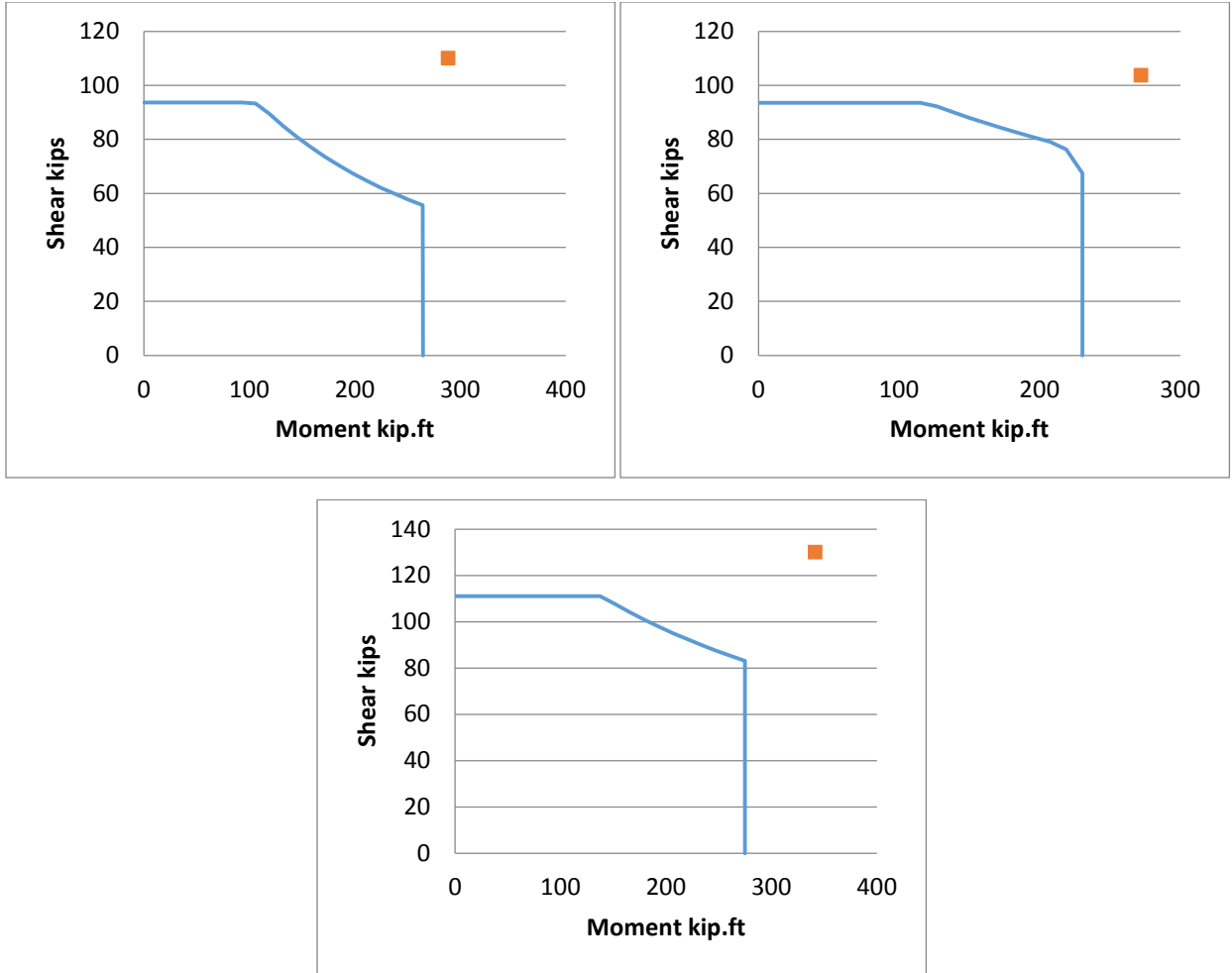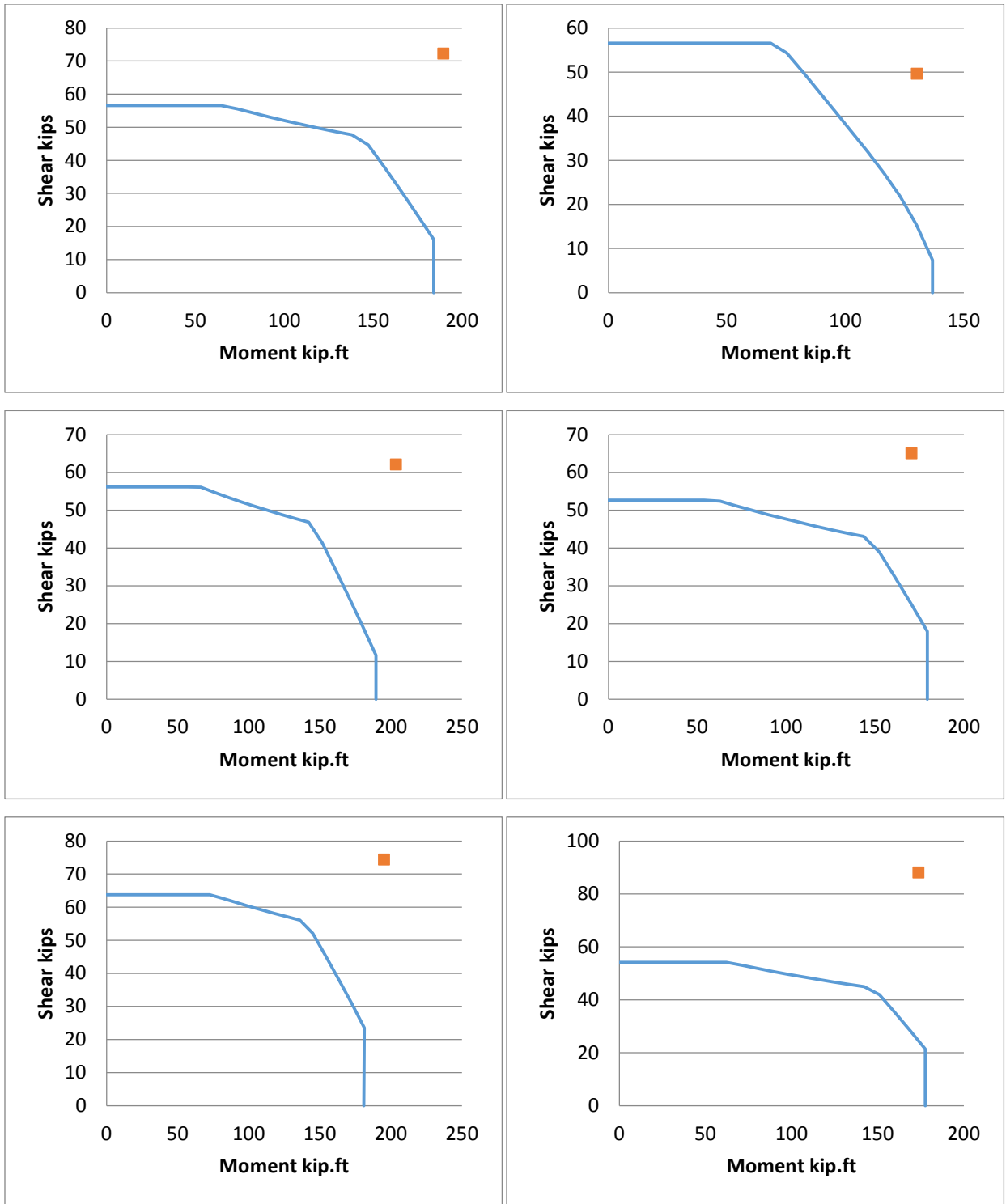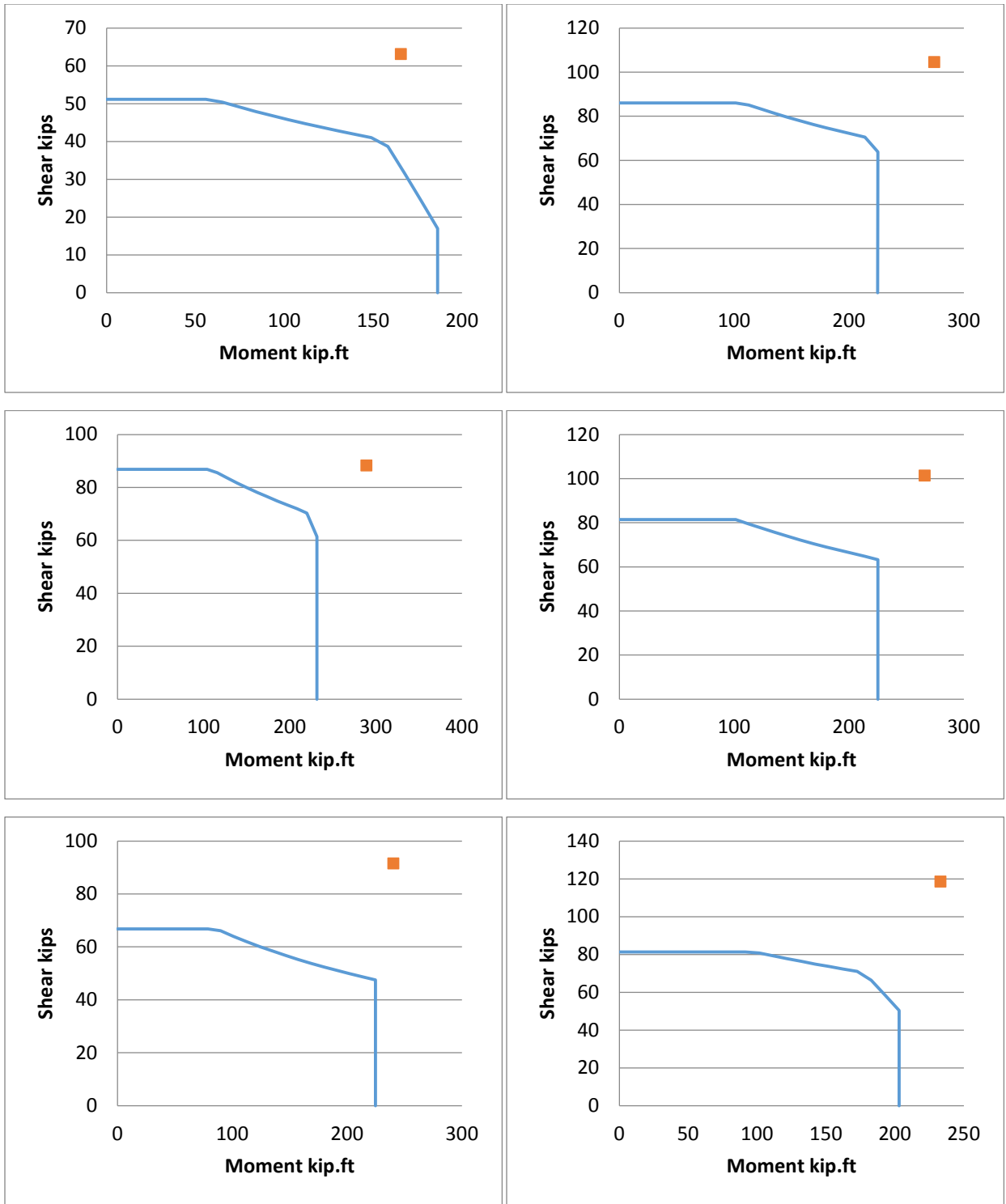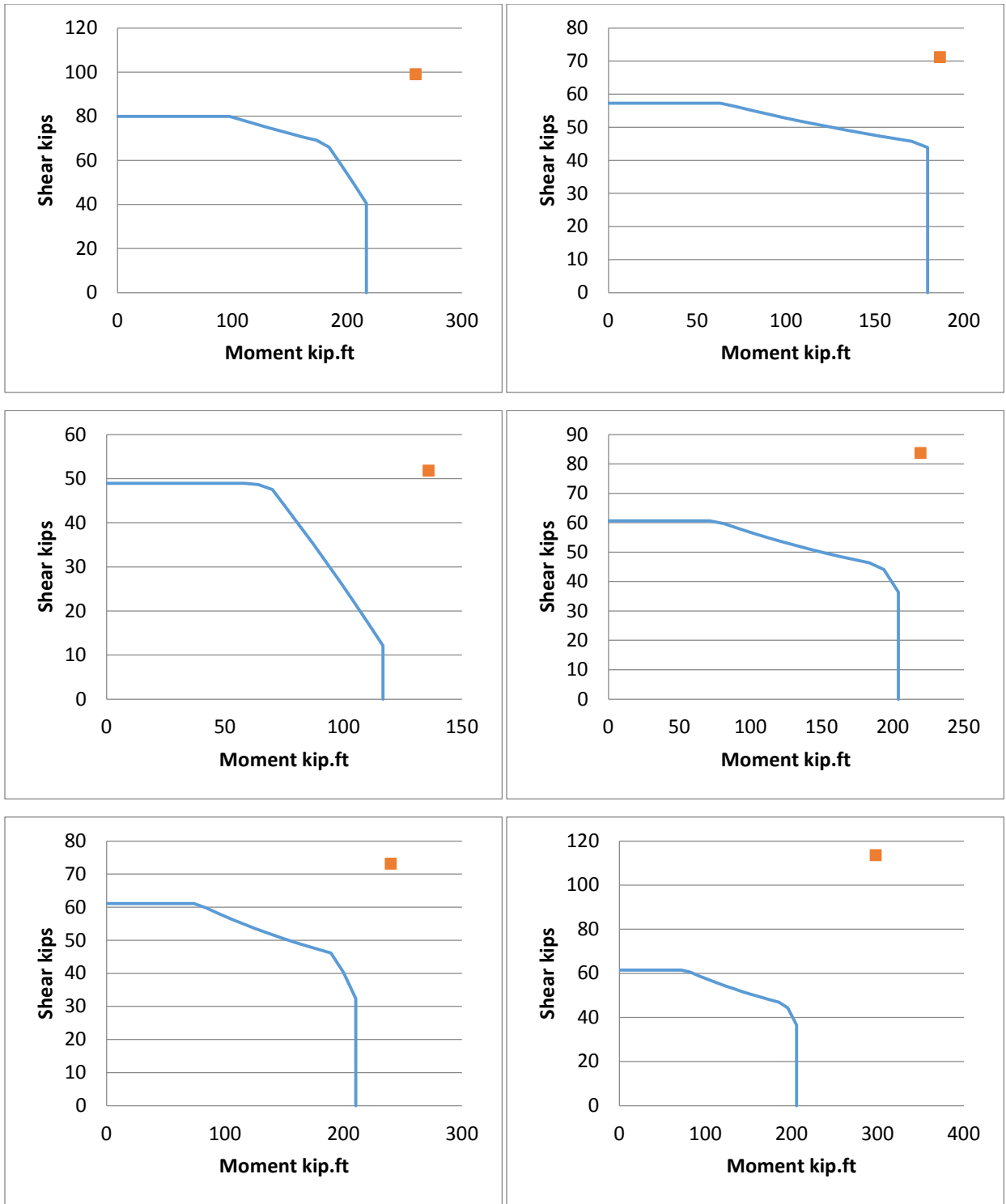**Figure 7.38: Ang et al. (1985) Interaction Diagrams (UNITs 13-18; Table 5.33)**
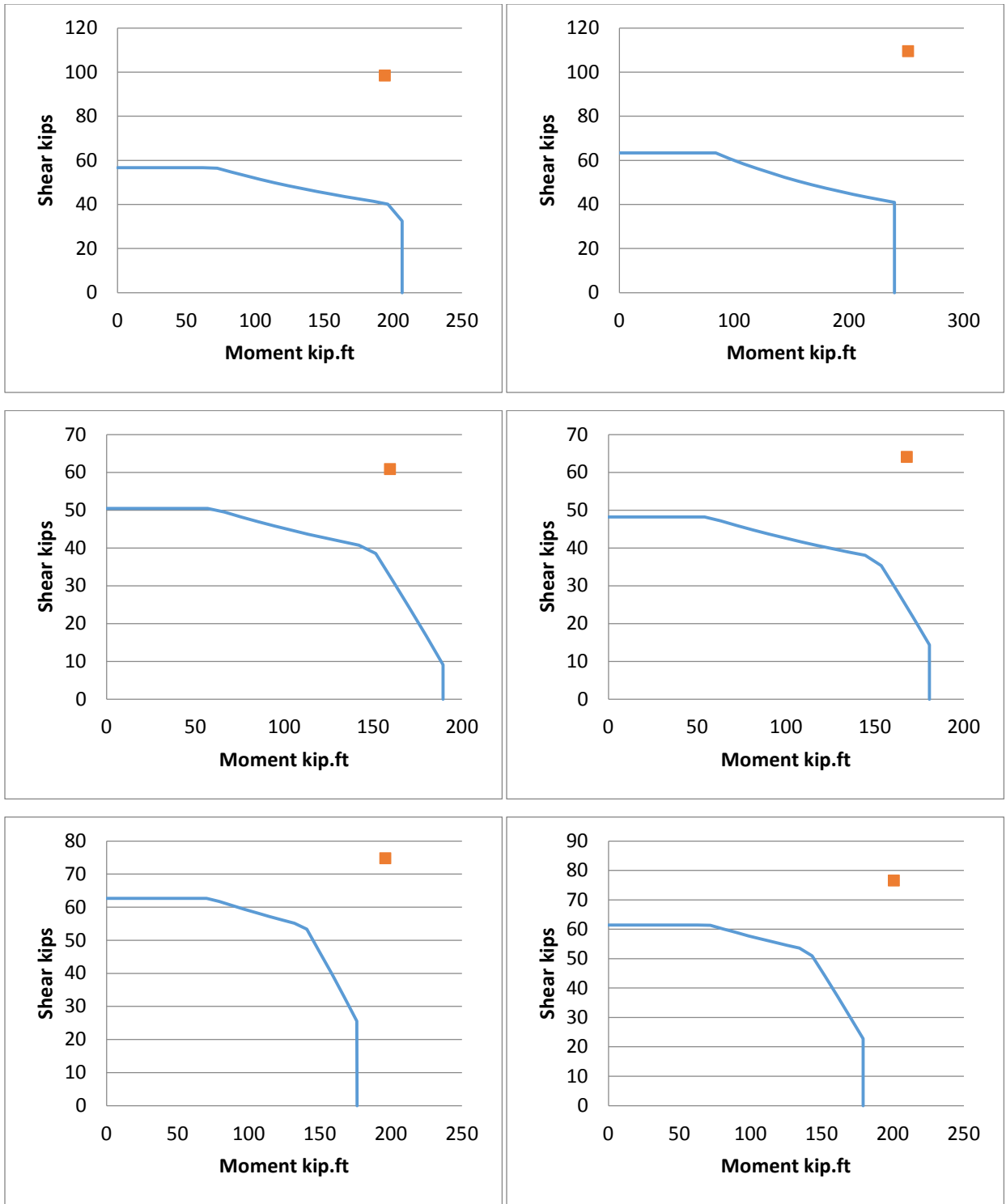
Figure 7.39: Ang et al. (1985) Interaction Diagrams (UNITs 19-24; Table 5.33)

Chapter 8: Conclusions

In this study, a formulation conforming to AASHTO (2014) LRFD Bridge Construction Specifications is developed to predict the axial force-shear-moment interaction diagrams of circular confined concrete bridge pier sections. Comparisons with a large database of experiments indicate the accuracy of the resulting diagrams. A further step was taken to improve the accuracy of the calculations.

Transverse steel area, spacing, cross section diameter, and applied axial force are the main keys to analyze and increase the shear capacity of the cross section. Treating the cracked concrete as a new different material proved to be a beneficial approach to predict the capacities and behaviors of sections.

On the other hand, comparisons against the AASHTO (1999) interaction diagram option in Response 2000 show that the latter yields incorrect predictions in moment-dominated failure. The author suggests that appropriate corrections be made to Response 2000 to correct these interaction diagram errors. The reader is also directed to use KDOT Column Expert for more accurate prediction of the interaction diagrams.

References

Abd El-Fattah, A.M., Rasheed, H.A., & Esmaeily, A. (2011). A new eccentricity-based simulation to generate ultimate confined interaction diagrams for circular concrete columns. *Journal of the Franklin Institute, 348*(7), 1163-1176.

ACI Committee 318. (2011). *Building code requirements for structural concrete* (ACI 318-11). Farmington Hills, MI: American Concrete Institute.

American Association of State Highway and Transportation Officials (AASHTO). (1999). AASHTO LRFD Bridge Construction Specifications (1999 Interim Edition). Washington, DC: Author.

American Association of State Highway and Transportation Officials (AASHTO). (2014). AASHTO LRFD Bridge Design Specifications (7th ed.). Washington, DC: Author.

Ang, B.G., Priestley, M.J.N., & Paulay, T. (1985). Seismic shear strength of circular bridge piers (Report 85-5). Christchurch, New Zealand: University of Canterbury.

Ang, B.G., Priestley, M.J.N., & Paulay, T. (1989). Seismic shear strength of circular reinforced concrete columns. *ACI Structural Journal, 86*(1), 45-59.

Arakawa, T., He, M.X., Arai, Y., & Mizoguchi, M. (1987). Ultimate shear strength of spirally-confined concrete columns. *Transactions of the Japan Concrete Institute, 9*, 305-312.

Bentz, E.C., Vecchio, F.J., & Collins, M.P. (2006). Simplified modified compression field theory for calculating shear strength of reinforced concrete elements. *ACI Structural Journal, 103*(4), 614-624.

Calderone, A.J., Lehman, D.E., & Moehle, J.P. (2001). *Behavior of reinforced concrete bridge columns having varying aspect ratios and varying lengths of confinement* (PEER Report 2000/08). Berkeley, CA: Pacific Earthquake Engineering Research Center.

California Department of Transportation (Caltrans). (2010). *Seismic retrofit guidelines for bridges in California* (Caltrans Memo to Designers 20-4). Retrieved from http://www.dot.ca.gov/hq/esc/techpubs/manual/bridgemanuals/bridge-memo-to-designer/bmd.html

Chai, Y.H., Priestley, M.J.N., & Seible, F. (1991). Seismic retrofit of circular bridge columns for enhanced flexural performance. *ACI Structural Journal, 88*(5), 572-584.

Cheok, G.S., & Stone, W.C. (1986). *Behavior of 1/6-scale model bridge columns subjected to cyclic inelastic loading*. Gaithersburg, MD: US Department of Commerce, National Bureau of Standards.

Elsanadedy, H.M. (2002). *Seismic performance and analysis of ductile composite-jacketed reinforced concrete bridge columns* (Doctoral dissertation). University of California, Irvine, CA.

Hamilton, C.H., Pardoen, G.C., & Kazanjy, R.P. (2002). *Experimental testing of bridge columns subjected to reversed-cyclic and pulse-type loading histories* (Report 2001-03, Civil Engineering Technical Report Series). Irvine, CA: University of California.

Henry, L., & Mahin, S.A. (1999). *Study of buckling of longitudinal bars in reinforced concrete bridge columns*. Sacramento, CA: California Department of Transportation.

Hose, Y.D., Seible, F., & Priestley, M.J.N. (1997). *Strategic relocation of plastic hinges in bridge columns* (Structural Systems Research Project Report No. SSRP-97/05). La Jolla, CA: University of California, San Diego.

Iwasaki, T., Kawashima, K., Hagiwara, R., Hasegawa, K., Koyama, T., & Yoshida, T. (1986). Experimental investigation on hysteretic behavior of reinforced concrete bridge pier columns. In Raufaste, N.J. (Ed.), *Wind and seismic effects: Proceedings of the 17th Joint Panel Meeting of the U.S.-Japan Cooperative Program in Wind and Seismic Effects, May 21-24, 1985.* Gaithersburg, MD: Center for Building Technology, U.S. National Bureau of Standards.

Jaradat, O.A. (1996). *Seismic evaluation of existing bridge columns* (Doctoral dissertation). Washington State University, Pullman, WA.

Joint ASCE-ACI Task Committee 426. (1973). Shear strength of reinforced concrete members. *Journal of the Structural Division, 99*(6), 1091-1187.

Kowalsky, M.J., & Priestley, M.J.N. (2000). Improved analytical model for shear strength of circular reinforced concrete columns in seismic regions. *ACI Structural Journal, 97*(3), 388-396.

Kunnath, S.K., El-Bahy, A., Taylor, A.W., & Stone, W.C. (1997). *Cumulative seismic damage of reinforced concrete bridge piers* (NCEER Technical Report 97-0006). Buffalo, NY: US National Center for Earthquake Engineering Research.

Lehman, D.E., & Moehle, J.P. (2000). *Seismic performance of well-confined concrete bridge columns* (PEER Report 1998/01). Berkeley, CA: Pacific Earthquake Engineering Research Center.

Lim, K.Y., & McLean, D.I. (1991). Scale model studies of moment-reducing hinge details in bridge columns. *ACI Structural Journal, 88*(4), 465-474.

McDaniel, C.C. (1997). *Scale effects on the shear strength of circular reinforced concrete columns* (Master's thesis). University of California, San Diego, La Jolla, CA.

Moyer, M.J., & Kowalsky, M.J. (2003). Influence of tension strain on buckling of reinforcement in RC bridge columns. *ACI Structural Journal, 100*(1), 75-85.

Munro, I.R.M., Park, R., & Priestley, M.J.N. (1976). *Seismic behavior of reinforced concrete bridge piers* (Report 76-9). Christchurch, New Zealand: University of Canterbury.

Nelson, J.M. (2000). *Damage model calibration for reinforced concrete columns* (Master's thesis). University of Washington, Seattle, WA.

Ng, P.L., Lam, J.Y.K., & Kwan, A.K.H. (2010). Tension stiffening in concrete beams. Part 1: FE analysis. *Proceedings of the Institution of Civil Engineers: Structures and Buildings, 163*(1), 19-28.

Nutt, R.V. (1996). *Improved seismic design criteria for California bridges: Provisional recommendations* (Report No. ATC-32). Redwood City, CA: Applied Technology Council.

Ohtaki, T., Benzoni, G., & Priestley M.J.N. (1996). *Seismic performance of a full-scale bridge column—as built and as repaired* (Structural Systems Research Project Report No. SSRP-96/07). La Jolla, CA: University of California, San Diego.

Petrovski, J., & Ristic, D. (1984). *Reversed cyclic loading test of bridge column models* (Report IZIIS 84-164). Skopje, Republic of Macedonia: Institute of Earthquake Engineering and Engineering Seismology.

Pontangaroa, R.T., Priestley, M.J.N., & Park, R. (1979). *Ductility of spirally reinforced concrete columns under seismic loading* (Report 79-8). Christchurch, New Zealand: University of Canterbury.

Priestley, M.J.N., Verma, R., & Xiao, Y. (1994). Seismic shear strength of reinforced concrete columns. *Journal of Structural Engineering, 120*(8), 2310-2329.

Ranf, R.T., Eberhard, M.O., & Stanton, J.F. (2006). Effects of displacement history on failure of lightly confined bridge columns. *American Concrete Institute Special Publication, 236*, 23-42.

Rasheed, H.A., Abd El-Fattah, A.M., Esmaeily, A., Jones, J.P., & Hurst, K.F. (2012). Software for adaptable eccentric analysis of confined concrete circular columns. *Computers and Concrete, 10*(4), 331-347.

Roeder, C.W., Graff, R., Soderstrom, J.L., & Yoo, J.H. (2001). Seismic performance of pile-wharf connections (PEER Report 2002/07). Berkeley, CA: Pacific Earthquake Engineering Research Center.

Saatcioglu, M., & Baingo, D. (1999). Circular high-strength concrete columns under simulated seismic loading. *Journal of Structural Engineering, 125*(3), 272-280.

Shahrooz, B.M., Miller, R.A., Harries, K.A. & Russell, H.G. (2011). *Design of concrete structures using high-strength steel reinforcement* (NCHRP Report 679). Washington, DC: Transportation Research Board.

Siryo, K.K. (1975). *Aseismic analysis of building structural members: A list of experimental results on deformation ability of reinforced concrete columns under large deflection* (No. 2). Japan: Building Research Institute, Ministry of Construction.

Sritharan, S., Priestley, M.J.N., & Seible, F. (2001). Seismic design and experimental verification of concrete multiple column bridge bents. *ACI Structural Journal, 98*(3), 335-346.

Standards New Zealand. (1995). Design of concrete structures. In *Concrete Structures Standard* (NZS 3101). Wellington, New Zealand: Author.

Stone, W.C., & Cheok, G.S. (1989). *Inelastic behavior of full-scale bridge columns subjected to cyclic loading* (NIST BSS 166). Gaithersburg, MD: National Institute of Standards and Technology.

Vecchio, F.J., & Collins, M.P. (1986). The modified compression-field theory for reinforced concrete elements subjected to shear. *ACI Journal Proceedings, 83*(2), 219-231.

Vu, N.D., Priestley, M.J.N., Seible, F., & Benzoni, G. (1998, June). *Seismic response of well confined circular reinforced concrete columns with low aspect ratios*. Paper presented at the meeting of the 5th Caltrans Seismic Research Workshop, Sacramento, CA.

Walraven, J.C. (1981). Fundamental analysis of aggregate interlock. *Journal of the Structural Division, 107*(11), 2245-2270.

Watson, S., & Park, R. (1994). Simulated seismic load tests on reinforced concrete columns. *Journal of Structural Engineering, 120*(6), 1825-1849.

Wong, Y.L. (1990). Squat circular bridge piers under multi-directional seismic attack (Doctoral dissertation). University of Canterbury, Christchurch, New Zealand.

Yalcin, C. (1997). *Seismic evaluation and retrofit of existing reinforced concrete bridge columns* (Doctoral dissertation). University of Ottawa, Ottawa, Canada.

Yarandi, M.S. (2007). *Seismic retrofit and repair of existing reinforced concrete bridge columns by transverse prestressing* (Doctoral dissertation). University of Ottawa, Ottawa, Canada.

Zahn, F.A., Park, R., & Priestley, M.J.N. (1986). *Design of reinforced concrete bridge columns for strength and ductility* (Report 86-7). Christchurch, New Zealand: University of Canterbury.

K-TRAN

KANSAS TRANSPORTATION RESEARCH
AND
NEW-DEVELOPMENT PROGRAM

AD ASTRA PER ASPERA

Kansas
Department of Transportation